Mixing Enhancement in Microfluidic Devices

A thesis submitted to The University of Manchester for the degree of Doctor of Philosophy in the Faculty of Science and Engineering

2017

Ulises Bautista Figueroa

School of Mechanical, Aerospace and Civil Engineering

Contents

Word count: 40166

List of Figures

List of Tables

Abstract

Microscale mixing is paramount for processing targeted drug delivery, chemical production and medical diagnostics. Mixing is often performed in a micromixer, which is a microfluidic device where the fluids are confined in micro sized channels in the order of 100-500 μm. Micromixing has many advantages over its macroscale counterpart, which include small sample consumption, portability, low cost, handling of dangerous materials, compact size and disposability. However, there are also many challenges for mixing enhancement that include low diffusivity rates, high surface-volume ratio, laminar flow, viscous effects, fluid confinement and surface defects are all significant challenges. This aim of this study is to design an effective and efficient micromixer that overcomes these limitations.

The literature review summarises the different approaches that have been reported to address these technical challenges, which included numerous sub-processes and micromixer designs. The most common technique involved forcing the liquid samples to mix through a complex microchannel pattern. However, this approach was limited by the high-pressure drop, complex manufacturing of the microchannel, cleaning difficulties and long mixing distances. Other mixing techniques made use of external energy sources such as sound waves, electromagnetic fields, pulsing the flow inlets, temperature gradients, in an attempt to enhance mixing. Although some were effective in specific cases, they did not offer a broad solution for many applications.

In order to address these issues, three novel micromixer designs were investigated and validated using a combination of numerical simulations and experiments; these included: 1) a micromixer with a modified geometry and synthetic jets, 2) a micromixer that exploited the multiphase flow principle and 3) a micromixer with a straight channel and a spinning disk.

The results confirmed that it was not feasible to develop a micromixer by scaling down a macromixer. However, by modifying the geometry and adding synthetic jets, it was possible to achieve the desired mixing degree of 90% in just 3 seconds at 350 μm downstream with a stroke length of 10.5 (Δ_{pp}=263 μm), Strouhal number of 0.525 (f=6 Hz) and Reynolds number of 0.25. However, the final design suffered technical issues and became complex. The second proposed solution relied on the multiphase flow principle that did not require a complex channel pattern, any external energy source or moving parts to effectively enhance mixing. A mixing quality of 95% was achieved within 0.2 seconds at 350 μm downstream with typical Re<1. Conversely, this design suffered poor mixing performance at Re>2, which was addressed by incorporating a straight channel and spinning disk that achieved a mixing quality of 90% for any Re<10 at a spinning frequency of 15 Hz. The promising results obtained with the multiphase principle and spinning disk make them serious candidates for being implemented in practical applications.

Declaration

No portion of the work referred to in the thesis has been submitted in support of an application for another degree or qualification of this or any other university or other institute of learning.

Ulises Bautista Figueroa

_____

28th of March 2017

Copyright statement

I. The author of this thesis (including any appendices and/or schedules to this thesis) owns certain copyright or related rights in it (the "Copyright") and s/he has given The University of Manchester certain rights to use such Copyright, including for administrative purposes.

II. Copies of this thesis, either in full or in extracts and whether in hard or electronic copy, may be made only in accordance with the Copyright, Designs and Patents Act 1988 (as amended) and regulations issued under it or, where appropriate, in accordance with licensing agreements which the University has from time to time. This page must form part of any such copies made.

III. The ownership of certain Copyright, patents, designs, trademarks and other intellectual property (the "Intellectual Property") and any reproductions of copyright works in the thesis, for example graphs and tables ("Reproductions"), which may be described in this thesis, may not be owned by the author and may be owned by third parties. Such Intellectual Property and Reproductions cannot and must not be made available for use without the prior written permission of the owner(s) of the relevant Intellectual Property and/or Reproductions.

IV. Further information on the conditions under which disclosure, publication and commercialization of this thesis, the Copyright and any Intellectual Property and/or Reproductions described in it that may take place is available in the University IP Policy (see http://documents.manchester.ac.uk/DocuInfo.aspx?DocID=487), in any relevant Thesis restriction declarations deposited in the University Library, The University Library's regulations (see http://www.manchester.ac.uk/library/aboutus/regulations) and in The University's policy on Presentation of Theses.

Acknowledgments

First, I want to thank Jehovah God for his priceless and countless blessings during my PhD journey.[1]

I would like to thank my supervisor Dr Iain Dupere for his comments and suggestions. They made me view things from a different angle. His continuous discussions, recommendations and praise made my PhD experience a great time in my life.

I also want to sincerely thank my family and friends for their encouragement and concerns over my wellbeing.

I would like to extend my thanks to Dr Robert Prosser for his recommendations made during my two examinations.

I am grateful for the financial support provided by the Consejo de Ciencia y Technologia (CONACyT) in Mexico.

[1]Proverbs 3:4,5 Trust in Jehovah with all your heart, and do not rely on your own undestanding. In all your ways take notice of him, and he will make your paths straight. *New World Translation of the Holy Scriptures.*

This thesis is dedicated to my parents

"It's far more difficult to be simple than to be complicated"[1]

[1]John Ruskin

Chapter 1

Introduction

1.1 General introduction

Microfluidics is a relatively new discipline, which appeared in the 1990s when the micro-electromechanical systems (MEMS) technology was used to manufacture new devices that could handle fluids. The devices first applications were in the chemical, biological and biomedical fields [1]. Interestingly, those first MEMS devices were handling fluid in unexplored domains at that time. The necessity to understand the flow behaviour in such a new length scale preceded the birth of a new discipline that was named "microfluidics" [1]. Microfluidics refers to the study of fluids, liquids or gas phases which are confined in a micro length scale (microchannel) [2].

Since its emergence, microfluidics have been used for a broad range of applications and continue their growth in many other areas. For example, drug design in life sciences [3], control and detection of chemical reactions [4] and diagnostic devices in biomedicine [5]. The diversity is due to its wide range of advantages over the conventional macroscale, which include low cost [6], portability [7], small sample consumption [8], [9] rapid analysis [10], and the possibility of carrying out studies in physical, chemical and biological processes [11], [12].

All of the microfluidics devices applications already highlighted are very different from each other. However, most of the microfluidics processes have something in common: the requirement of mixing, which is an important stage in many microfluidic processes. Liquid samples commonly referred as reagents very often require mixing before they reach or perform a new stage in a microdevice. For example, homogenization of solutions in chemical reactions [13], mixing solutions containing macromolecules such as Deoxyribonucleic acid (DNA) [14], [8], mixing different liquid samples containing enzymes and proteins in biological processes [15], [16], [17], or for the production of nanoparticles [18].

Unfortunately developing new microfluidic devices for mixing at the microscale, is very complex. The main problem lies in the nature of shrinking down a macroscale process. As a consequence, several mechanisms become more relevant. For example, mixing is influenced by low diffusivity rates, high surface-volume ratio, laminar flow, viscous effects, fluid confinement and surface defects [19]. In order to achieve the full potential of microfluidics devices, it is therefore very essential to further our understanding of the mechanisms and develop solutions to these limitations.

1.2 Motivation

Over the last two decades, the microfluidics market has grown significantly. The three main growth areas are pharmaceutics, point-of-care and biotechnology, which can be seen in Figure 1.1. This forecast is supported by several other studies that claim considerable growth will take place in the years to come [20], [21], [22], [23]. For instance, in one market report [20], it was predicted that the market would grow from $3.1 Billion in 2015 to $7.5 Billion by 2020 at a compound annual growth rate (CAGR) of 19.3%. A similar figure was predicted by Roussel [21] who claimed that market would grow from $2.56 Billion in 2015 to $5.95 Billion in 2020 with a CAGR of 18%. The predicted market growth of $3 Billion in 2016 seen in Figure 1.1 is confirmed by the actual growth of $3.65 Billion reported in [24]. Therefore, being aware of these market predictions encourages further research in microfluidics to fulfil future needs. This

potential has been the driving force of several microfluidics companies that are currently diversifying their products to reach a broader range of customers in the near future [21].

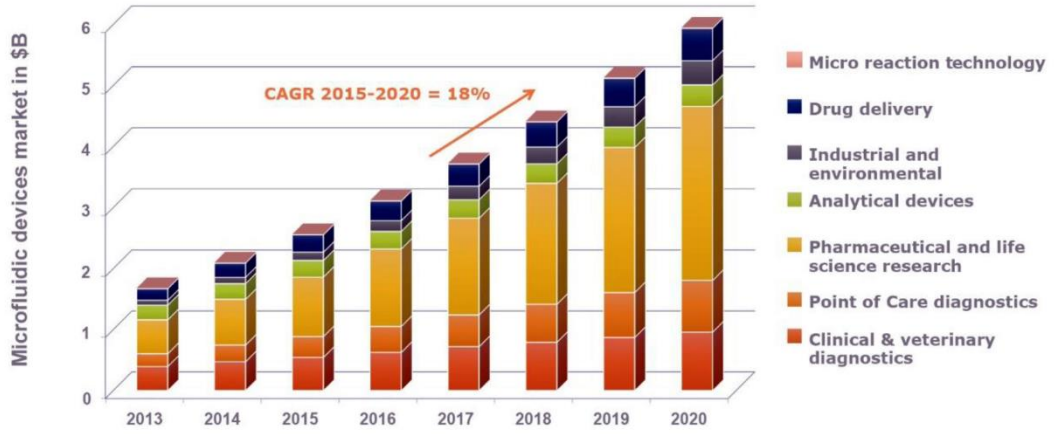

Figure 1.1 Microfluidics devices market in $Billion, June 2015 [21].

Figure 1.1 shows that the biggest growth of microfluidic devices is predicted to be in pharmaceutical and life science research. Nevertheless, to commercialise effective and efficient devices, a continuous development will be essential to achieve such growth. Meanwhile, in addition to the devices themselves, all related components will also have to be developed. For example, micromixers to perform DNA analysis or chemical reactions in a microreactor.

Realising the potential of microfluidic devices, the next step was to understand the technical limitations and the standard requirements of commercial devices, which mainly depend on the application. For example, technical issues for micro-chemical reactions [25] will be completely different for those of point-of-care diagnostics [26]. Being aware of the different kind of technical difficulties will help overcome them in future microfluidics devices.

When the first microfluidic devices were manufactured, most of their manufacturing methods were originated from the area of MEMS [2], which by comparison was a mature technology that was developed in the 1980s. Therefore, most of the technology used to manufacture microfluidic devices relied on the methods and processes utilised in MEMS.

MEMS technology has been widely developed in the last two decades, but did not experience rapid commercialization or significant growth in the 1980s [27]. However, this changed from 2005 onwards when the MEMS market grew and is anticipated to continue growing to reach 26.14 billion USD by 2022 [28].

To estimate the percentage of the microfluidic market within the MEMS market, the predicted trend in recent years is shown in Figure 1.2 [29]. It is evident that the microfluidic market will reach about a quarter of the total MEMS market by 2017.

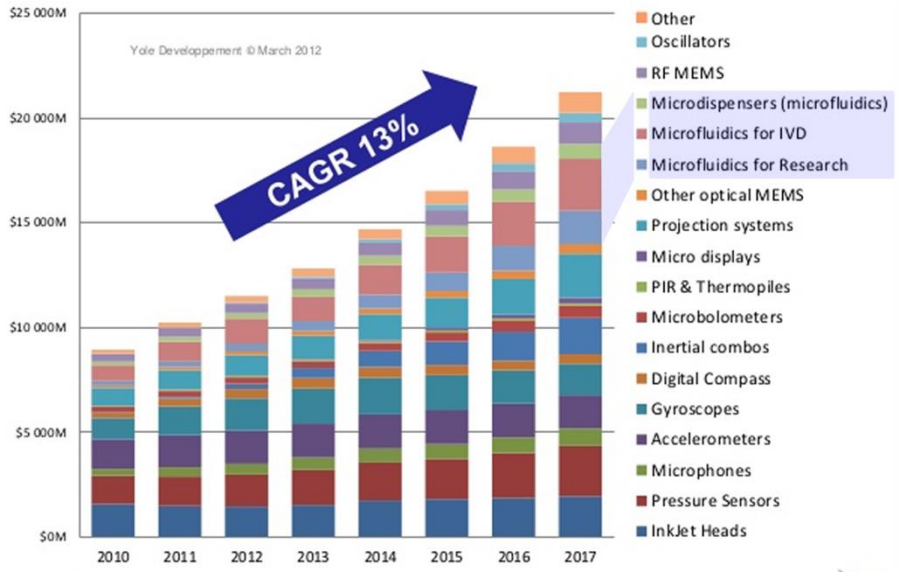

Figure 1.2 Microfluidics market forecast within the MEMS market [29].

To successfully develop and commercialise a new microfluidic device, there are many other components that also have to be developed. For instance, in a microdevice that is used to perform chemical processing, components such as micropumps, electrowetting techniques and micromixers may be required.

In many processes carried out in microdevices, mixing is one of the most important stages of the process where the extent of mixing indicates the quality of the final product. For example, mixing liquid samples to trigger chemical reactions. From Figure 1.3, micromixing is just one of many requirements not only for the development of current microfluidics devices, but also for emerging devices such as electrowetting, digital microfluids and microreactors, amongst others.

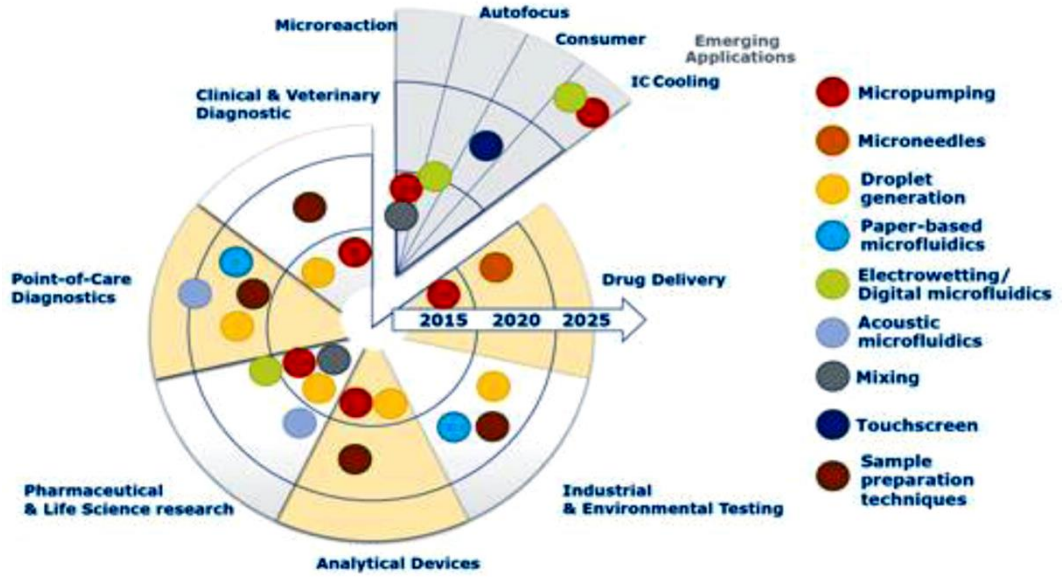

Figure 1.3 Microfluidics technology and applications [21].

However, mixing in microfluidic devices is not a simple process and involves many challenges. One of them is the length scale. In a micromixer the high surface-volume ratio has a significant impact on the patterns of the fluids to be mixed, which is mainly caused by the reduced length scale of the device. Another issue is related to the ratio between the viscous forces and the inertial forces. At the micro scale, the viscous forces become dominant over the inertial forces, which increase the complexity of mixing [19].

To address these mixing issues in microdevices, numerous mixing techniques have been investigated since the discipline of microfluidics began in the 1990s. Mixing techniques such as splitting and recombining the working fluid, patterning grooves on the inner surface of microchannels, using a microstirrer, acoustics and periodic flow pulsation at the inlets, have all been proposed as a solution to the mixing issue in microdevices [15], [30], [31], [32]. However, despite the continuous efforts being made to design and fabricate an efficient micromixer, the mixing problem remains unsolved; this is because most of the mixing techniques does not fulfil the requirement of mixing at the low Reynolds number (Re) encountered in microdevices. It is for this reason why many researchers continue proposing new alternatives in the hope of discovering a practical solution.

1.3 The need of mixing in microdevices

Mixing is a very common phenomenon in our everyday life. When mixing of two or more liquids, the natural thing do is to stir which seems very simple. However, when the length scale is several orders of magnitude smaller than our reference macroscale, homogeneous mixing becomes challenging due to the: laminar flow, boundary layer thickness, surface defects, surface-volume ratio and low diffusivity rates [5], [19].

It is therefore reasonably to ask why attempt to mix fluids in microscale. The answer lies in the opportunity to exploit the numerous benefits that microfluidic devices have in comparison to their macroscale counterparts. For instance, it is only possible to manipulate small quantities of samples when they are expensive, dangerous or simply not available in large amounts such as DNA [4], [8], [9]. Microdevices also possess the capability to perform high quality separation and detection processes, which reduces the required time for their analysis. This is in addition to other notable advantageous characteristics that include their compact size, portability and disposability. Furthermore, a micromixer device, for example, can also be integrated with other processes in a single device [33], [34], [35]. All of these advantages make the development of microfluidic devices a very attractive area of research for practical applications. However, to be able to harness all the advantages it is necessary to develop efficient devices with effective processes, which includes mixing as already established [36].

Unfortunately, a trait that most micromixers have in common is poor mixing. Although continuous development has led to some improvements, many have not yet been successfully commercialised. Limiting factors such as manufacturing complexity, high cost, complex control systems or poor mixing performance are some of the causes. The main difficulty of mixing in microdevices is their highly laminar flow [37], which is often represented by the Reynolds number (Re); this dimensionless number indicates

the ratio between inertial forces to viscous forces. Typical Re in microfluidic devices are below one [38], [1], [39], [37], [40], which contribute to mixing difficulties.

In an attempt to address the mixing problem at such low Reynolds numbers, two alternative approaches are proposed in this study: mixing with 1) synthetic jets and 2) multiphase flow.

1.4 Aims and objectives

The overall aim of this project is to investigate the possibility of mixing enhancement in microfluidics devices using two new alternatives: synthetic jets and multiphase flow. The mixing investigation is intended to provide design rules for effectively mixing liquid samples in microfluidic devices and better understanding of these two mixing technique that are not fully explored.

1.4.1 Design criteria

- **Short mixing time**

The time required to mix liquid samples in microfluidic devices is usually one of the most critical parameters in a microfluidic process. The time required to mix different chemical reagents in a microreactor, for example, dictates the quality of the final product [41]. In such processes, the time scale is in the order of a few hundred milliseconds. While other applications may not require such short mixing times, it is always desirable. Therefore, the final micromixer design should be able to deliver 90% mixing quality within a few miliseconds.

- **Simple design**

A simple micromixer design is ideal because it is directly related with the manufacturing complexity and the final cost. Complex designs also have the issues of cleaning and a high-pressure drop [42], [43], for example, which is related to high power consumption when pumping the fluids to mix, making the mixing device less efficient.

- **Minimum energy consumption**

One of the most effective techniques for enhancing mixing in microfluidic devices is using an external energy source which is often used to disturb the flow and promote mixing. In some cases, the energy required to drive the liquids is relatively high. For example, in a micromixer that uses an electric field [44]. Therefore, low energy consumption is desirable. In fact, an ideal scenario would be to eliminate the need of an external source of energy altogether.

- **Mixing degree above 90%**

Another requirement of the micromixer is related to the final quality of the mixture. A mixture quality of 90% is often considered acceptable in microfluidics applications [45], which is derived from the mixing degree (MI) calculation of the final mixture. The convention used in this study is that a MI=0 indicates no mixing and a MI=1 represents complete mixing. Therefore, to achieve 90% mixing quality, the mixing degree has to be 0.9.

- **Short mixing distance downstream**

Mixing by molecular diffusion takes unpractical long microchannel distances [1]. An efficient micromixer should therefore mix within short distances, which are also beneficial in applications where the working fluid is limited or in an integrated micromixer of a more complex Lab-on-a-Chip processes [46], [47].

- **Simple system of control**

Complex control systems are not only difficult to operate but also complex to manufacture, assemble and maintain. Thus, a novel micromixer design should have a simple control system or not utilise any at all.

There is the possibility that some of the criteria conflict with each other. For example, short mixing times and the mixing degree are achieved but do not fulfil the low energy consumption aim, for example, too high. Compromises may therefore be required in order to propose the most efficient and effective micromixer.

1.5 Structure of this thesis

In Chapter 1, the background, the motivation, aims and objectives are presented. In Chapter 2, a review of the available mixing techniques is introduced, which includes the driving mechanisms and mixing techniques used for enhancing mixing in microfluidics devices. In Chapter 3, the methodology used to perform all the numerical simulations and the experimental tests is detailed. In Chapter 4, 2D numerical simulations of a macromixer with four synthetic jets are first presented. Then, a simplified macromixer with two pairs of synthetic jets is considered. The chapter continues with an even simpler macromixer design consisting of one pair of synthetic jets, which is then scaled down to a typical micromixer size. Next, an optimised synthetic jet micromixer design is presented and discussed in some detail. In Chapter 5, the multiphase flow approach for mixing enhancement in microfluidics is introduced and the mixing performance of a micromixer using such a method is investigated at the typical Re found in microfluidic devices. In Chapter 6, a novel micromixer that could mix liquid samples at $Re \leq 10$ is proposed and discussed. The micromixer design consists of a straight channel and spinning disk that is located on the bottom wall of the straight microchannel of the micromixer with the purpose of enhancing mixing. Finally, in Chapter 7, the conclusions and future work of the mixing investigation are presented.

Chapter 2

Literature Review

2.1 Introduction

In the preceding chapter, we considered the importance and the potential practical applications that an efficient micromixer could have in the area of microfluidics. Mixing in these devices, however, is not straightforward. This is because the fluids in such devices are under certain conditions that make mixing difficult, which are mostly associated with their length scale.

Due to the practical applications and advantages, many attempts have been made to design and fabricate an efficient micromixer. However, many issues related to mixing in the micro length scale have to be overcome. For example, the laminar flow, high surface-volume ratio, high diffusivity values of the species to be mixed and the difficulty to generate chaos and turbulence, all of which contribute to mixing complications in microdevices. Hence, in this chapter we described and discussed the current proposed attempts to overcome the mixing issue.

The present chapter begins by introducing the concept of mixing from a macro scale view point and continues by considering mixing in microsystems. After this, the mixing mechanisms of molecular diffusion, chaotic advection and the hydrodynamic techniques are discussed that have been used to enhance mixing. The chapter will be concluded by reviewing the mixing techniques used currently in microdevices based on synthetic jets and multiphase flow.

2.2 Mixing

In our everyday life, mixing is a common process. We all mix liquids or solids in one way or another sometimes without even knowing it. For example, when we make a cup of coffee. If we look at nature, mixing is also present in many natural phenomena such as in the Earth's mantle [48], in the sea; when sea water mixes with fresh water or in the atmosphere; when two air streams of hot and cold air meet. But how can we define mixing? Nguyen [49] defines mixing as a transport process of species, temperature and phases to reduce inhomogeneity. Another definition is given by Villermaux et al. [50] and it is referred as an operation consisting of putting together two or more constituents in order to reach uniformity. Therefore, we can infer that mixing is a process where the objective is to uniformly distribute the samples to be mixed.

However, a question arises when it comes to evaluating the homogeneity of a mixture: how do we know if the final mixture is properly mixed? The evaluation of mixing is challenging because it is a dynamic and three-dimensional (3D) system. One potential option to evaluate mixing is using Poincaré maps. A Poincaré map can be seen as a cross-section or map at a certain location within the mixture [51]; hence, it is considered a two dimensional (2D) map of the mixture. This technique simplifies the 3D mixing system into 2D [52]. Consequently, there are some key limitations. For example, the Poincaré maps are a qualitative technique that only allows a visual examination of the distributions of the fluids to be mixed. Therefore, Poincaré maps are typically used in mixing problems where the working fluid is composed of small particles (several orders of magnitude smaller than the fluid domain) as a visual aid to evaluate mixing in microdevices [14], [53], [54], [55], [56].

However, the most common technique that is used to quantitatively measure the mixing quality of a mixture is to determine the concentration variance of one of the components within the final mixture [57]. To achieve this, a mean value of the mixture concentration is defined, for example, the concentration target of the final mixture, which can be expressed as:

$$\overline{c}_i = \frac{1}{n-1}\sum_{i=1}^{n} c_i \tag{2.1}$$

while the variance of the concentration is:

$$\sigma^2 = \frac{1}{n-1}\sum_{i=1}^{n}(c_i - \overline{c}_i)^2 \tag{2.2}$$

where c_i is the concentration of the selected sample, n is the number of samples analysed, $\overline{c}_i$ is the mean concentration of the sample which is 0.5 for complete mixing. This leads to having values of the concentration variance of 0.5 for an unmixed mixture and a concentration variance of zero for a fully mixed mixture. This value is therefore directly related to the quality of the mixture. In practical applications, for example, the variance of the concentration is recommended to be 0.05, which indicates a complete mixing [52], [58], [59], [60], [61], [62], which corresponds to 95% mixing [58], [62].

However, reporting the concentration variance value is not a common way of defining the quality of the mixing. Instead, the most commonly used method involves indicating the quality by mixing degree. This convention was used by Johnson et al. [63] and Glasgow and Aubry [63] who normalised the variance concentration by the mean value of the concentration $(\overline{c}_i = 0.5)$ and then subtracted that result from 1 to give:

$$MI = 1 - \frac{\sqrt{\frac{1}{n-1}\sum_{i=1}^{n}(c_i - \overline{c}_i)^2}}{\overline{c}_i} \tag{2.3}$$

where *MI* is known as the degree of mixing of the mixture, where a value of 0 indicates no mixing and a value of 1 represents complete mixing.

2.3 Mixing in microsystems

Mixing in microsystems is difficult mainly because the flow regime is highly laminar [64]. Hydrodynamic instabilities do not develop, resulting in no chaos and turbulence unless they are induced by external sources. Chaos is not easy to define and understand. It may give us an idea that chaos signifies random motion but that is not necessarily the case. Ottino [51] defines chaos as a system that experiences rapid divergence of its initial conditions. In other words, chaos can be defined as how much a fluid is stretched from its initial conditions. But a laminar flow in microdevices is not stretched significantly at usual operating conditions and chaos does not develop. On the other hand, Lesieur [65] states that a turbulent flow is a flow that experiences disorder in time and space. In a different paper, Ottino [66] gives a similar definition. He states that

a turbulent flow is a flow that is able to produce spatial and temporal disorder. In contrast to a turbulent flow, a laminar flow is often considered a highly ordered flow where disorder does not take place [64].

If chaos and turbulence are not an option in laminar flows, then, a question arises of how can fluids in such a regime mix? There are several alternatives, like for example; molecular diffusion [67], chaotic advection [68], or by the manipulation of the hydrodynamics by external energy sources [1] to enhance mixing.

2.3.1 Mixing by molecular diffusion

In his pioneering work on diffusion, Fick [69] states that the diffusion of a species is due to the influence of molecular forces. To mathematically represent his idea, he made an analogy with the thermal conduction equation proposed by Fourier [70], saying that the molecular diffusion follows the same law. Fick concluded that molecular diffusion can be modelled in Cartesian co-ordinates as:

$$J_1 = Aj_1 = -AD\frac{\partial c_1}{\partial z} \tag{2.1}$$

where A is the surface area at which diffusion takes place, c_1 is the concentration of the sample to diffuse, z its position and D the diffusion coefficient of a particular specie. Equation (2.1) was later known as Fick's law.

The diffusion coefficient D is a parameter that depends on the nature of the specie to diffuse [71]. However, if we consider that a fluid is constituted of spherical particles, the diffusion constant can be approximated by the Einstein-Stokes equation [72] as:

$$D = \frac{kT}{6\pi\mu R} \tag{2.5}$$

where k is the Boltzmann constant, T the absolute temperature, R the radius of the spherical particles and μ the dynamic viscosity of the fluid.

However, we need to define diffusion to have a better understanding of its meaning. But before doing that, we first need to explain the terms solute and solvent. A solute is the specie to diffuse, for example, small particles, enzymes or small proteins; while a solvent, is the flow phase where the solute is dissolved, for example, a liquid. Thus, we can define diffusion as the motion of the solute through the solvent and always occurs from high to low concentration [71].

Although in many microfluidic devices mixing is usually achieved by diffusion, it has some limitations. For example, diffusion is a slow process and often requires a considerable amount of time to completely diffuse a solute. Table 2.1 shows some mixing times at several length scales where we can see that in the case of diffusing enzymes or small proteins in a microreactor, the mixing time is one thousand seconds (t≈16 min) when using a microchannel of 100 μm [1].

Table 2.1 Mixing times of some samples at several length scales [1].

System	Diffusion time
Dye in water in a glass of 10 cm	10^5 s
Enzymes and proteins in a microreactor of 100 μm	1000 s
Dye in water in a microsystem of 100 μm	10 s
Dye in water in a microsystem of 1 μm	10^{-3} s

One way of reducing the diffusion time is by decreasing the transverse distance that the solute has to travel to be fully diffused or mixed. This can be seen in the last two examples provided in Table 2.1 where dye is diffused in water using two different cross-sections of microchannels: one with 100 μm and another with 1 μm. The channel reduction results in a significant decrease of the diffusion time to mix the samples which goes from 10 s to 10^{-3} s. Nevertheless, this approach might not be very practical in microfluidic devices where typical microchannel sizes are in the order of 100-500 μm [49].

An alternative way of reducing the distance that the solute has to travel to mix in the solvent is by splitting the fluid stream into several sub-streams. Hismann et al. [73] proposed a micromixer based on pure diffusion where they fabricated an array of microchannels at the fluid confluence of a Y-micromixer, see Figure 2.1. They claim that rapid mixing takes place in the micromixer as a result of the reduced distance of sub-streams. This mixing approach has also been investigated in other papers [74], [75], [76]. However, the manufacturing complexity, cleaning issues and possible high-pressure drop are some of the limitations of this mixing approach.

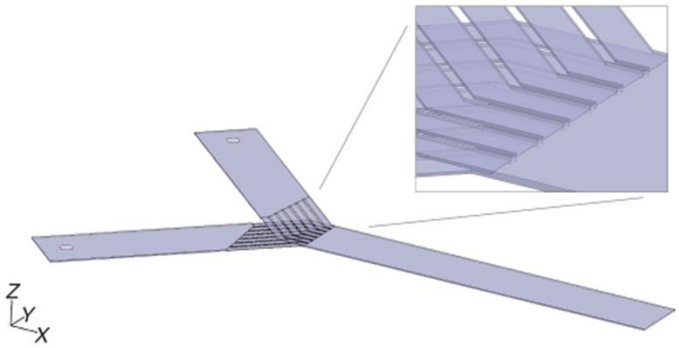

Figure 2.1 Micromixer with an array of microchannels at the confluence of the fluids to be mixed [73].

To avoid the manufacturing of such a complex array of microchannels, another approach was proposed by Knight et al. [77], which consists of focusing the fluids to mix at the micromixer inlets as shown in Figure 2.2. They state that fast mixing is achieved because the flow injected from the left horizontal inlet rapidly diffused into the two opposite side inlet streams. This approach has been successfully applied in a practical study of cells infected by different concentrations of virus [78]. However, it is only useful to diffuse the solute into the solvent but not to have a uniform mixture of all the working fluids downstream.

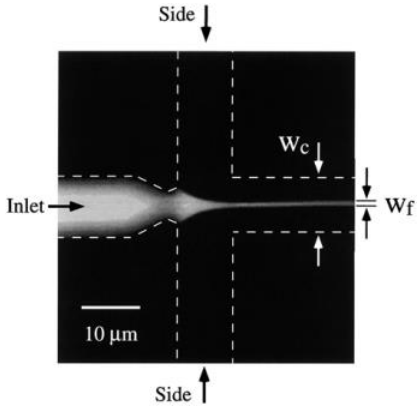

Figure 2.2 Mixing with a hydrodynamic focusing technique [77].

To improve the micromixer reported in [77], Floyd et al. [79] proposed a micromixer where the fluid to be mixed was injected from multiple inlets into one microchannel as depicted in Figure 2.3. The inlets of the fluids were arranged in an alternative manner aiming to reduce the transverse distance that they have to travel to diffuse between each other. This effect is also beneficial to increase the interface area to enhance mixing. Qualitatively, the mixing improvement seems significant but the

Reynolds number in this study was about 40 which is considerably high for most microfluidics applications where Re<1 [1], [37], [38], [39].

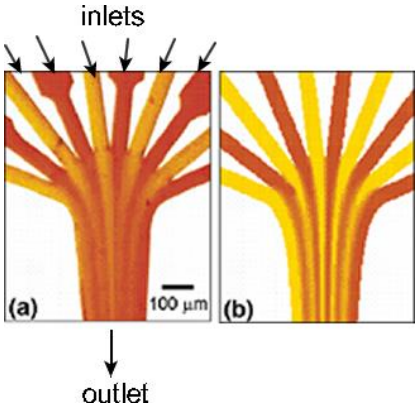

Figure 2.3 Micromixer base on hydrodynamic focusing, a) experiment (modified from [79]), and b) numerical simulation.

2.3.2 Mixing by chaotic advection

Chaotic advection is an alternative approach for mixing enhancement at the laminar regime. Aref [80] performed a 2D numerical study where mixing was enhanced by chaotic advection in a hypothetical stirring tank. In a later numerical work, Aref and Balachandar [81] state that chaotic advection can also be produced at low Reynolds numbers. Such numerical works were then experimentally validated by Chaiken et al. [82] in which they successfully reproduced the vortical structures identified by Aref and Balachandar [80], [81]. The structures show concentric patterns which they named "whorl" and "tendril" structures, which indicate chaotic advection. In an attempt to generate such flow structures and improve mixing in microfluidic devices, numerous researchers have proposed micromixer designs based on chaotic advection [38], [51], [55], [68], [83], [84], [85], [86].

Nevertheless, we do not know what chaotic advection is. Chaos has already been defined as the rate of stretching that a fluid experiences in relation to its initial conditions but what about advection? Advection can be defined as the transport of particles that are driven in the direction of the working fluid [68]. Hence, chaotic advection can be referred to as the stretching of the working fluid in directions different to the main flow [37].

However, changing the direction of the flow to generate chaotic advection is challenging in microfluidics devices and is mainly because of the laminar flow. One way of forcing the main flow to alter its direction and generate the chaotic advection effect is

by modifying the path and/or the shape of the microchannel. A good example of this is the micromixer reported by Kim et al. [86]. The micromixer consists of a channel formed in an F-shape with an alternatively orientation to form the path of the microchannel as shown in Figure 2.4. The chaotic flow behaviour is generated by the three-dimensional path that the flow suffers when it is forced through the F-shape channels. The mixing performance of this particular micromixer design was evaluated at several Reynolds numbers ranging from 0.44 to 10.53. Interestingly, a mixing quality of 90% was only achieved at Re=0.44 while the mixing performance of the rest of the cases were below 90%. Although 90% mixing quality is reported at low Reynolds numbers, the quantification of the mixture was at 40 times the size of the channel inlet downstream, which is significantly large for practical microfluidic applications.

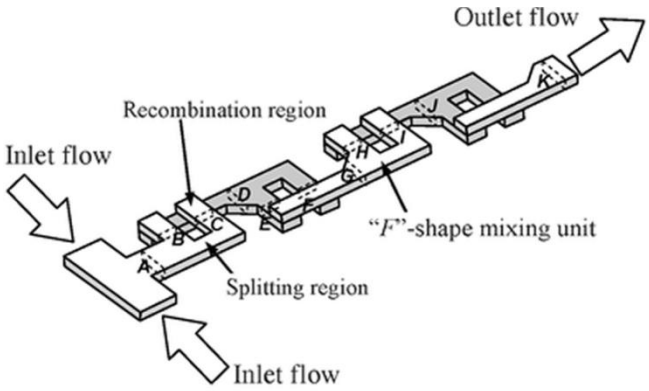

Figure 2.4 Passive micromixer based on chaotic advection [86].

Stroock et al. [13] introduced another approach to induce chaotic advection in a micromixer. They manufactured grooves on the bottom wall of a straight microchannel to force the fluid to change its direction and promote mixing as shown in Figure 2.5. The channel patterning promotes the formation of transverse velocity components indicated by the red and green lines in Figure 2.5.

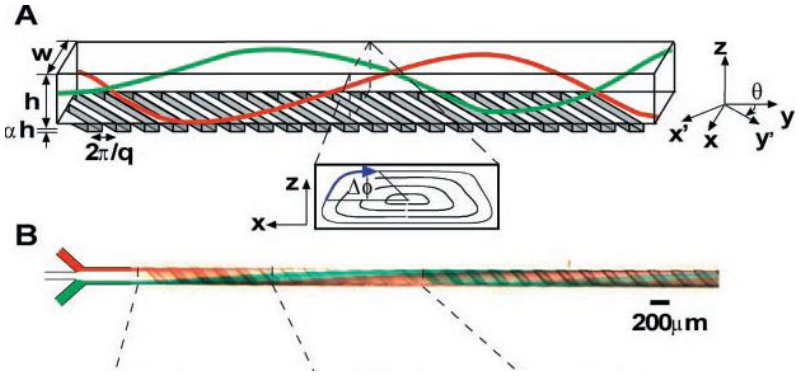

Figure 2.5 Three-dimensional twisting flow in a channel with obliquely oriented ridges on the bottom wall [13].

Strook et al. [13] state that this mixing technique can mix fluids in a wide range of Reynolds numbers (0.1<Re<100). Nevertheless, this micromixer has some drawbacks such as the relative long distance to achieve good mixing (15 times the channel width from the inlets), see Figure 2.6, difficulty in manufacturing and cleaning and a possible high-pressure drop caused by the grooves. These are characteristic limitations of these sort of micromixers (passive micromixers), which still leaves a window opened for simpler and more efficient designs.

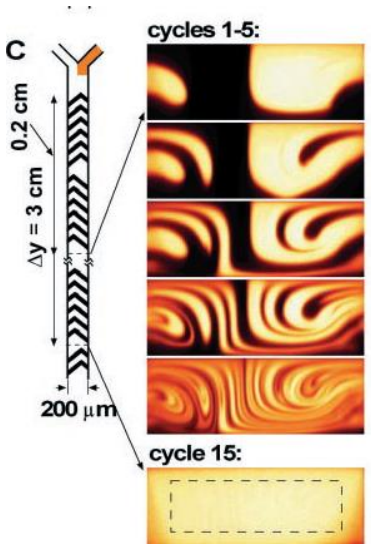

Figure 2.6 Micromixer with pattern grooves on a microchannel [13].

Mixing with chaotic advection has been widely investigated and many micromixer designs consisting of a zigzag channel [87], 3D serpentine structures [88], twisted channels [89] and embedded barriers [90], take advantage of such effects. However, issues like difficult manufacturing, low mixing at Re<1, high-pressure drop and cleaning issues, are some of the limitations of most of these micromixers.

2.3.3 Manipulation of the hydrodynamics by external energy sources

An alternative way of enhancing mixing in microfluidic devices is by manipulating the hydrodynamics of the fluid to be mixed by external energy sources. Micromixers based on these mixing techniques are known as active micromixers [15]. Numerous micromixers with this approach have been proposed to enhance mixing and they can be classified according to the sort of energy they use to stir the fluids. Nguyen [37] classified the active micromixers as: a) serial segmentation, b) pressure disturbance

across the mixing channel, c) integrated microstirrer, d) electrohydrodynamic disturbance, e) dielectrophoretic disturbance, f) electrokinetics disturbance in a mixing chamber and g) electrokinetics disturbance, h) transverse temperature gradient, see Figure 2.7. Some of the active micromixers are more complex to manufacture and control than others but to have a better understanding of the working principles on which they are based, we will review them in detail next.

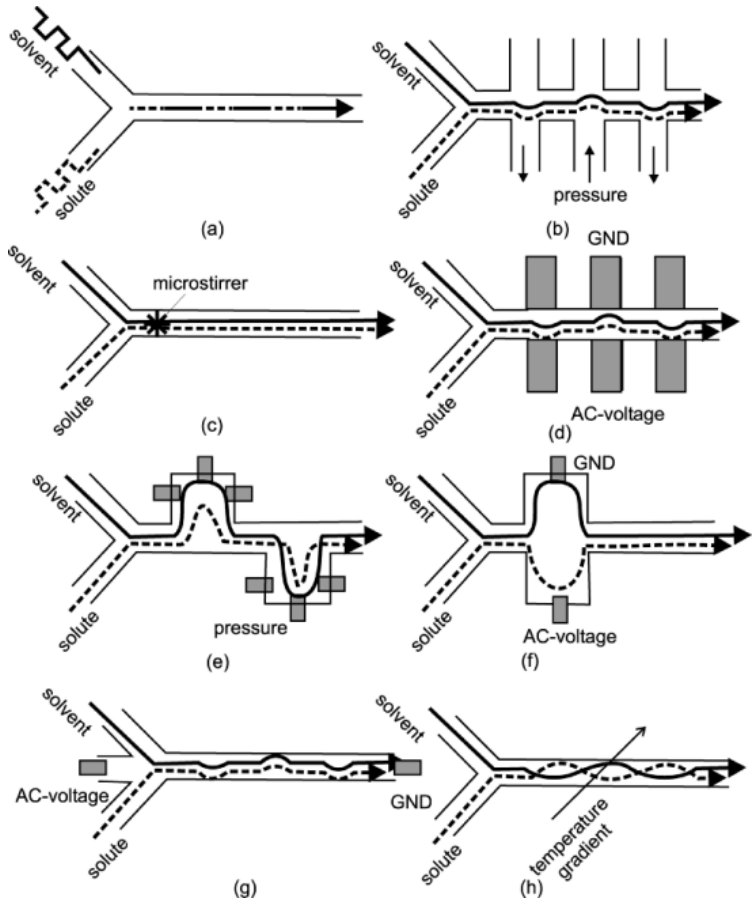

Figure 2.7 Active micromixers classification [37]

2.3.3.1 Pressure-driven disturbance

One of the first pressure-driven disturbance micromixers reported in the literature, is the one proposed by Deshmukh, et al. [91]. It consists of a Y-shape inlet from which the flow is pulsed as shown in Figure 2.8 and its working principle is based on perturbing the working fluid while they are pumped alternatively. Regarding mixing enhancement, it was demonstrated that the alternative flow injection led to the sequential segmentation of the fluids downstream. Their work was one of the first of its kind, as previously mentioned, and focused on the fabrication technique and operating conditions rather than on the mixing performance of the device. The mixing

quantification is not reported, however, from their experimental results. We can see that the two liquid phases are still noticeable downstream, which suggests that mixing was not fully completed.

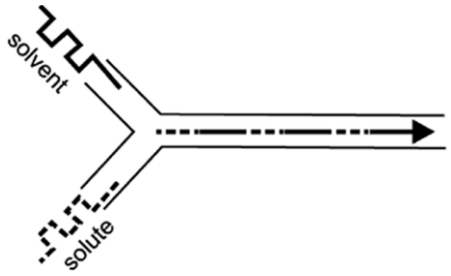

Figure 2.8 Y-shape micromixer with pulsing flow at the inlets [37]

A slightly different pressure-driven micromixer design was proposed by Glasgow et al. [92] which is considered to be a T-shape mixer. They performed a mixing study at several out of phase pulsing modes. Their findings suggest that the best mixing performance was achieved when the fluids were pulsed at 180 degrees out of phase. Although the mixing study was performed at Re=0.3, the quatified mixing degree was 0.56, which is considered as poor mixing.

Another T-shape pressure-driven micromixer was reported by Ma et al. [93] for several Reynolds numbers between 2.4 and 0.048. They state that a mixing degree of 75% was achievable at Re<0.24 and a mixing degree of 90% for Re>2.4. Although the mixing quality was significantly high, the micromixer has some drawbacks. For example, the mixing quantification was performed at a considerable distance from the confluence of the liquids, about 12 times the microchannel width of the micromixer inlet. Another issue is that the flow was pulsed at a frequency of 100 Hz to reach 90% mixing quality at (Re=2.4). This could be a serious limitation in scenarios where the energy consumption is a restrictive parameter.

2.3.3.2 Integrated microstirrer

Another alternative for mixing enhancement in microdevices is integrating a microstirrer in a microchannel [94], [95]. Lu et al. [94] used this technique to stir the fluids to mix at their confluence, as shown in Figure 2.9. The working principle of this micromixer consists of driving the microstirrer with an external magnetic field. The angular velocity of the microstirrer is controlled by the intensity of the external magnetic field. They claim that the rotating speed should be between 100 and 600 rpm to obtain a

homogeneous mixture. However, the major difficulty with this approach is the complex manufacturing of the microstirrer and the relatively high energy consumption to drive it.

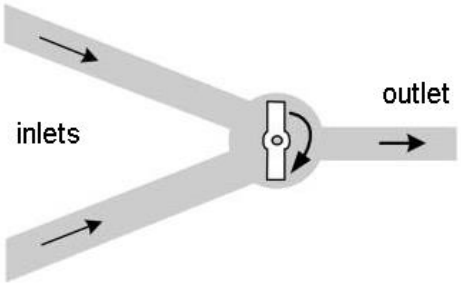

Figure 2.9 Micromixer with an integrated microstirrer in a microchannel [95].

2.3.3.3 Electrohydrodynamic (EHD) disturbance

Mixing enhancement is also possible when disturbing the flow with electrodes placed close to a microchannel [44], [96], [97]. One example of this mixing technique is the micromixer reported by Moctar et al. [44] which is composed of four pairs of transverse electrodes to the main channel, as shown in Figure 2.10. The way this micromixer design works is by energising the electrodes with an oscillating signal, which produces a magnetic field that perturbs the flow along the microchannel to promote mixing. Moctar et al. [44] claim "good" mixing at Reynolds numbers as low as 0.0174 and in less than 0.1 seconds. However, to reach a mixing degree of 80%, the electrodes required an electric field intensity of 7 E^{+05} V/m (200 V).

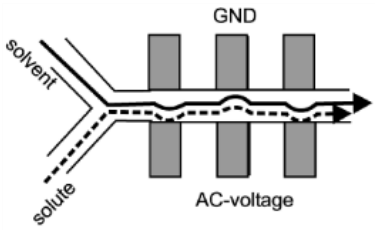

Figure 2.10 Micromixer configuration based on electrohydrodynamic disturbances [37].

Overall, several issues limit the practical application of these micromixers. For instance, the need for a complex system of control which impacts on its final cost and, most importantly, the working fluid has to respond to the electric fields to enhance mixing.

2.3.3.4 Acoustic disturbance

Acoustic energy is another source of energy that has been used for mixing enhancement in micromixers [98], [99], [100], [101], [102]. These micromixers use ultrasonic sound waves that are transmitted to the working fluid by piezoelectric transducers [100], [101], see Figure 2.11.

Acoustic mixing is a very effective method for mixing enhancement in microdevices. For example, in the acoustic micromixer proposed by Jang et al. [101] it is evident that the sound waves can stretch and fold the fluid interface to promote mixing. This effect is also reported by Yang et al. [100]. Nevertheless, these sorts of micromixers are usually operated with high frequencies, (KHz or MHz) [100], [101], [98], which impacts on the energy consumption of the micromixer device. In addition, the increase of temperature due to ultrasonic waves [100], [102] and the need of a mixing chamber [98], [100], [101] are some concerns that could be a problem in practical applications in microfluidic devices.

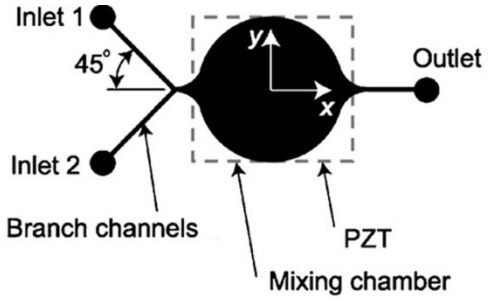

Figure 2.11 Acoustic micromixer with a piezoelectric transducer (modified from [101]).

2.3.3.5 Thermal disturbance

Temperature disturbances have also been used in several micromixers as an external energy source for mixing enhancement [103], [104], [105], [106], [107]. The working principle of these types of micromixers is based on the recirculation of the working fluid by applying transverse temperature gradients across a straight microchannel, as shown in Figure 2.12 [103]. Darhuber et al. [103] demonstrated that such temperature gradients can induce helical paths that increase the interface area of the fluids which ultimately enhances mixing. They claimed that this method can be used to mix ultra-small volumes using just 2-3 Volts of energy. However, they did not report how efficient this method is in terms of the quality of the final mixture.

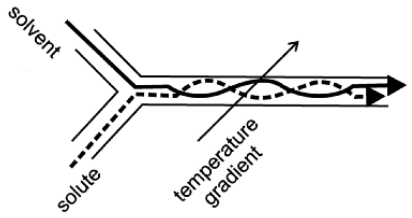

Figure 2.12 Thermal disturbance in a microchannel [37].

Several limitations are directly related with the thermal mixing approach. For instance, the changes in temperature may cause also changes in the properties of the working fluid. One of the most important of these properties is the diffusivity of the liquid samples. Increasing the temperature of the samples may lead to an increase in the diffusivity, which will lead to easier mixing [108]. However, temperature increases may damage living cells like enzymes and proteins often used in microfluidic applications [7], [109].

2.4 Dimensionless numbers in microfluidics

Dimensionless numbers are very useful to help identify the importance of competing transport processes often linked with forces, different types of energy and time scales [37]. A dimensionless number is useful to identify which transport process dominates over others [110]. In a mixing process, for example, the dimensionless numbers could be useful when identifying if the diffusion process dominates over the convection process or vice versa. They are also convenient to simplify complex systems where the governing equations are difficult to solve either analytically or numerically. Systems such as stirring liquids in a tank [80], the deformation and breakup of a droplet [111], a fluid boiling in a microchannel [112], flows in porous media and atmospheric flow [64], are some examples of complex systems where dimensionless numbers are very convenient to study such flow phenomena.

Dimensionless numbers are also advantageous in microfluidic devices. For example, they can be used to study the physical phenomena that are present in numerous microflow processes like in the generation of droplets [111], [113], mixing of chemical and/or biological samples [2], design and fabrication of micropumps, valves, and flow sensors [114]. Some of the most common dimensionless numbers to analyse microfluidics devices are the following:

The Reynolds number. The Reynolds number gives us a loose indication of the importance between the inertial forces and viscous force [37] and it is represented mathematically as:

$$\mathrm{Re} = \frac{\rho U D_h}{\mu} = \frac{U D_h}{\nu} \tag{2.6}$$

where ρ represents the fluid density; U the mean velocity of the fluid; D_h hydraulic diameter of the microchannel and μ the dynamic viscosity.

The Péclet number. The Péclet number denotes the relation between the advection and diffusion transport [37] and it is represented as:

$$Pe = \frac{UL}{D} \tag{2.7}$$

where U is the mean velocity of the fluid; L characteristic length of the channel and D the diffusion coefficient of the specie to diffuse (solute).

Capillary number. It compares the viscous over the interfacial forces [49] and is determined by:

$$Ca = \frac{\mu U}{\gamma} \tag{2.8}$$

where μ is the dynamic viscosity; U the velocity of the fluid and γ the surface tension between immiscible phases.

Bond number. The Bond number can be designated as the ratio between the surface tension forces and the gravitational force [110] which is estimated as:

$$Bo = \frac{\Delta\rho g R^2}{\gamma_i} \tag{2.9}$$

where $\Delta\rho$ signifies the mass difference between two fluids, g the acceleration due to gravity, R the characteristic length (often the radius of a fluid droplet) and γ_i the surface tension force.

The Strouhal number. Although the Strouhal number is not very common in microfluidics, it can be useful to analyse micromixers that include any sort of actuation to perturb the working fluid. Then, the Strouhal number can be considered as the relation between the duration of a single actuation period over the fluid velocity of the working fluid [115]. In other words, the rate of the sequential segmentation of the working fluid and it is expressed as:

$$St = \frac{fL}{U}$$

where f is the actuation frequency; L the characteristic length and U the mean velocity of the flow.

2.5 Mixing with synthetic jets

A synthetic jet can be considered as an artificial jet of fluid that is generated from the working fluid of the system by the alternating motion of a diaphragm or piston [116]. A synthetic jet device consists of three basic components: a cavity, a moving piston or membrane and an orifice as shown in Figure 2.13. The geometry of the cavity can be of any shape, however cavities with circular geometry are more widely used than other shapes in synthetic jet applications [117], [118], [119]. Circular orifices are also frequently used in many synthetic jet configurations but other shapes like squares or rectangular shapes (slots) can also be implemented [120], [121].

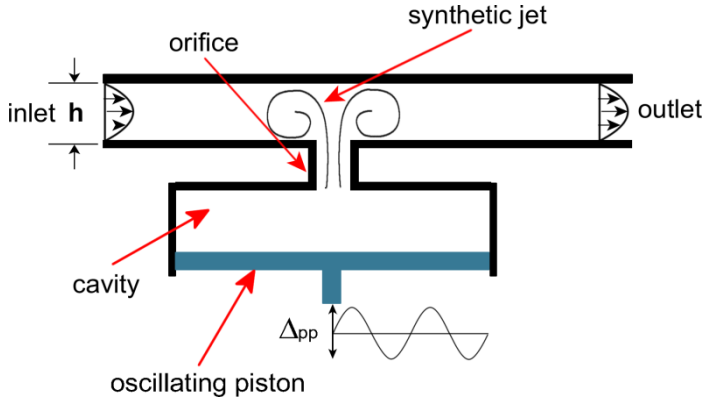

Figure 2.13 A synthetic jet device with its main components: a cavity, an oscillating piston and an orifice (not to scale).

To generate synthetic jets with the geometrical configuration shown in Figure 2.13, two steps should be taken: 1) when the moving piston moves downward, some of

the working fluid from the transverse channel is ingested into the cavity, 2) when the piston displaces upward, the working fluid contained in the cavity is expelled through the orifice in a form of a jet, see Figure 2.13. This process is repeated as long as the piston is in motion and at certain operating conditions vortical structures can be produced [122].

The applications of synthetic jets are broad and could be implemented in flow control [123], delay of boundary layer separation [124], acoustics [125], enhancement of heat transfer [125], improvement of the mixing of fuels in engines and turbines [120], [126], amongst others.

Synthetic jets can be studied in two main scenarios: one is in quiescent conditions [117] and the other is in cross-flow conditions [127]. A synthetic jet device working in quiescent conditions is that which the working fluid outside the cavity is at equilibrium when it starts to operate. In contrast, a synthetic jet operating in a cross-flow is one in which the surrounding fluid is in constant motion, usually transverse to the synthetic jets direction, before actuating it.

Synthetic jet devices working in cross-flow could also be classified into two categories: 1) cross-flow in an unconfined fluid, like the one shown in Figure 2.14 and 2) cross-flow in a confined fluid as shown in Figure 2.13. Synthetic jets in an unconfined cross-flow configuration has been studied considerably by many researchers [123], [127], [128], [129]. However, synthetic jets in a confined cross-flow setting have not had the same interests [122], [130]. This leaves room to further investigate the operating conditions of synthetic jets and the possibility of applying them in applications like mixing enhancement of viscous liquids.

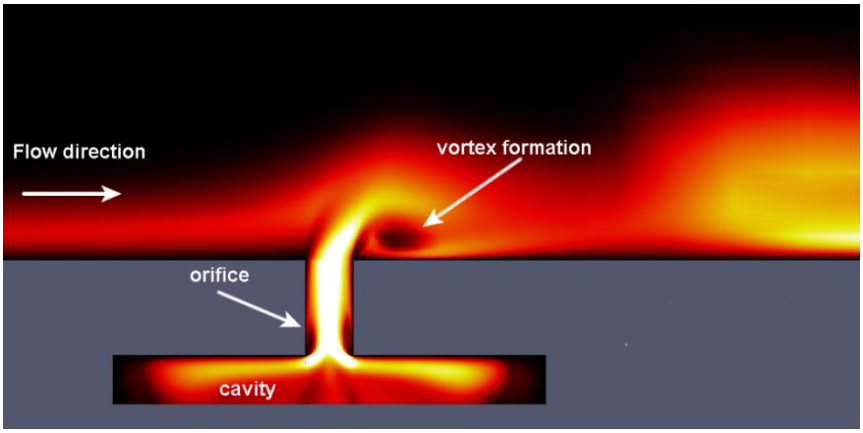

Figure 2.14 Synthetic jet in cross flow conditions [131].

The interaction between synthetic jets and an unconfined cross-flow was investigated by Glezer and Amitay [123]. They found that the interaction between synthetic jets and a cross-flow can induce recirculation regions at certain operating conditions. Their study was carried out at macro scale and at unconfined cross-flow.

An experimental work in the field of mixing with synthetic jets at low Reynolds numbers (Re=2) was recently carried out at the University of Manchester [132], [133]. The investigation consisted of the design and fabrication of a macromixer with multiple opposite synthetic jets operated in a confined cross-flow setting. The data reported in such a study suggest that it is possible to improve mixing at low Reynolds numbers (Re=2) to an extent of 90% mixing quality at certain operating conditions. Those operating conditions varied depending on the actuation frequency and amplitude of the synthetic jets. For example, if fast mixing is required, it is recommended that the synthetic jets should be operated with a Strouhal number of 3.2 (f=8 Hz), a stroke length of 2.0 (Δ_{pp}=0.2 mm) while driving the synthetic jets 180 degrees out-of-phase.

Nevertheless, such macromixers also have some issues: 1) the mixing quantification was taken at a relatively long distance from the mixing area. It was 14.5h downstream, where h is the channel height (h=8 mm). This leaves room to wonder if the mixing quality of the mixture decreases or remains the same at a shorter distance downstream.

On the other hand, mixing in a straight microchannel was studied by Mautner [130] in which he numerically investigated mixing in a confined cross-flow using synthetic jets. His data indicates that it is possible to perturb the fluids to enhance mixing using synthetic jets. Another numerical work considering a confined cross-flow is reported by Timchenko et al. [122]. This study suggests that it is possible to improve the heat transfer rate in a microsystem using a single synthetic jet placed transverse to a straight microchannel.

Due to the fact that there are not many investigations reported in the literature regarding micromixers with synthetic jets, we will discuss the previous two works [122], [130] in more detail next.

Mautner [130] numerically studied the possibility of using synthetic jets to enhance mixing in a straight microchannel. His study consisted of two synthetic jet configurations: 1) mixing with a single synthetic jet and 2) mixing with two staggered synthetic jets, see Figure 2.15. He carried out his study varying the cavity size,

diaphragm displacements and orifice dimensions of the synthetic jet micromixer in an effort to find the optimal geometry and operating condition to enhance mixing.

Mautner's results suggest that it is possible to perturb the flow with synthetic jets in a microchannel. The main fluid within the microchannel seemed to be considerably perturbed by actuating the synthetic jets. Furthermore, the actuation of the synthetic jets appears to trigger some recirculation zones along the microchannel as shown in Figure 2.15b.

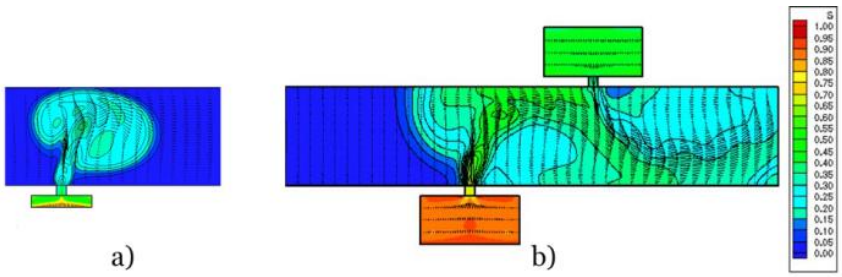

Figure 2.15 Concentration contours and velocity vectors for a) a single synthetic jet, b) two staggered synthetic jet, Re =10 [130].

However, there is an issue with the study carried out by Mautner [130]. The problem lies in the way he initialized the liquids to be mixed in his numerical domain. It does not represent a real scenario because he defined the whole microchannel with only one fluid (blue colour) and the synthetic jet cavities with another fluid, see Figure 2.15a. Furthermore, in the case of mixing with the staggered jet configuration (Figure 2.15b) the bottom cavity was defined with one fluid and with one concentration while the upper cavity was defined as a fully mixed mixture.

These considerations made by Mautnet [130] are only useful to visualize the flow pattern of the synthetic jets when they are actuated but do not represent a real scenario. In a real scenario, the liquids to mix should flow along each other through the main microchannel. Hence, the synthetic jet cavities should be filled with one of those fluids to mix but not with fully mixed fluid (mixture). Overall, we do not know if the synthetic jet micromixer investigated in [130] is able to reach a mixing degree of 90%.

Another numerical work considering synthetic jets in confined cross-flow is reported by Timchenko et al. [122]. The system investigated consists of a single synthetic jet located perpendicular to a main microchannel as shown in Figure 2.16. It is worth mentioning that has not mixing enhancement purpose but heat transfer enhancement. However, it is useful for reviewing the flow pattern produced in a cross-flow setting.

The authors claim that a significant improvement in heat transfer was achieved and the good performance of the cooling device was attributed to the formation of vortical structures not only inside the cavity but along the microchannel, as shown in Figure 2.17. An important factor to notice with this work is the possibility to generate vortical structures in a confined synthetic jet working in cross-flow. Although the Reynolds number (Re=125) and the operating frequency (f=10 KHz) of the synthetic jet membrane were relatively high for microfluidic applications, this synthetic jet arrangement could be useful to try to produce those vortical structures for enhancing mixing a micromixer.

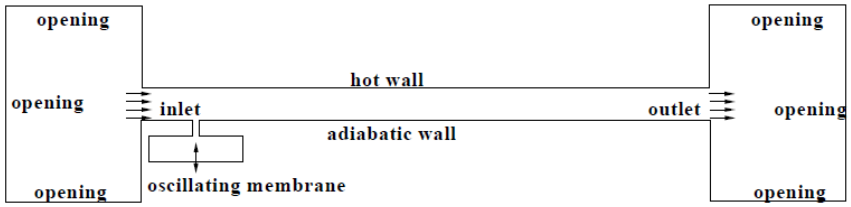

Figure 2.16 Synthetic jet arrangement for enhancing heat transfer [122].

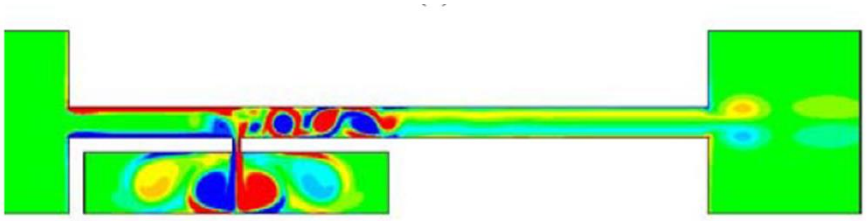

Figure 2.17 Vorticity contours of the cooling system at f=10 KHz, Δpp=42 μm, Re=125 [122].

2.5.1 Actuation methods to generate synthetic jets

The way to actuate a synthetic jet in microfluidics applications is not straightforward and it is mainly due to the micro scale. The most common techniques utilized to actuate synthetic jets are with oscillating membranes driven by electromagnetic [134] or piezoelectric actuators [135].

Regarding the electromagnetic method, it is mainly composed of a pair of permanent magnets and driving coils [134], as seen in Figure 2.18. The periodic displacement of the synthetic jet membrane is generated by an alternating signal which is

fed to the coils and then triggers the oscillation of the synthetic jet membrane. This periodic oscillation leads to the generation of synthetic jets.

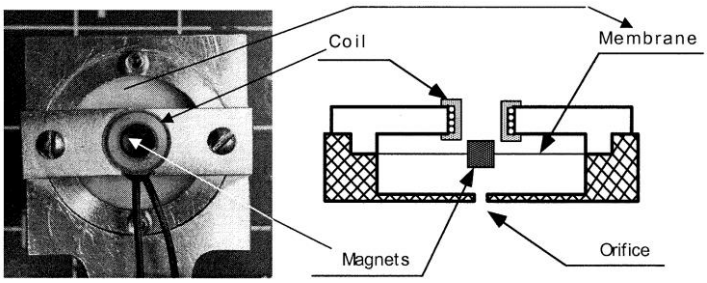

Figure 2.18. Electromagnetic actuator: a) Top view of the device, b) Main components [134].

Another method to actuate a synthetic jet membrane is by piezoelectric actuators [135]. A lateral view of a synthetic jet device using a piezoelectric actuator is displayed in Figure 2.19. The device consists of an elastic and impermeable membrane located at the bottom of the synthetic jet cavity and a piezoceramic disk bonded on the outside face of the membrane. Thus, the membrane is actuated up and down when the piezoactuator is activated, leading to the generation of synthetic jets.

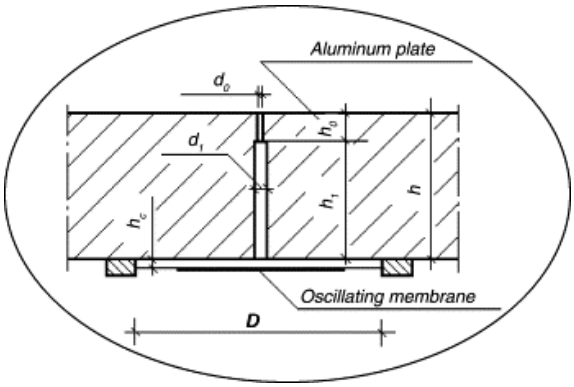

Figure 2.19 Synthetic jet actuated by a piezoelectric disk [135].

One of the restrictions of the previous actuating devices is their size, which are usually a few centimetres long. On the other hand, piezoelectric and electromechanical actuators can also be fabricated in smaller dimensions to fit the size requirements using MEMS technology [33]. However, the reduction in the dimension of the actuators also affects its force and displacement capacity. In most cases, the force and the displacement delivered by the actuators are not enough to operate a microdevice like a micropump [136]. Therefore, the size and the force of an actuator seem to be an important limitation to implement a micromixer with synthetic jets.

2.6 Mixing in multiphase flow

An alternative way for mixing miscible phases in a microfluidics device is by using the multiphase flow principle [49]. A multiphase flow refers to multiple fluid phases that are in contact with each other [49]. Regarding mixing, two miscible phases and one immiscible phase should compose the mixing system.

To characterise multiphase flows in microdevices, the dimensionless number known as the capillary number (Ca) is often used. The capillary number can be seen as the importance between the viscous forces and the interfacial forces that are present in a multiphase system in microfluidics [113]. Depending on the value of the capilarry number, the fluids contained inside a microchannel can experience different behaviour such as the formation of fluid droplets, slugs, stratified flows [113] or thin wetting films [49]. In the case of the formation of fluid droplets, it is considered a segmented flow and, according to Günther et al. [137], this effect can be used for mixing enhancement. The fast mixing in droplets is attributed to the fluid motion that the droplets experience while they are flowing along a microchannel.

A typical arrangement of a multiphase flow micromixer is shown in Figure 2.20 [37]. It consists of injecting the miscible phases (solute and solvent) in an immiscible phase (fluid carrier) to form a droplet and promote the mixing while driven downstream [37], [137]. The most common fluid carrier in microfluidics is oil and it is only used to transport the miscible phases [2], [37], [138], [139], [140].

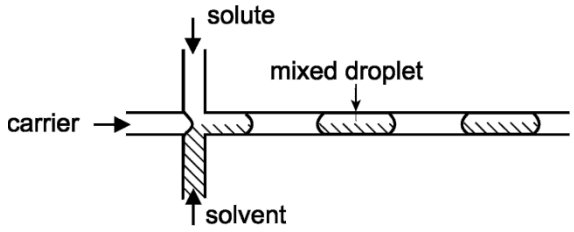

Figure 2.20 Micromixer arrangement based on multiphase flow [37].

However, this mixing technique is not very effective when a straight channel is used. Bringer et al. [140] show experimentally that poor mixing occurs in a droplet that flows along a straight microchannel, see Figure 2.21. They attributed such poor mixing to the steady and symmetrical flow pattern that a droplet suffers while flowing downstream. Such flow pattern was confirmed experimentally by Günther et al. [137],

who used the micro Particle Image Velocimetry (μPIV) technique to visualise the velocity profile in the droplet.

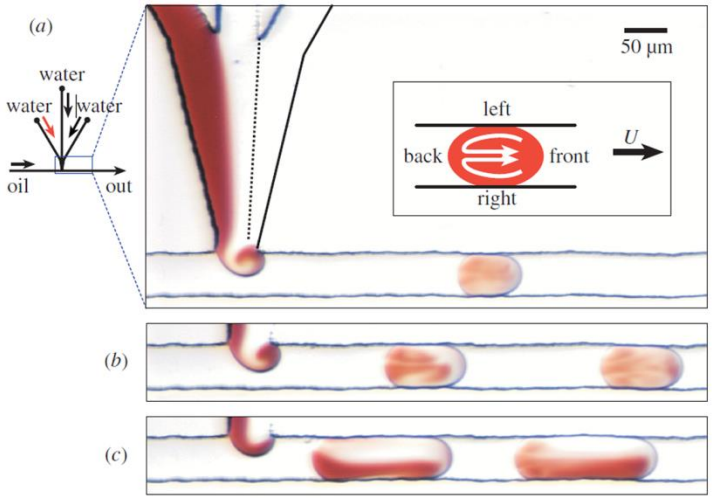

Figure 2.21 Mixing two miscible fluids in a droplet using a multiphase flow [140].

To address the issue of poor mixing in a droplet that flows through a straight microchannel, Song et al. [85] manufactured a wavy microchannel in an attempt to induce chaotic advection, as shown in Figure 2.22. This geometry change influences the flow patterns of the miscible phases to significantly enhance mixing [85], [37]. A slightly different approach was made by Liau et al. [141] using protuberances on the inner part of the serpentine microchannel to promote fast mixing in solutions with high proteins concentration.

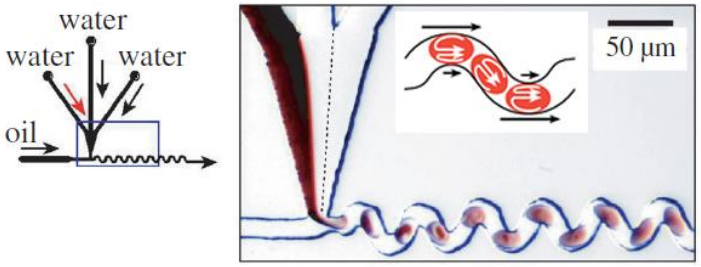

Figure 2.22 Mixing droplets in a wavy microchannel to promote chaotic advection [140].

Mixing using multiphase flow in microfluidic devices has been not widely investigated, [85], [137], [142], [143], [144], [145], due to the need of an additional process to separate the miscible phase from the immiscible. Furthermore, from the point of view of simplicity, most of the multiphase micromixers require a serpentine path and a relatively long distance to effectively mix the fluids of interest [85], [140].

Chapter 3

Numerical and Experimental Methodology

3.1 Introduction

In the previous chapter, we have reviewed the mixing mechanisms and techniques used to enhance mixing in microdevices. As we have seen, numerous techniques have been implemented in an attempt to overcome the problem of mixing in microdevices.

In this chapter, we describe the methodology followed to investigate the performance of the mixing devices proposed in this thesis. Such mixing devices are based on two different approaches: 1) mixing with synthetic jets and 2) mixing in multiphase flow.

The structure of this chapter consists of two main parts: 1) the numerical and experimental methodology considered to design, operate and analyse a macromixer, 2) the approach considered to numerically simulate a micromixer based on both the synthetic jet and the multiphase flow principle. In the first part, we explain the considerations made when designing a macromixer as well as the equipment used to operate it. Moreover, a dimensionless analysis is also presented to characterise the macro and micromixers with synthetic jets. The second part is focused on the settings

considered to simulate numerically the mixing of the macro and microdevices which are presented in Chapter 4, 5 and 6. Finally, the mesh sensitivity study and the validation of the numerical simulations are discussed.

3.2 Background of the synthetic jet micromixer

Regarding mixing with synthetic jets, we started off reviewing the possibility to manufacture a micromixer with a synthetic jet arrangement. Although the fabrication, assembly and operation of a micromixer is challenging at microscale, the major difficulty was to find a suitable actuator to operate it; an actuator of reduced cost and easy to control.

After a thorough search for an actuator to meet these requirements, none were found that fulfilled the specifications to implement it in a synthetic jet micromixer. The most promising were mainly based on the piezoelectric principle [146], but they have some limitations. For example, they only deliver a very short stroke length which is of paramount importance to create the synthetic jets in the micromixer. Moreover, to reach the maximum actuation displacement, the piezoactuators have to be operated with frequencies above 100 Hz. Another issue is their complex system of control which is more expensive than a piezoactuator. For instance, the cost of a piezoactuator can vary from £300 to £600 and an amplifier to actuate between £1000 and £1700, depending on the number of connexions (quotation in 2015) [146].

It was clear, therefore, that all these limitations are not in agreement with our aims, which are to design a low cost and a low energy consumption micromixer. These technical difficulties may be solved later when suitable and low cost actuators are available on the market. However, to asses a mixer with synthetic jets at Re=0.5, it was decided to fabricate a macromixer.

3.3 Considerations for the macromixer design

Before starting the fabrication of a macromixer, several numerical simulations were carried out to have a preliminary understanding of the mixing performance of the mixer design. The results of the simulations were promising in regards to mixing performances at Re=0.5, (see Chapter 4). That is why the manufacturing of such

macromixer was carried out. To perform such simulations, however, the geometry of the new mixer had to be defined first. As mentioned in Chapter 2, a previous macromixer design was manufactured in The University of Manchester [132] and it was considered a guide for a new macromixer design; a diagram of it is shown in Figure 3.1.

Some of the geometrical parameters of the mixer reported in [132] were kept the same. For example:

- The aspect ratio of the main channel is kept at 5.
- The dimensions of the orifice depth and width of the synthetic jet are kept at h/2; where h is the rectangular channel height (h=4 mm).
- The separation between synthetic jets (pitch) is at 2h.

Although these dimensions were kept constant, several improvements were also made in the new mixer design. One of them was regarding the synthetic jet cavity which was changed from a circular to a rectangular shape. With this change, we do not expect to have areas of unmixed fluids (dead zones) which were one of the issues of the mixer reported in [132]. Another modification was made at the channel inlets, which were perpendicular to the main channel and placed opposite to each other as shown in Figure 3.2. Furthermore, an asymmetric cavity was also considered in this mixer design in order to create liquid jets with different strengths.

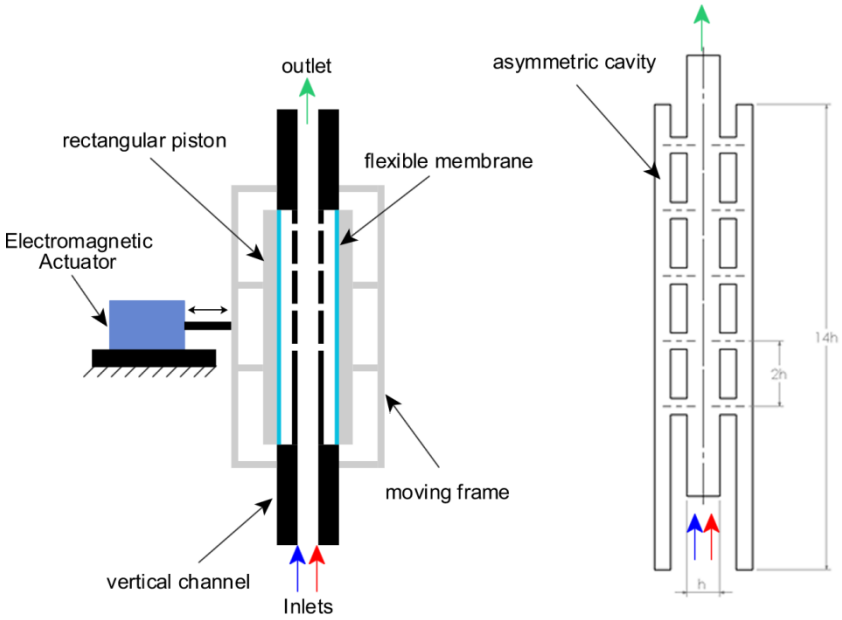

Figure 3.1 2D diagram of the macromixer with four pairs of opposite synthetic jets.

3.3.1 Construction of a macromixer

As was previously mentioned, numerical simulations were only carried out to have a preliminary understanding of the possible mixing performance of the synthetic jet macromixer. Once the preliminary simulations provided a notion of what to expect in a real scenario, a question arose related to the issue of how accurate the mixing performance of the macromixer was compared to reality? To answer this question, a test rig was built to perform the corresponding experiments.

3.3.2 Macromixer design and its components

To have a better understanding of the macromixer design, a 3D modelling was created with a Computer-Aided Design (CAD) software (Solidworks) [147], see Figure 3.2. The mixer design consisted of a vertical channel, a mixing area where the synthetic jets are located, two opposite inlets and a 90 degrees channel outlet. The vertical arrangement of this design was proposed to avoid the force of gravity interfering in the mixing process of the fluids. Hence, the fluids to be mixed should be pumped upwards from the bottom of the main channel and flowed along each other through it. The complete test rig including all its components is presented in Appendix A.

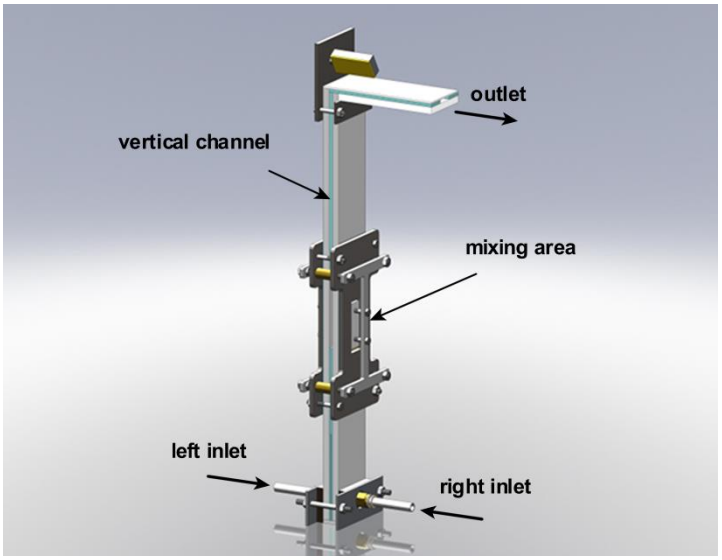

Figure 3.2 Final macromixer design with synthetic jets.

3.4 Mode of actuation of the synthetic jets

In order to create synthetic jets to enhance mixing, they had to be actuated by the pair of opposite pistons attached to a moving frame (see Figure 3.1). A simplified diagram of the macromixer is displayed in Figure 3.3 to illustrate this. The motion of the pistons is transmitted from an electromagnetic actuator by means of a moving frame, see Figure 3.1. The electromagnetic actuator was driven by means of a sinusoidal signal 180 degrees out of phase to create the synthetic jets. This sort of signal is often used to actuate synthetic jets [121], [122], [125], [148]. The control of the frequency and strength of the synthetic jets were achieved by controlling the peak-to-peak displacement (Δ_{pp}) and the actuation frequency on an electromagnetic actuator.

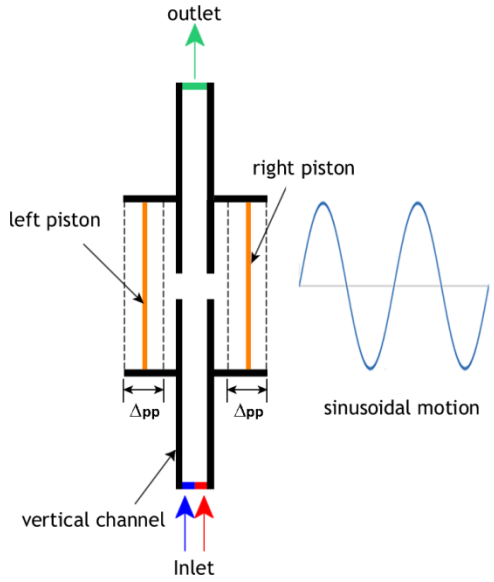

Figure 3.3 Diagram showing the piston configuration to generate synthetic jets.

A diagram of the whole macromixer arrangement is shown in Figure 3.4 and its working principle is as follows:

- The fluids to be mixed are stored in two separate containers.
- The fluids are pumped through the vertical channel by means of two gear pumps. The pumps are controlled by a power supply (not shown in Figure 3.4).
- Two flowmeters are installed before the channel inlets to visually monitor the flow rate.
- When the fluids leave the flowmeters, they flow towards the main vertical channel and hit an aluminium sheet, change their direction and flow downstream.

- After some time, the working fluids fill the whole channel and there is a clear distinction between the two fluids shown in the right corner in Figure 3.4.
- In order to enhance the mixing degree of the two parallel streams, the opposite rectangular pistons are actuated 180 degrees out-of-phase which area attached to a moving frame and actuated by an electromagnetic actuator. The out of phase actuation leads to the generation of synthetic jets within the rectangular channel.
- To get an alternative motion on the moving frame, the electromagnetic actuator is driven by means of a sinusoidal signal.
- The sinusoidal signal is controlled by means of a data-adquisition (DAQ) card and a LabVIEW interface.
- The mixing performance of the mixer is investigated by varying the displacement and the actuation frequency of the electromagnetic actuator systematically.

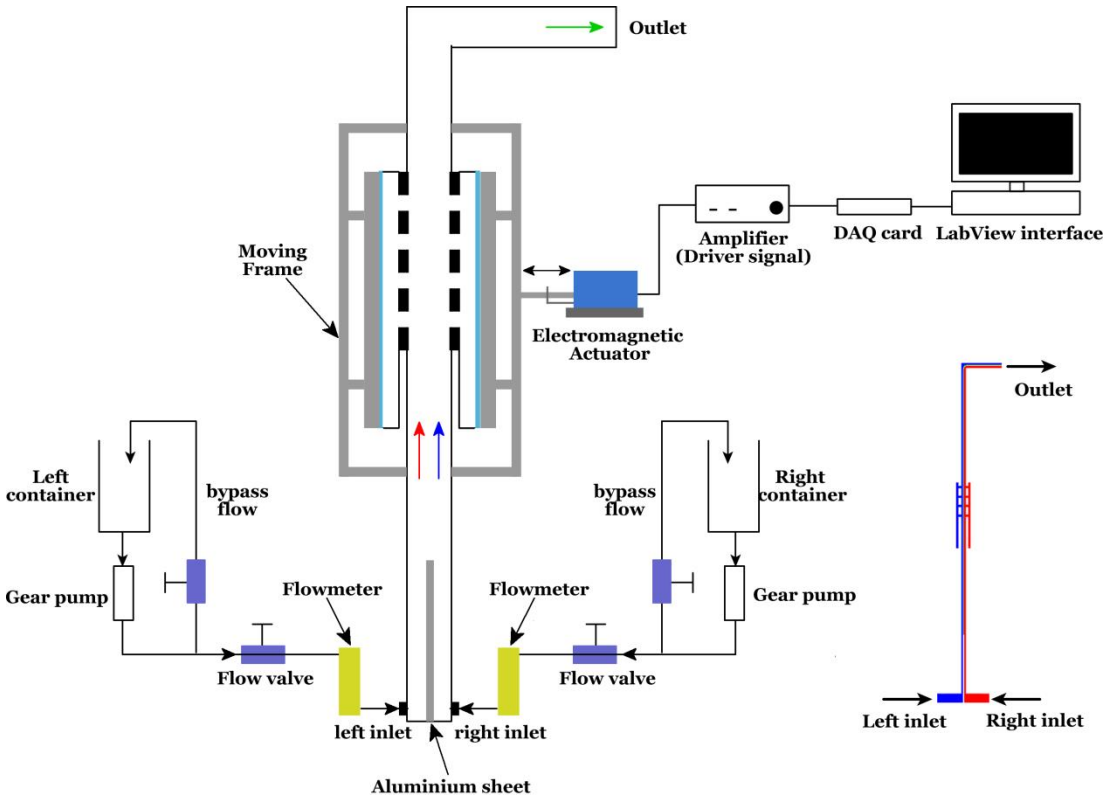

Figure 3.4 Diagram of the experimental set-up of the macromixer with four synthetic jets (not to scale).

3.5 Test rig

After the fabrication of the macromixer with four opposite synthetic jets (see Appendix A), we found out that it is very difficult to visualise the mixing process inside the rectangular channel. This difficulty was primarily due to the reduced area designated to visualise the mixing process; it was just 4 mm wide. The completed macromixer design is shown in Figure 3.5 which displays the area where visualising the mixing process was intended to take place.

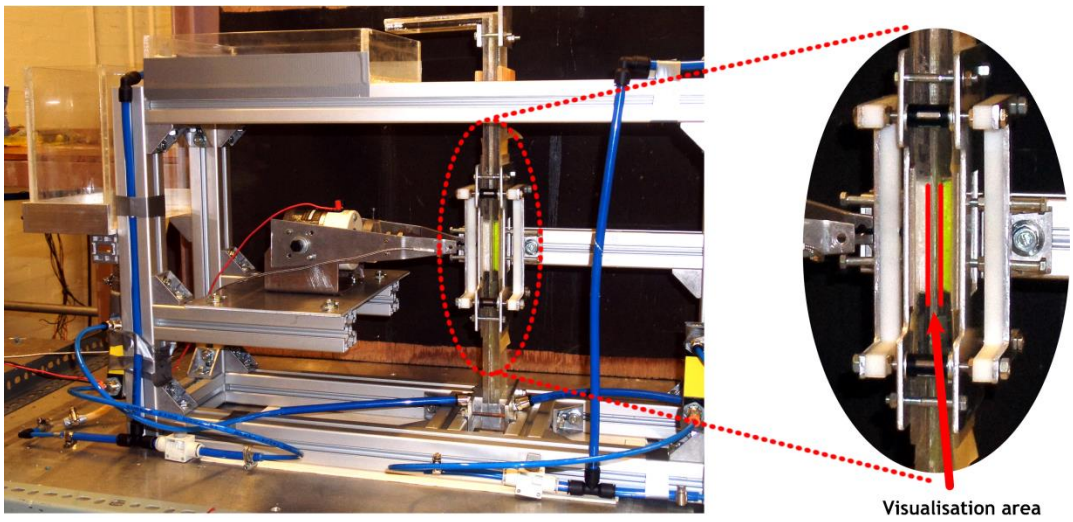

Figure 3.5 Lateral area of the macromixer designated for the visualisation of the mixing process.

One possibility to address the visualisation issue was to design and manufacture a larger macromixer. However, before doing this, the mixing performance of the macromixer was investigated by means of numerical simulations to assess its feasibility for mixing at Re=0.5, see Chapter 4.

3.6 Experimental settings

- **Selection and preparation of the working fluid**

Regarding mixing, we considered using a water-sugar solution for the working fluid in the experiments presented in this thesis. The reason for this was due to the fact that adding certain amounts of sugar to pure water can increase the dynamic viscosity of the solution. We should remember that we want to mix two liquids at Reynolds numbers below 1. Therefore, increasing the dynamic viscosity of the fluid makes the

desired Reynolds number easier to achieve. A concentration of sugar of 58.2% in water gives a dynamic viscosity of 0.050 Pa·s at 18 °C [149]. This dynamic viscosity is 50 times higher than the viscosity of water which is also appropriate to use to perform the mixing experiments in this thesis. Additionally, the concentration of sugar also modifies the fluid density of the working fluid to 1277 kg/m^3 [132], which is one of the parameters required to determine the Reynolds number.

- **Mixing visualisation**

As we utilised a working fluid constituted by sugar and water, the resulting solution was clear and transparent. It was evident that we needed to use a sort of tracer to visualise the mixing process. Therefore, we used two commercial water based paints to perform the visualisation the mixing process in the synthetic jet mixer. Reeves acrylic paint [150] with a medium yellow and cobalt blue colour was used to colour the working fluid. The paints are made of a high pigment concentration.

Once the viscosity of the water-sugar solution was ready, we proceeded to colour half of it yellow and the other half blue. Hence, this was the working fluid used to perform the experiments of the macromixer with one single synthetic jet (see Chapter 4, section 4.4).

The reason behind the use of the two different paints was because when the two colours mix (yellow and blue), they create a new colour (green), which indicates mixing. This mixing technique was used by Koch et al. [75] to characterize a micromixer based on pure diffusion. They utilized two commercial inks to study mixing in their micromixer device, claiming that this technique is simple and does not need any colour calibration because the colour change is only due to diffusion. Other techniques are based on measuring the colour intensity of fluorescent dyes [51], [91], [100], [151], [152], [153], or determining the amount of potential of hydrogen in the mixture (pH), [52], [75], [98], [154], [155].

3.7 Method for the quantification of mixing

In this thesis, mixing enhancement is investigated by means of numerical simulations and experiments. However, to know the quality of the final mixture we were required to quantify it. Therefore, as already mentioned in Chapter 2, section 2.2, the

most widely accepted method for the mixing quantification is by determining the variance of the concentration across the mixing channel.

- **Numerical simulations**

The mixing quantification method of the numerical results presented in this thesis is based on the determination of the variance of the concentration of one of the two fluids to be mixed [63], [92]. In the case of numerical simulations, the quantification of the mixing was performed by extracting all the values of the concentration of the mixture from each numerical cell at the desired location. These were used to determine the mixing degree of the mixture using equation (2.3). Hence, the fluid designated as dyed-water is selected to evaluate the mixing degree of the mixture. The variance of the concentration of the fluids to be mixed is then normalized by the mean value of the concentration ($\overline{c_i} = 0.5$) to define the mixing degree of the mixture is determined as:

$$MI = 1 - \frac{\sqrt{\frac{1}{n-1}\sum_{i=1}^{n}(c_i - \overline{c_i})^2}}{\overline{c_i}} \tag{3.1}$$

where c_i is the concentration of the selected sample, n is the number of samples analysed, *MI* is known as the degree of mixing of the mixture where: a value of 0 indicates no mixing and a value of 1 represents complete mixing.

As we already mentioned in Chapter 2, section 2.2, a mixing quality of 95% is considered to be a complete mixing in macromixers [58], [62]. However, in microfluidics a 90% mixing is considered to be a fully mixed mixture [63], [77], [85], [87], [90], [97], [44], [156]. Therefore, in this thesis a mixing degree of 90% will be considered as complete mixing.

- **Experiments**

To quantify the quality of the mixture in an experiment, we used the technique reported by Stroock et al. [13] which consists of determining the pixel intensity of an image which is then normalized to emulate the concentration of the fluids. This quantification technique is used in many other works [51], [157], [91], [100], [151], [152].

In order to quantify the mixing degree of the mixture from the experimental results, a Matlab [158] programme was coded to extract the pixel intensity of each image. The procedure considered was as follows:

1. An image is imported into the Matlab programme.

2. A horizontal line is drawn across the area of interest (using the computer mouse)

3. A plot containing the different colour intensities is automatically shown, see Figure 3.6b.

4. The Matlab program saved the value of such colour intensities in separate variables, which are named as Red-Green-Blue (RGB).

5. To quantify the pixel intensity of one colour, for example red (R), the pixel values were normalized with respect to the other two colours as:

$$c_i = \frac{R}{\sqrt{R^2 + G^2 + B^2}} \tag{3.2}$$

7. After the normalization of the colour intensity values, we can consider the pixel intensity as the concentration of one of the fluids to be mixed. Finally, those normalized pixel values are used to calculate the mixing degree of the mixture using equation (3.1).

To validate our Matlab programme, we used one experimental image reported in [133] (see Figure 3.6a), which displays the concentration contours of a tracer (Rhodamine B). The image was obtained with the planar laser-induced flourescence (PLIF) technique [159].

Therefore, we determined the mixing degree of the mixture at the same location as in [133] with our Matlab programme. A mixing degree of 0.4985 was quantified using equation (3.1) at that location. If a comparison is made with the mixing degree of 0.5 reported in [133], it gives a 0.1% difference which is in excellent agreement, giving us confidence in the technique. Therefore, we conclude that the Matlab programme is sufficiently accurate to quantify the mixing degree of the mixture in the experimental results.

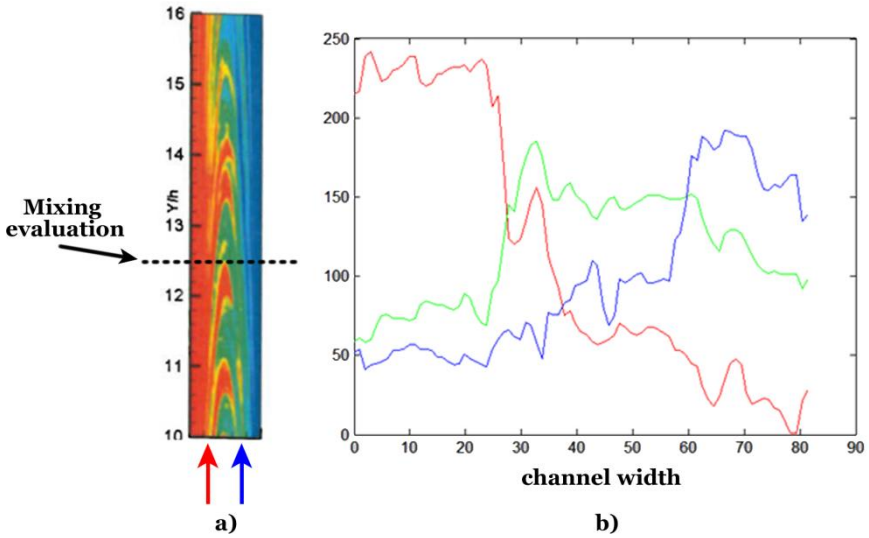

Figure 3.6 a) Concentration contours of a PLIF image [133], b) Pixel intensity at 12.5h.

3.8 Dimensionless study

There are many variables that could affect the mixing process. Variables like the frequency at which the synthetic jets are created, the viscosity of the working fluid, geometric parameters like the orifice depth and width and the cavity size, are all related to the performance of a synthetic jet mixer. Therefore, it is challenging to decide which variables are important and which ones are not. We cannot select all the variables that influence the mixing because the number of experiments and/or simulations could be considerable. Hence, we decided to analyse the synthetic jet mixer by making use of dimensionless numbers. This will help us to select only the critical dimensionless numbers that influence the mixing performance of the synthetic jet mixer. According to the theorem of Buckingham [110], [160], we first have to identify all the variables that are involved in the mixing system, which are:

- Average velocity in the main rectangular channel, U_m
- Flow velocity of the synthetic jets, U_j
- Width of the rectangular channel, W_c
- Height of the rectangular channel, h
- Diameter and width of the synthetic jet orifices d_0, d_w
- Dynamic viscosity, μ
- Density of the working fluid, ρ

- Actuation frequency of the synthetic jets, f
- Peak-to-peak actuation (amplitude), Δ_{pp}
- Diffusivity of the fluids, D
- The length that a jet travels after being expelled from the cavity, L_o

After considering all the previous variables, the mixing degree (MI) can be written as a function of them all:

$$MI = f(U_m, U_j, w_c, h, d_0, D_c, \mu, \rho, f, \Delta_{pp}, D, L_o) \tag{3.3}$$

If we select d_0, ρ, U_m as the variables to form the basic dimensions in the Buckingham's theorem, we have the following dimensionless parameters:

$$\pi_1 = \frac{\mu}{\frac{\rho d_o^{\,3}}{d_o\left(\frac{d_o}{\overline{U}_n}\right)}} = \frac{\mu}{\rho d_o \overline{U}_n} \quad (Reynolds\ number) \tag{3.4}$$

$$\pi_2 = \frac{\mathrm{D}}{\frac{d_o^{\,2}}{d_o / \overline{U}_n}} = \frac{D}{d_o \overline{U}_n} \quad (Peclet\ number) \tag{3.5}$$

$$\pi_3 = \frac{f}{\frac{1}{d_o / \overline{U}_n}} = \frac{f d_o}{\overline{U}_n} \quad (Strouhal\ number) \tag{3.6}$$

$$\pi_4 = \frac{L_o}{d_o} \quad (stroke\ length) \tag{3.7}$$

$$\pi_5 = \frac{h}{d_o} \quad (channel\ height\ and\ orifice\ ratio) \tag{3.8}$$

In a synthetic jet mixer, two Reynolds numbers are present: 1) The Reynolds number due to the main flow inside the channel and 2) the Reynolds number of the synthetic jet itself. Hence, the two Reynolds number can be determined with:

$$\mathrm{Re}_m = \frac{\rho h U_m}{\mu} \quad (Reynolds\ of\ the\ main\ flow) \tag{3.9}$$

where U_m is the velocity of the main flow inside the channel and

$$\mathrm{Re}_j = \frac{\rho d_0 U_j}{\mu} \quad \textit{(Reynolds number of the synthetic jet)} \tag{3.10}$$

where U_j is the velocity of the expelled synthetic jet.

Referring to the dimensionless number of the stroke length, equation (3.7), it can be re-defined using the synthetic jet velocity as:

$$L = \frac{L_0}{d_o} = \frac{U_j}{d_0 f} \tag{3.11}$$

The stroke length can be regarded as the strength of the liquid jets. It is also related to the distance that the synthetic jets can travel when they are expelled from the synthetic jet orifice.

Regarding the Strouhal number (Str), it is helpful to know the rate of the sequential segmentation of the mixing fluids. In other words, the distance between successive jets. It is mathematically represented as:

$$Str = \frac{f\, d_0}{U_m} \tag{3.12}$$

Therefore, we can conclude that the mixer could be characterised using the Reynolds number (Re), Péclet number (Pe), the stroke length (L) and the Strouhal number (Str).

3.9 Design of experiments

The mixing performance of a mixer with synthetic jets could be influenced by many variables. For example, the properties of the fluids, the geometry or the operating conditions. However, to identify the most influential variables regarding its mixing performance, a design of experiment (DOE) was considered.

A design of experiment could be defined as a plan to conduct a series of tests and then analysed them to obtain valid and objective conclusions [161]. The objective of a DOE is to uncover the most significant variables that influence the process of interest. Each process could be different from each other. That is why there are several types

DOEs. These are briefly reviewed next in order to select the most suitable for the mixing problem.

- **One factor design**

This is the simplest DOE type which tests one single factor or variable and its objective is to identify the significance of the selected factor with respect to the variable of interest [161]. For instance, if the actuation frequency is selected for improving the mixing performance of a mixer with synthetic jets, this could represent the single factor. Meanwhile, the variable of interest in the case of mixing could be the mixing quality. Nevertheless, this DOE design is not robust enough in most processes because it disregards other important variables and their interaction.

- **Factorial design**

This sort of design of experiment is used not only to test all the possible combinations between the variables of interest, but also their possible interaction. It consists of selecting the variables of interest and vary them all together. The advantage of the factorial design is that it could deal with several factors or variables of interest at the same time. However, if the number of factors is increased to more than four, the experiment becomes too large and could impact on its practical application [161].

- **Fractional factorial design**

The drawback of the factorial design is that when the number of factors increases, the number of tests also increases. For example, an experiment with 10 factors and two levels each will requires 1024 tests. This number of experiments is in most cases infeasible because its cost and time to perform them. There is where the fractional factorial design becomes useful. The fractional design could be seen as a fraction or sub set of tests taken from the whole factorial design [161]. However, caution has to be taken when selecting the array of experiments to have reliable results.

- **Response surface experiments**

This type of DOE, also known as Response Surface Methodology (RSM), is useful when the important factors have been already identified in a process. The

objective of the response surface experiments is to have a model to predict the relation between the factors and the response. This technique is helpful to find other operating conditions where the response variable is also achieved [162]. In other words, it is a method to optimise the operating conditions of the system of interest.

The RSM is most widely used in industrial processes where several input variables influence the response. It is not an uncommon feature in industrial processes to have more than one response variable. One good example where the RSM could be applied is in a process involving a chemical reaction. The reaction time and temperature could be the input variables and the rate of production and quality of the desired product could be the response variables [163].

After reviewing the DOE types, we concluded that a factorial design was the best option to test the mixing performance of the mixer with synthetic jets. The reason for this was because it is robust and considers the testing of all the combinations of the factors and their interaction. This is important due to their possible contribution to increase or decrease the mixing quality. However, the robustness of these methods also suggested a large number of experiments.

This concern indicated that the DOE selected (factorial) should be simplified somehow. One way of doing it was using a dimensional analysis to group variables in dimensionless numbers. After performing the corresponding dimensional analysis, it indicated that the mixer with synthetic jets could be investigated with five dimensionless numbers: the Reynolds number, the Péclet number, the stroke length, the Strouhal number and the ratio between the orifice and cavity of the synthetic jet device.

If we consider the five dimensionless numbers (factors) in our factorial DOE and then varied them within four levels, the DOE was still large enough and not very practical. Hence, a further simplification was required. The simplification was performed observing the variables contained in each dimensionless number. First, we decided to kept the Reynolds number constant (Re=0.5). This was due to the fact that in microfluidics the typical Reynolds numbers are between 0.1 and 1. With this assumption, the variables contained in the Re were also kept constant. Next, the Péclet number was maintained constant. This was considered because the typical diffusivity found in microfluidics ($D=10^{-11}$ m^2/s) remained constant during the mixing process. Another dimensional parameter found was the orifice-cavity ratio. In order to reduce the number of factors it was kept constant (fixed geometry). Therefore, the only two

dimensionless numbers left were the stroke length and the Strouhal number. These two parameters involved two important operating variables: the actuation amplitude and frequency of the synthetic jets.

3.10 Numerical simulation settings

To successfully simulate the macro and micromixers, several options need to be selected in the software. One of the most important is the selection of the correct numerical model or solver and the appropriate boundary conditions. In the next subsections we will address this.

3.10.1 Governing equations using ANSYS Fluent

To mathematically represent the fluid behaviour and its mixing process in the mixing devices, the working fluid in a macro and microchannel is assumed to be a continuum fluid system [2], [19]. Considering that the fluids to be mixed are Newtonian and incompressible [64], the set of governing equations to model such system are:

- **The continuity equation** [110]

$$\nabla \cdot \vec{V} = 0 \tag{3.13}$$

where $\vec{V}$ is the velocity vector.

- **The momentum equation** [110]

$$\frac{\rho D\vec{V}}{Dt} = -\nabla P + \mu \nabla^2 \vec{V} + \rho g \tag{3.14}$$

where ρ is the density of the working fluid, P the pressure in the system, μ the dynamic viscosity and g the accelelation due to gravity.

- **The species transport equation** [164]

$$\frac{Dc_i}{Dt} = \boldsymbol{D}\nabla^2 c_i \tag{3.15}$$

where c_i is the concentration of the species and $\boldsymbol{D}$ is the diffusivity constant of the specie to diffuse.

3.10.2 Numerical method to solve the governing equations

The governing equations of the macro and micromixers are difficult to solve analytically because they are non-linear partial differential equations [165]. Hence, numerical methods are frequently used to have approximate solutions.

To simulate the mixing process in a macro and micromixer numerically, the software Fluent version 14.0 from ANSYS [166] was used, which is based on the finite volume approach [165]. The model selected from the software to simulate the mixing of two different fluids was the *species transport model without chemical reactions* [167].

Options selected in the numerical simulation were:

- Both the *laminar* and the *species transport without chemical reaction* models were activated.
- Mixing is a time dependent problem. Hence, the transient option is considered.
- The *pressure-based solver* is selected due to the laminar flow regime (Re<2).
- The spatial discretization is set to *second order upwind scheme*.
- The transient formulation is left as default (*first order implicit*). This cannot be set to a higher order due to the sort of moving mesh used (layering moving mesh).
- *The simple scheme* is chosen as the solution method.
- The convergence criteria for the continuity, the convection-diffusion and the momentum equations are set as 10^{-6}. To reach such convergence criteria, a maximum number of 120 iterations per time steps are required.

3.10.2.1 Boundary conditions

The governing equations need to be solved within a fluid domain. Therefore, the fluid domain has to be enclosed using boundary conditions. Boundary conditions are very important to obtain correct solutions [168]. Every boundary condition used to simulate each type of mixer will be commented on its corresponding chapter. However, the boundary conditions to simulate the macro and micromixers with synthetic jets were similar which are:

- **Inlets**

A parabolic and well developed velocity profile is defined at the inlet of the mixing channel. It is set up in the software ANSYS Fluent with the help of a User-defined Function UDF (see Appendix B).

- **Outlet**

The *pressure outflow* boundary condition is selected at the channel outlet.

- **Static walls**

In terms of the static walls, the *non-slip* boundary condition is considered [165].

- **Moving wall**

To implement the moving wall boundaries and generate the synthetic jets, it was achieved by defining it using a UDF in the form of:

$$v(t) = \pi\left(\frac{\Delta}{2}\right) f \cos(2\pi ft) \tag{3.16}$$

where f is the oscillating frequency of the moving walls, t the time step and Δ_{pp} the peak-to-peak displacement. The boundary condition in the moving wall was using a sinusoidal motion, which is the most used in synthetic jet devices [121], [122], [125], [148].

- **Initial conditions (initialisation)**

In order to provide the initial conditions to start the numerical simulation, the fluid domain must be defined. Hence, it is initialised assuming that the two fluids flow along each other without significant mixing. According to this assumption, we define half of the domain as water and the other half as dyed-water. The initialisation is also coded using a UDF.

3.10.3 Governing equations using OpenFOAM 2.3.1

The governing equations required to numerically simulate the mixing process in a multiphase flow setting using OpenFOAM 2.3.1 are similar to the equation used in ANSYS Fluent and their mathematical representation is:

- **The continuity equation**

$$\Delta \cdot \vec{V}_m = 0 \tag{3.17}$$

- **The momentum equation**

$$\frac{\rho D\vec{V}_m}{Dt} = -\nabla P_m + \mu\nabla^2\vec{V}_m + \gamma + \rho g \tag{3.18}$$

- **The species transport equation**

$$\frac{Dc_i}{Dt} = \boldsymbol{D}\nabla^2 c_i \tag{3.19}$$

where the sub index m indicates mixture. We should remember that we have two miscible liquids and one immiscible, and each of them is governed by a continuity equation. The sum of them gives a final continuity equation. In the momentum equation, the term γ represents the surface tension force acting on the interface formed between the miscible and immiscible phases and in the transport equation, the term c_i is the concentration of the corresponding species and D is the diffusivity constant of the miscible phases.

These equations are very similar to the governing equations already discussed above. The only difference is that this time a multiphase flow is considered. Notice that the time term is included in every equation because the mixing process is time dependent. The concentration of the miscible phases change with time and the interface between the liquid-solid-gas also evolves with time. Therefore, to investigate the mixing process in the multiphase micromixer, time dependent numerical simulations have to be performed.

3.11 Mesh sensitivity study for the macromixer

The objective of performing a mesh sensitivity study is to make the results of the numerical simulations independent from the mesh density of the fluid domain. To do so, the velocity and the concentration of the fluid are the two variables considered in the mesh study. It is worth mentioning that the macromixer with four pair of synthetic jets was used to carry out the mesh sensitivity study.

To carry out the mesh sensitivity study, four different mesh sizes are considered, and are named: Mesh 16, 32, 64 and 128. The consideration to refine the mesh of the fluid domain was dividing the channel width into, for example, 16 equally spaced cells and then doubling it to refine the next mesh. Another important consideration regarding the mesh study was that all the mesh cases had a structural mesh configuration with an aspect ratio of 1 for each numerical cell.

The velocity profiles corresponding to the different mesh sizes tested are shown in Figure 3.7. The results indicate that the velocity profile designated as Mesh 16 did not match the rest of the velocity profiles. The discrepancy is attributed to the fact that such mesh was the coarsest mesh out of four. In contrast, the rest of the mesh sizes agreed very well with each other. Therefore, *Mesh 16* is discarded to perform the numerical simulations.

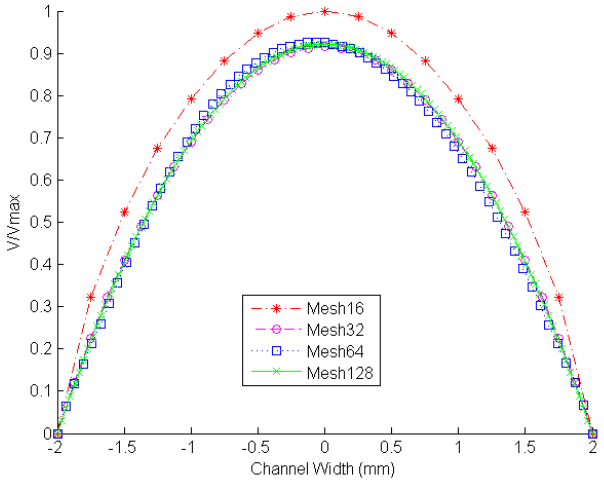

Figure 3.7 Velocity profile of the four mesh sizes considered: Mesh 16, 32, 64, 128.

The next variable considered to verify the mesh sensitivity is the concentration of the fluids to mix. The concentration of the fluid known as dyed-water is plotted after one oscillating cycle (t=0.5 seconds, f=2 Hz) for each mesh size. The concentration was measured at 4 mm from the last synthetic jet orifice downstream. The concentration profiles for each mesh size can be seen in Figure 3.8. The biggest variation is observed once more for Mesh 16 due to the poor mesh density. Regarding Mesh 32, a slight variation in the concentration profile is observed if it is compared with the finer meshes (Mesh 64 and Mesh 128). On the other hand, the concentration of dyed water of Mesh 64 and Mesh 128 seem to have a very similar pattern. Therefore, it is reasonable to select Mesh 64 for getting reliable numerical results.

After the selection of Mesh 64 for simulating the macromixer, a time step study was also carried out for that particular mesh. We have to remember that all the numerical simulations required to simulate a synthetic jet mixer have to include a *moving mesh*. In general, the time step is one parameter required to run numerical simulations

and it depends on several factors. In our case, it depends on the mesh size but it also depends on the velocity at which the mesh moves.

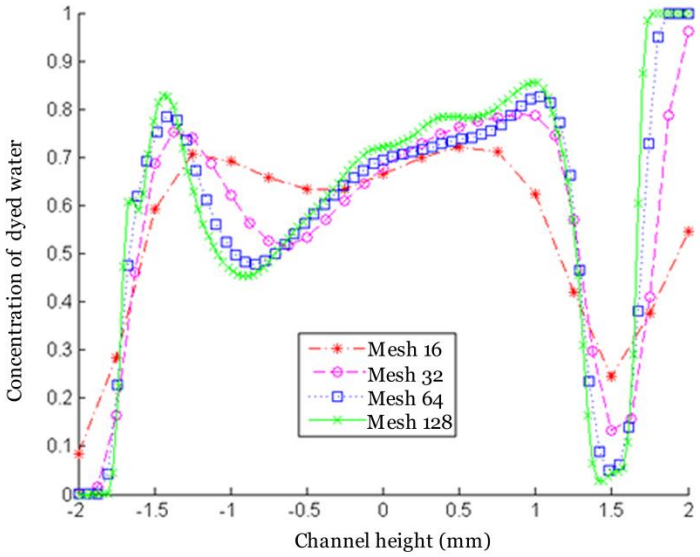

Figure 3.8 Concentration of the dyed-water phase of four different mesh sizes.

Having said this, three different time steps are tested to verify if the concentration profile is affected by it. The three time steps considered were at t = 0.001, 0.0005 and 0.00025 seconds and the concentration profiles are shown in Figure 3.9. We can observe that the mass fraction corresponding to t=0.0005 seconds agrees very well with t=0.00025 seconds. In contrast, a higher time step (t=0.001 seconds) showed a slight discrepancy when compared with the other time steps. Such difference is mainly evident in the middle of the concentration profile.

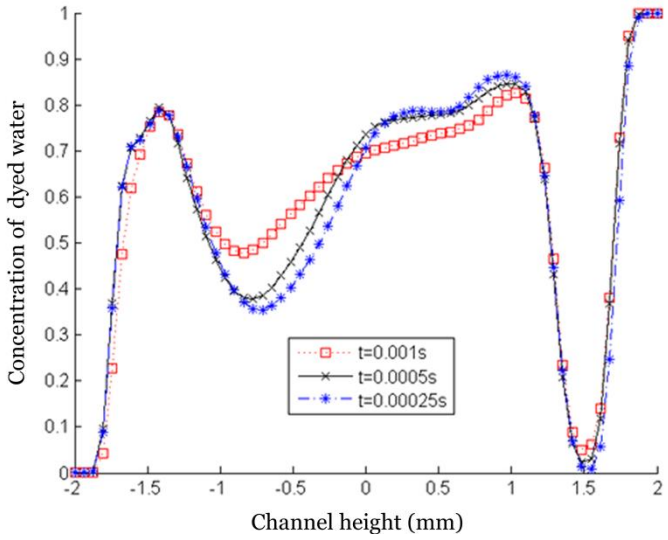

Figure 3.9 Concentration profile at three different time steps.

Therefore, based on the previous mesh sensitivity analysis, the most adequate mesh and time step to perform the numerical simulations of the macromixer is *Mesh 64* with a time step of 0.0005 seconds.

3.12 Micromixer settings

To numerically simulate a micromixer, we first need to set up the numerical case correctly and then validate it with experiments.

3.12.1 Set up and validation of the micromixer in ANSYS Fluent 14.0

Before carrying out the numerical simulation of the micromixer, the micromixer reported by Glasgow et al. [92] was numerically replicated. This was done to verify that the numerical simulation was set correctly. The reason for selecting such a micromixer case was because it also included an experiment which helped to validate the numerical simulation. Furthermore, it was also suitable because the Reynolds number was 0.3, which is a typical Reynolds number found in microfluidic devices, [1], [38], [39].

In Figure 3.10, the concentration of the fluids (numerical case performed in ANSYS Fluent 14.0) is visually compared with the concentration of the micromixer published in [92]. When we qualitatively compare our numerical case (Figure 3.10c) with the numerical case reported in [92] (Figure 3.10b), they agree very well. The concentration contours at the cross section also indicate a very similar distribution of the concentration in the liquids to be mixed. On the other hand, to properly validate those numerical simulations, they have to be compared with an experiment. Hence, Figure 3.10a shows the experimental results of the micromixer which prove that our numerical simulation is in good agreement. The fluid interface of the two fluids to be mixed is clearly seen in the experiment, which signifies that little mixing occurs at Re=0.3. The quantification of the mixing degree reported in [92] at 2 mm from the confluence is 0.12, while the mixing degree in the replicated case is 0.11, giving 8% difference. In other words, 6% less mixing is predicted in the replicated case. Therefore,

we conclude that the numerical settings selected to simulate the micromixer with synthetic jets was set correctly.

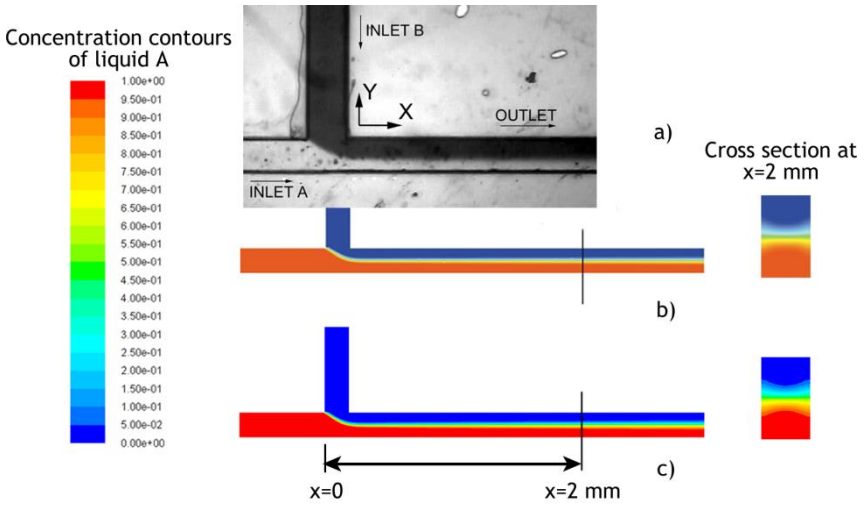

Figure 3.10 Comparison between experimental and simulating results: a) Experimental results of the case at Re=0.3, b) Concentration contours reported in [92], c). Replicated case to validate the settings of the numerical simulations.

The previous validation was performed just to be certain that the case was set up correctly. However, the mesh size used in reference [92] cannot be used for our micromixer case. The reason for this is because the dimensions of the cross-section of the microchannel studied in [92] and the one studied in this thesis are different. In the case of Glasgow et al. [92], the dimensions of the cross-section of the microchannel are 200 μm wide and 120 μm depth. In our case, however, the dimensions of all the micromixers studied in this thesis will be 350 μm wide and 175 μm depth. The last dimensions were considered because they were the ones used by Dolomite [169]. Therefore, because of these differences in dimensions, we also performed a mesh sensitivity study to simulate the micromixer with synthetic jets numerically.

3.12.2 Mesh sensitivity study for the micromixer

Regarding the mesh sensitivity study, a new mesh study was required to carry out the numerical simulations of the micromixer. The two variables considered to make the results independent of the mesh size were the velocity and the concentration of the fluid known as dyed water as in the macromixer mesh study. We also considered four different mesh sizes for the discretization of the fluid domain. Such mesh sizes were named: Mesh 4, Mesh 8, Mesh 16 and Mesh 32. These meshes are named according to the number of numerical cells contained in the cross section of the microchannel.

The results obtained regarding the velocity variable and the four mesh sizes tested are shown in Figure 3.11. We can observe that the less dense meshes, Mesh 4 and Mesh 8, indicate a dramatic discrepancy when they are compared with finer meshes (Mesh 16 and Mesh 32). In contrast, Mesh 16 and Mesh 32 were in good agreement with each other. The difference in the average velocity was about 1%. Therefore, we could use Mesh 16 or Mesh 32 to perform the numerical simulations. However, before making that decision, we have to look at the other variable of interest: the concentration of dyed water.

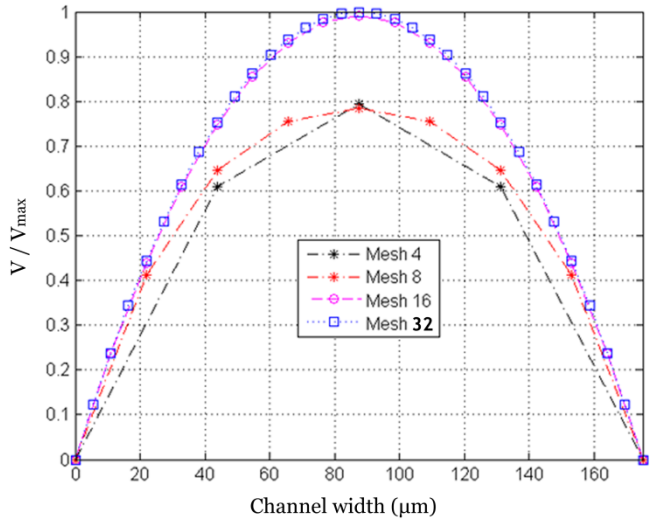

Figure 3.11 Velocity profiles of the four different mesh sizes tested.

The concentration profile of dyed water across the microchannel of the four mesh sizes tested is shown in Figure 3.12. We can see that Mesh 4 shows the greatest difference in the concentration profile when it is compared with the rest of the mesh sizes. Mesh 8 is in a relative good agreement with finer meshes but not its velocity profile, see Figure 3.11. The concentration profile of finer mesh sizes, Mesh 16 and Mesh 32, agree very well with each other; the difference is about 0.01%.

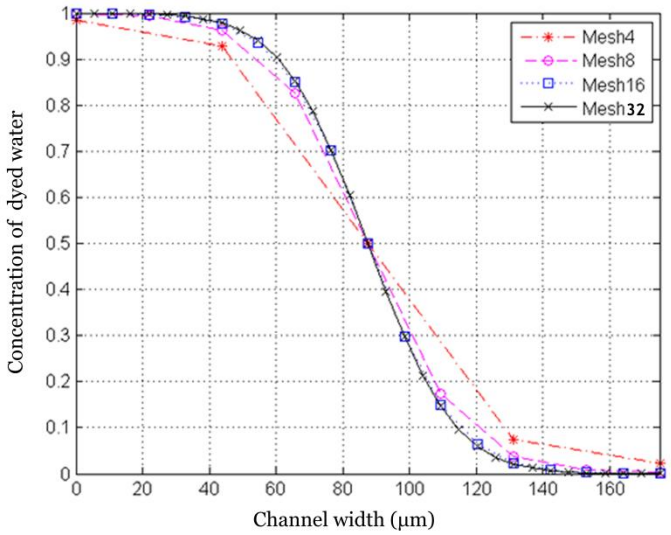

Figure 3.12 Concentration contours of dyed water across the microchannel for the four different mesh sizes tested.

According to the mesh study of the micromixer, the optimum mesh to perform the numerical simulations in ANSYS Fluent 14.0 is Mesh 16.

3.12.3 Simulation validation in OpenFOAM 2.3.1

The same work published in [92] was utilized to validate the software settings of the numerical simulations performed in OpenFOAM 2.3.1. Figure 3.13 shows the concentration in the T-micromixer reported in [92] and also the replicated simulation performed in OpenFOAM 2.3.1 (Figure 3.13c). A qualitative assessment of the replicated case shows that it corresponds well with the numerical simulation reported in [92]. The interface of the fluid is well defined downstream and mixing only takes place by molecular diffusion, as stated in [92]. If we look at both cross-sections of the microchannel, the concentration distribution appears to be quite similar in both cases after 2 mm from the confluence of the fluids. The quantification of the mixing degree at 2 mm from the fluid confluence is 0.13, which is about 8% higher than the 0.12 reported by Glasgow et al. [92]

The relatively good agreement between the replicated and the numerical simulation reported in [92] give us confidence that the numerical case is set correctly. Additionally, the micromixer simulated in OpenFOAM 2.3.1 involves a multiphase flow where the fluid interphase between the liquid and gas phase is tracked with time. Hence, the finest mesh of the previous mesh study (mesh 32) will be used in all the numerical

simulations. The reason for this is because it will give better resolution of the liquid-gas interface.

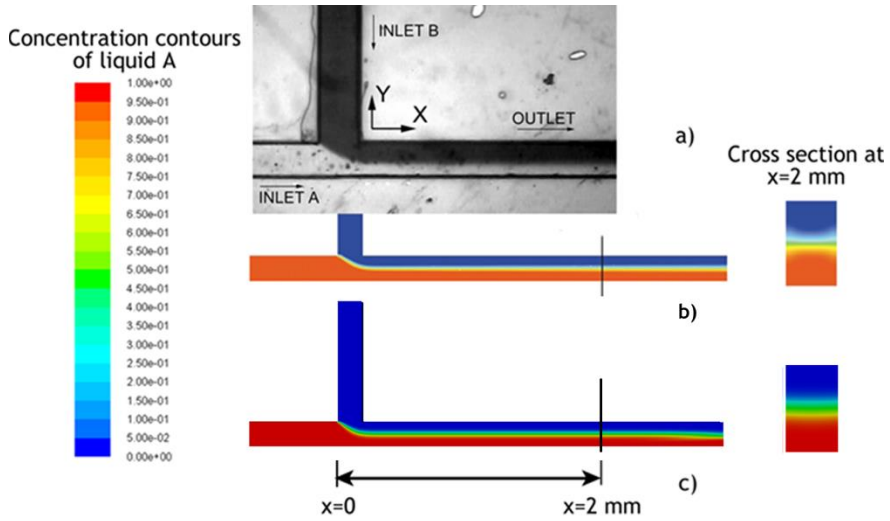

Figure 3.13 Concentration of the liquids to mix in a T-micromixer, a) Experiment [92], b) Simulation reported in [92] and c) Replicated simulation performed in OpenFOAM 2.3.1.

Chapter 4

Mixing with Synthetic Jets

4.1 Introduction

In Chapter 2, we reviewed not only the mechanisms for improving mixing in microfluidic devices, but also the mixing techniques and micromixer designs currently proposed to improve mixing. Additionally, the limitations of those micromixer devices were also highlighted.

In this chapter, an investigation of the mixing performance of a micromixer with synthetic jets was conducted. The practical implementation of a micromixer with synthetic jet was not a simple matter because of the reduced length scale (micrometres). Issues such as the type of actuator to drive the synthetic jets, the difficulty to place the piston at certain distance for the synthetic jet orifice, sealing of a flexible membrane located between the piston and the working fluid and the system of control to actuate the pistons to generate the synthetic jets were all major limitations of a synthetic jet micromixer.

However, since the mixing performance of such device is currently of interest, an alternative method was proposed to investigate the effect of synthetic jets on mixing at low Re. The approach considered was to fabricate a scaled up micromixer device (macromixer) with dimensions of the order of a few centimetres rather than micrometres.

The first approach was using a macromixer which consisted of four opposite synthetic jets. This was considered because it was believed that having an array of synthetic jets could enhance mixing in a great extent. Nevertheless, that mixer design consisted of a complicated geometry which involved numerous components. The design did not allow the visualization of the mixing process in a practical setting. In an attempt to address that issue, the project progressed proposing a second alternative which consisted in the reduction of the number of synthetic jets from four to two. The excellent mixing performance of that macromixer suggested that it was possible to simplify the mixer with four pairs of synthetic jets. However, the whole design was very close to the previous macromixer (four synthetic jets), which meant that it was challenging to observe the mixing process in a practical scenario.

The third option to tackle the mixing process consisted of the redesign of the whole macromixer. The main changes were made in the channel orientation (from vertical to horizontal) and the reduction of the number of synthetic jets to just one pair of opposite jets. The proposed mixer design was first studied using numerical simulations. Once the mixing performance reached the desired quality, it was then manufactured. The fabrication, assembly and tests of the mixer were carried out to validate its effectiveness in a real scenario. The project continued scaling down the macromixer to a typical micromixer size. Interestingly, the poor mixing performance of the scaled micromixer showed that it was not possible to design a micromixer from a macro point of view. This issue was addressed in the last section of the chapter, making a modification to the micromixer with synthetic jets which enabled it to deliver the mixing target of 90% set in the objectives of the project.

4.2 Mixing with a macromixer with four opposite synthetic jets

To start our study, we designed a macromixer with four opposite jets, taking into account a previous work reported by Xia [133] who suggests that a macromixer with three opposite jets can effectively mix liquid samples at Re=2. Therefore, we proposed to increase the number of synthetic jets to four pairs in an attempt to enhance

mixing at even lower Reynolds numbers found in microfluidic applications (Re<1) [1], [37], [38], [39], [40].

4.2.1 Definition of the problem

Consider the macromixer system illustrated in Figure 4.1. It consists of one vertical and rectangular channel and a mixing area where synthetic jets are implemented. The liquids to be mixed are pumped through the channel by means of two opposite inlets located at its lower extremity Figure 4.1a. They flow upwards passing through the area where the synthetic jets are located and then continue flowing to the channel outlet. At low Reynolds numbers, (Re<2), in the absence of the actuation of the synthetic jets the fluids flow alongside each other through the channel without a significant mixing, as shown in Figure 4.1a.

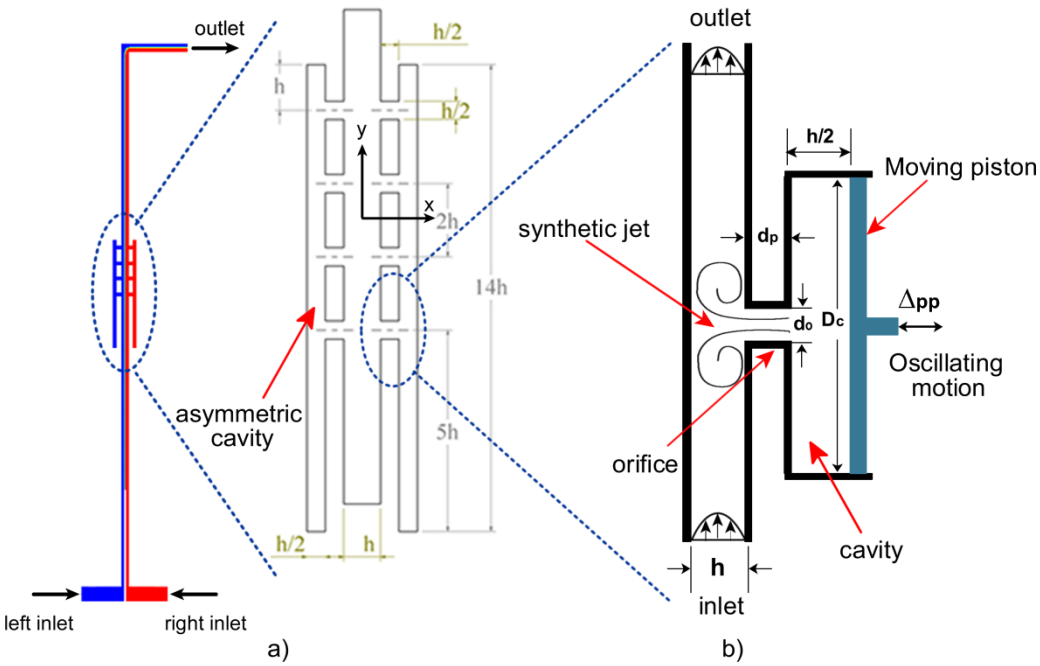

Figure 4.1 Macromixer with four opposite jets: a) Dimensions of the mixing area, b) Synthetic jet in a cross-flow setting (not to scale).

The dimensions of the cross section of the rectangular channel are 4 mm high (h) and 20 mm wide (w), giving an aspect ratio of 5. The synthetic jet orifice depth d_p is $h/2$ and its diameter d_0 is 2.5 mm, as shown in Figure 4.1b. The synthetic jet orifices are extended along the main channel width and can be considered slots rather than orifices. The separation between the synthetic jet orifices is 2h. This last dimension is

based on previous numerical simulations carried out by the author of this thesis, which suggests that the optimal orifice separation is 2h to avoid the synthetic jets interfering with each other. It is important to highlight that the cavities are much smaller than in [133] and their shape is rectangular and not circular but with an asymmetric setting. With this design we expect to avoid possible unmixed fluid due to the difference in shape of a cavity and piston as considered in [133].

What we want to achieve with the synthetic jet mixer is to enhance mixing at low Reynolds numbers (Re=0.5). However, as we have determined in Chapter 3, mixing with a mixer with synthetic jets depends on two main variables: the actuation frequency and amplitude of the actuator. These variables are directly related to the dimensionless numbers of the Strouhal number and the stroke length. To investigate the effect that these dimensionless numbers have on the mixing of the samples, an independent variation will be carried out.

As we mentioned in Chapter 3, section 3.5, the fabricated test rig presented some technical difficulties regarding the visualisation of the mixing process inside the channel. Nevertheless, the investigation of the mixing performance of the macromixer was performed using numerical simulations.

- **Stroke length**

In the case of the stroke length, it was varied from 0.88 up to 3.52 with an increment of 0.88, as shown in Table 4.1. The only parameter varied to obtain those stroke length values was the peak-to-peak displacement (Δ_{pp}) of the actuating pistons, which was varied from 0.5 mm to 2.0 mm in steps of 0.5 mm. Notice that the Strouhal number was kept constant, Str=0.33 (f=1 Hz), to avoid any possible influence on the mixing performance caused by it.

Table 4.1 Variation of the Stroke length keeping the Strouhal number constant.

Actuation displacement Δ_{pp} (mm)	**Stroke length (L)**	**Strouhal number (Str)**
0.5	0.88	0.33 (f=1 Hz)
1.0	1.76	0.33
1.5	2.64	0.33
2.0	3.52	0.33

- **Strouhal number**

Regarding the Strouhal number, it was varied in a similar manner. It was increased from 0.33 to 3.66 in steps of 0.33, while keeping the stroke length constant to 0.88, as shown in Table 4.2. The range of Strouhal numbers tested corresponds to the range of actuation frequencies between 1 to 10 Hz in steps of 1 Hz.

Table 4.2 Strouhal number tested keeping the stroke length constant.

Strouhal number (Str)	**Stroke Length (L)**
0.33 (f=1Hz)	0.88 (Δ=0.5 mm)
0.66 (f=2Hz)	0.88
0.99 (f=3Hz)	0.88
1.32 (f=4Hz)	0.88
1.65 (f=5Hz)	0.88
1.98 (f=6Hz)	0.88
2.31 (f=7Hz)	0.88
2.64 (f=8Hz)	0.88
2.97 (f=9Hz)	0.88
3.30 (f=10Hz)	0.88

4.2.2 Numerical simulations

In order to numerically simulate the macromixer with four synthetic jet orifices, appropriate boundary conditions should be defined to the computational domain which are indicated in Figure 4.2. The boundary conditions are: 1) two inlets from which the two liquids to be mixed are pumped, 2) one single channel outlet 3) two moving walls which are actuated along the x co-ordinate to create the synthetic jets and 4) the rest of the fluid domain is considered as static walls.

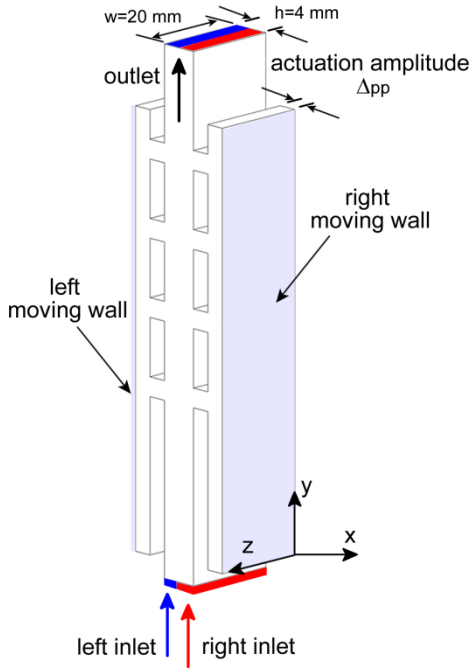

Figure 4.2 Fluid domain configuration of the macromixer with four synthetic jets.

In order to simulate the fluids as close as possible to the fluid conditions found in microfluidic devices, we will consider a typical value of diffusivity. The diffusivity is a very important parameter to consider in the numerical simulations, its importance is because at high diffusivities mixing becomes easier than at low diffusivities. Unfortunately, this is not the case in microfluidic devices where typical diffusivity values of the liquid samples are $D=10^{-10}$ and $D=10^{-12}$ m^2/s [49], [71], [157], [113].

In our case, we will consider a diffusivity of 10^{-10} m^2/s which is considered as the diffusion average of small proteins in many Bio-microelectro-mechanical systems (BioMEMS) [92], [115].

The validation of the numerical simulation was performed as discussed in Chapter 3. A mesh sensitivity study was also carried out due to the change in dimensions of the computational domain and it was considered to make the mesh density independent to the variables of interest (velocity and concentration).

The numerical simulation of the 3D domain is considerable expensive in terms of computational time and resources. To verify that the numerical simulations were numerically symmetric and avoid performing simulations in 3D, a single case was simulated with an actuation frequency and amplitude of 8 Hz and 2 mm, respectively. The results of this case are shown in Figure 4.3. Three surface planes along the main

mixing channel indicate qualitatively that the concentration contours are symmetric across the rectangular channel. Therefore, we assumed that the flow is symmetric across the macromixer channel and proceeded to perform 2D numerical simulations to investigate the mixing performance of the macromixer. It is worth mentioning that this consideration reduced the computational time by 15%.

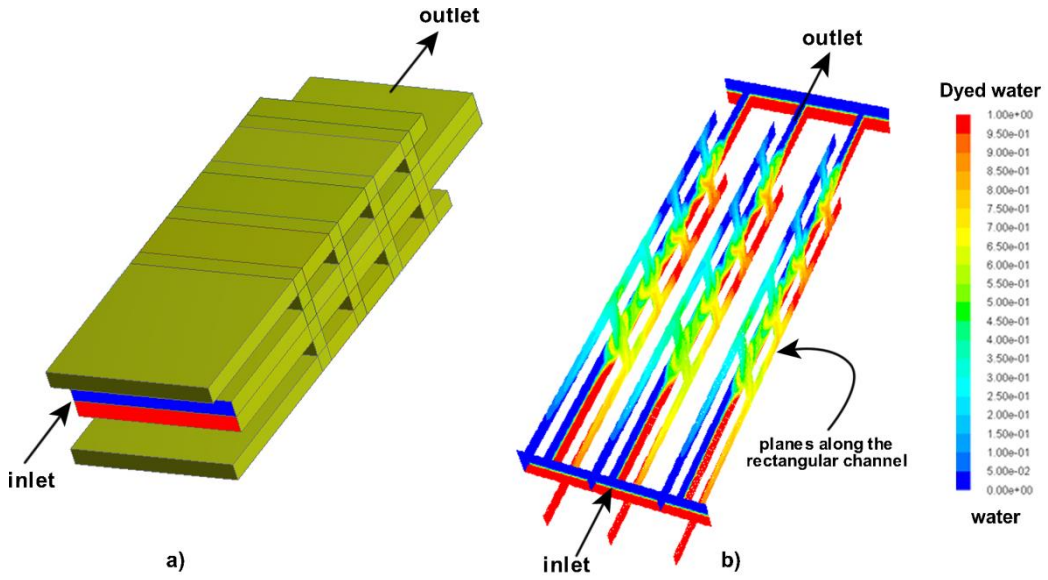

Figure 4.3 Symmetric flow in the numerical domain of the mixer with four opposite synthetic jets, Re=0.5, f=8 Hz, Δpp=2 mm.

4.2.3 The effect of the stroke length on mixing

In order to investigate the effect that the stroke length has on the liquids to mix, we proposed to investigate it by considering the systematic variation shown in Table 4.2. This study consisted of varying the actuation displacement of the moving walls while the actuation frequency was kept constant to 1 Hz. The outcome of the study at 6 seconds of mixing time is presented in Figure 4.4.

Overall, the stroke length study showed that the mixing of dyed-water and water is enhanced when the stroke length is increased from 0.88 to 3.52. For example, the mixing degree was significantly improved at L=2.64 and L=3.52 which is indicated by the green colour code along the channel. Interestingly, mixing seems to occur only along the main channel and not inside the synthetic jet cavities at low stroke lengths (L=0.88 and L=1.76). This effect leads to a lower rate of stretching and folding of the fluid interface, which is ultimately the main mechanism for enhancing mixing. Another interesting observation was that the vortical structures, which are characteristic of

synthetic jets, are not yet seen in any of the instantaneous pictures displayed in Figure 4.4. Mixing enhancement appears to take place due to the constant and alternative segmentation of the fluid interface along the main channel.

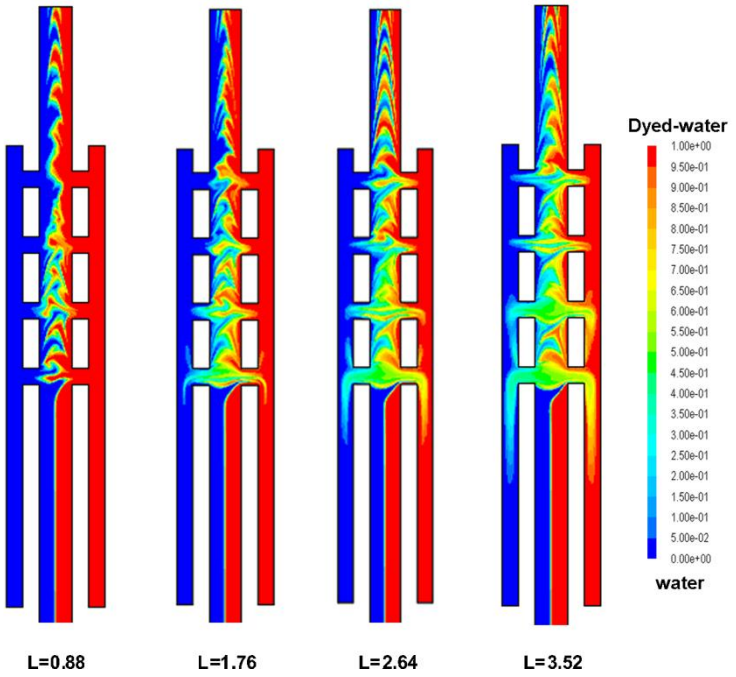

Figure 4.4 Concentration gradients of the stroke length study after 6 seconds of mixing time (t=6T), Str=0.33 (f=1Hz), Re=0.5.

4.2.4 The effect of the Strouhal number on mixing

We will now investigate the effect that the Strouhal number (Str) has on the fluids to mix. The systematic variation of the Strouhal number was performed as shown in Table 4.2. This time the Strouhal number was varied from Str=0.33 to Str=3.33 in steps of 0.33 while maintaining the stroke length to its minimum value (L=0.88). The instantaneous concentration contours are shown in Figure 4.5 at t=6 s.

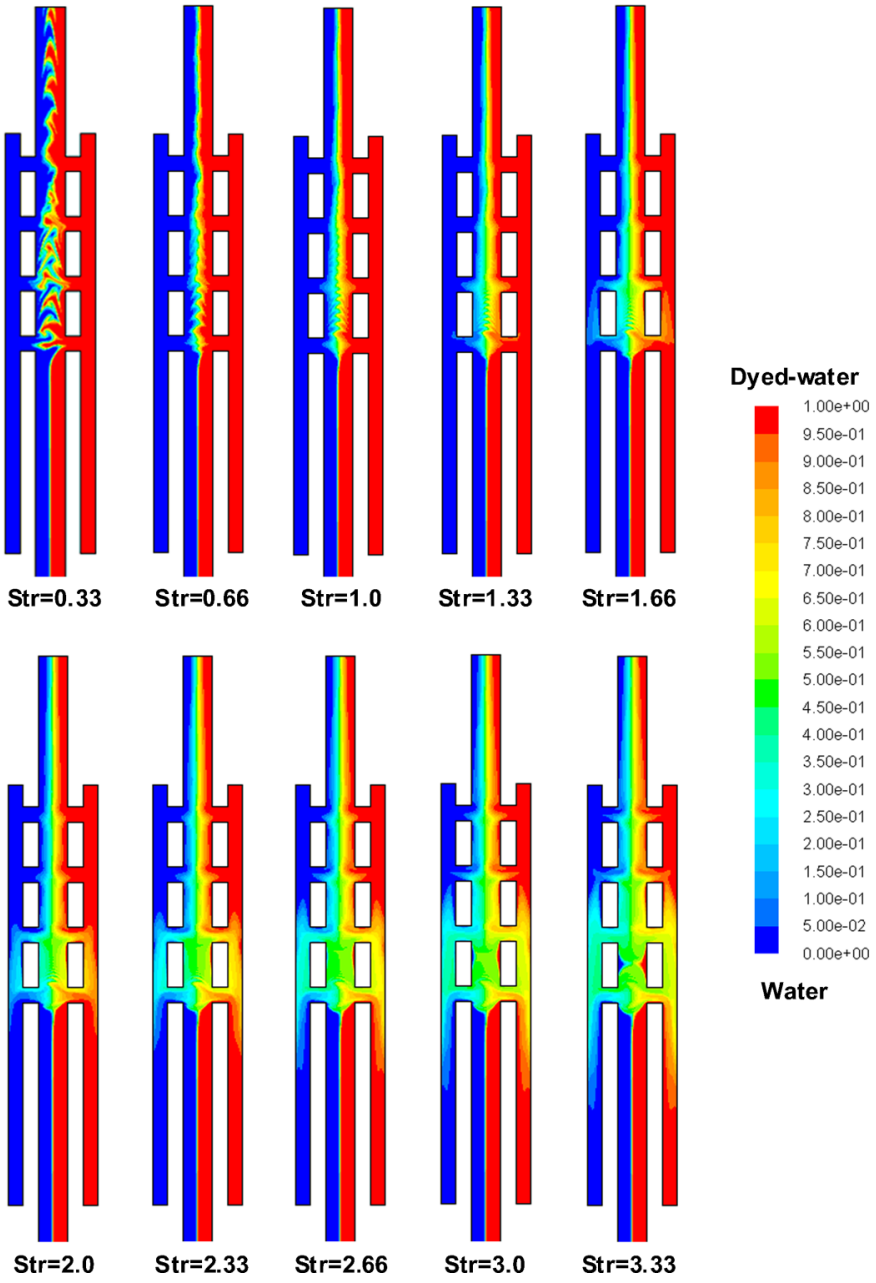

Figure 4.5 Concentration gradients for the Strouhal number study after 6 seconds of mixing time, L=0.88 (Δpp=0.5 mm), Re=0.5.

In general, we can state that increasing the Strouhal number from 0.33 to 3.33 has a significant effect on the mixing of the fluids. This was evident in most of the cases where the Strouhal numbers was above 1.6 (f=5 Hz). Concentrations close to a value of 0.5 (green), not only along the main channel but also inside the synthetic jet cavities suggests that mixing enhancement took place. An interesting result is at Str=0.33, where the fluid interface is considerably stretched and folded in the first two synthetic jet

orifices. This is mainly caused by the different strengths of the liquid jets due to the asymmetric cavities. However, when the Strouhal numbers was increased above a value of 0.66, such segmentation effects were less significant along the channel outlet.

As a summary we can say that increasing the Strouhal number had a remarkable effect on the mixing of the liquid samples, especially for Strouhal numbers above 2.0. Mixing enhancement mainly occurred along the main channel, however, unmixed fluid still remained inside the synthetic jet cavities, even at the highest Strouhal number tested (Str=3.33). Those unmixed fluids are injected to the already mixed samples in the main channel and may influence the final quality of the mixture.

4.2.5 Mixing quantification

To evaluate how well the macromixer performed with four opposite synthetic jets, the concentration of one of the fluids was quantified in the way discussed in Chapter 3, section 3.7. The mixing degree was determined by considering a time-average of five different images within one oscillating cycle. The location at which the concentration was determined is shown in Figure 4.6. It was at just one channel height (h=4 mm) after the last synthetic jet orifice downstream. The reason for quantifying the mixing quality of the mixture is because short distance is a desired characteristic of any mixer design in microfluidic applications [4], [8], [9].

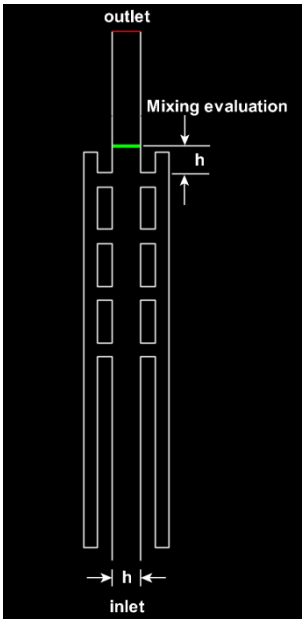

Figure 4.6 Location at which the mixing degree was measured (one h downstream from the last synthetic jet orifice).

4.2.5.1 The effect of the stroke length on mixing

In order to investigate how the mixing degree of the mixture changed while varying the stroke length, we proceeded to quantify it within the 6-7 seconds of mixing time. The mixing degree results as a function of the stroke length is displayed in Figure 4.7. Overall, it can be seen that increasing the stroke length has an important effect on improving the mixing degree of the mixture. The most significant improvement of the mixing degree was at L=3.52, reaching a mixing degree of 0.30 or 30% mixing quality. Interestingly, this corresponds to the maximum actuation amplitude tested (Δ_{pp}=2.0 mm). However, it was just 2.3% above the next lowest stroke length (L=2.64). Lower values of stroke length show poor mixing degrees, which are mainly attributed to the lower rate of stretching and folding of the fluid interface.

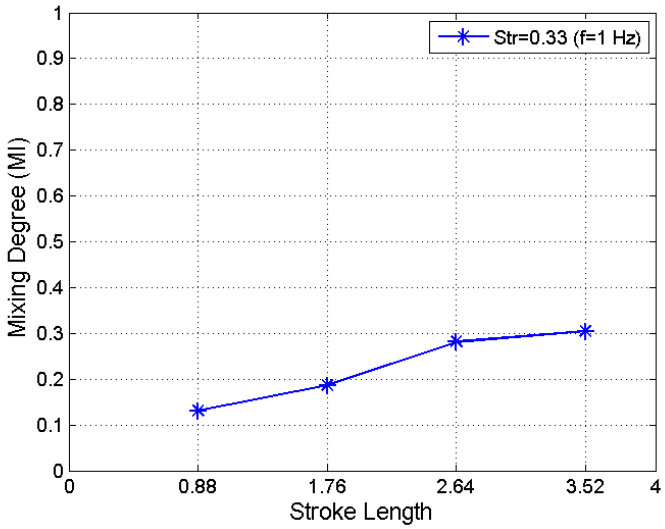

Figure 4.7 Time averaged of the mixing degree for the four stroke lengths tested, Str=0.33, Re=0.5, t=6-7 seconds.

4.2.5.2 The effect of the Strouhal number on mixing

To have quantitative data of how the Strouhal number influences the mixing degree of the mixture, we continue with its quantification at the same location and mixing time as the stroke length study. Figure 4.8 shows how the mixing degree evolved while increasing the Strouhal number from 0.33 to 3.33 in steps of 0.33. It shows that the mixing degree rises sharply while increasing the Strouhal number from 0.66 to 3.3. The mixing improvement is about 4-5% for each case tested. The maximum mixing degree measured was 0.43 or 43%, which corresponds to a Str=3.33 (f=10 Hz). In other

words, the maximum mixing degree was reached at the maximum actuation frequency (f=10 Hz).

An interesting result is the one corresponding to Str=0.33 (f=1 Hz). In this particular case, the mixing degree seemed to be very close to the value of the Str=0.66 (f=2 Hz). This can be attributed to the considerable segmentation of its fluid interface, as can be seen in Figure 4.5.

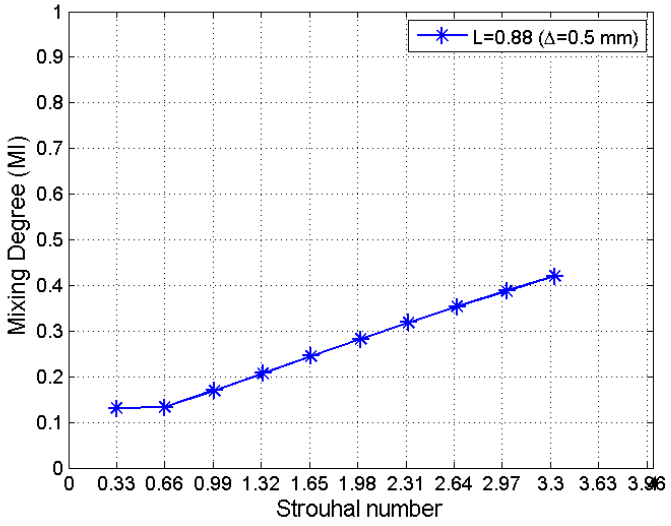

Figure 4.8 Time averaged of the mixing degree varying the Strouhal number, L=0.88, Re=0.5 t=6-7 seconds.

4.2.5.3 Varying the stroke length and the Strouhal number

In the previous two sections, we have studied the influence that the two dimensionless numbers, the stroke length and the Strouhal number, have on the mixing degree of the mixture. The findings suggested that it is possible to enhance mixing by either increasing the stroke length or the Strouhal number. However, varying only one of those dimensionless numbers and keeping the other at its minimum value did not lead to the mixing degree target of 0.90, which is considered as an acceptable mixture quality in microfluidic applications, see Chapter 2, section 2.2.

In order to reach that mixing degree target, we proposed to further explore the working conditions of the synthetic jet mixer. To do this, we will keep the four stroke lengths considered in Table 4.1 but vary the Strouhal number from 0.66 to 3.33 in steps of 0.66 (f=2 Hz). The mixing degree of such a variation is graphically displayed in

Figure 4.9. Overall, it shows that increasing the Strouhal number and the stroke length at the same time has a remarkable impact on the mixing degree. With these results, we can identify the operating conditions at which the mixing degree is equal to 0.9 or 90%. Hence, the best operating condition is at L=3.52 (Δ=2 mm) and Str=2.64 (f=8 Hz), where the mixing degree is 0.93 or 93% of mixing quality. The criterion of selecting this operating condition was based on the energy consumption to reach a mixing degree of 0.9. Although a mixing degree above 0.90 was also reached at Str=3.30 (f=10 Hz), it required operating the mixer 2 Hz higher than at Str=5.64 (f=8 Hz). A more detail explanation of the energy consumption issue will be addressed later on this chapter.

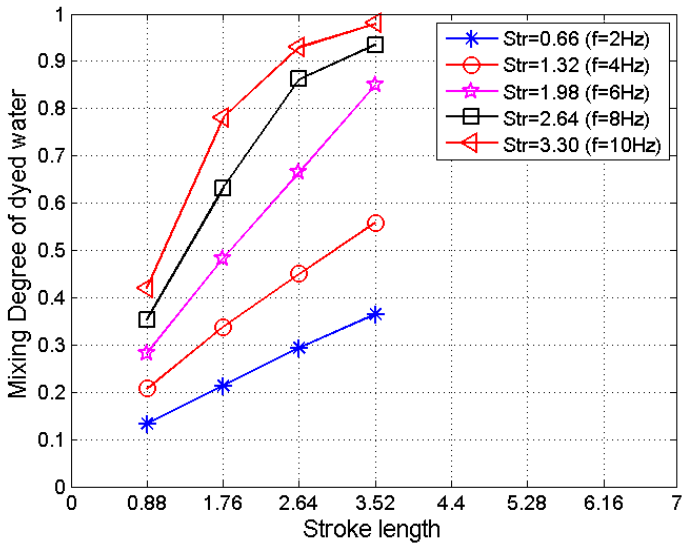

Figure 4.9 Variation for the Strouhal number and the stroke length, Re=0.5, t=6-7 seconds.

4.2.5.4 Time sequence of the optimal operation condition

Once we have found the best operating condition of the mixer to reach the mixing quality of 90%, we will investigate how the mixing process takes place within the mixing channel and how the flow pattern evolved with the synthetic jets. Therefore, we selected this optimal operating condition and looked at its concentration gradients at an early stage of the mixing process. Figure 4.10 shows a time sequence of the concentration contours of this mixing condition. We can see that at t=0.1 s, the fluid interface was considerably stretched and folded inside the mixing channel and in the left cavity. Another observation is that the liquid jets stretched the fluid interface at different

length due to the asymmetric cavities. A similar flow pattern was observed in the opposite cavity at t=0.15 s.

The continuous and alternative actuation of the synthetic jets significantly enhanced the mixing of the two liquids at Re=0.5 and the mixing time required to reach a 90% mixing degree at the selected location was 7 seconds, as shown in Figure 4.10. Interestingly, the homogeneous mixing of the fluids is evident in the whole fluid domain which suggests that complete mixing took place.

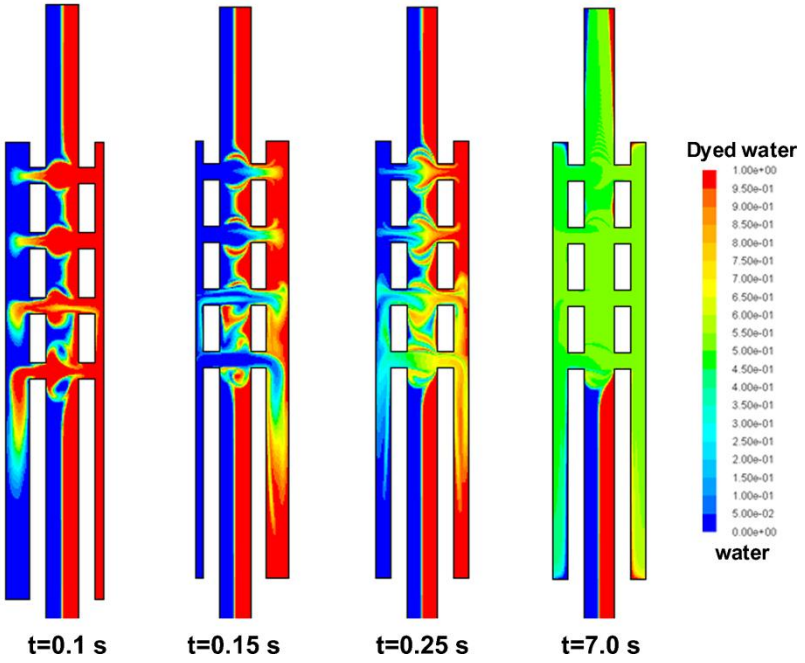

Figure 4.10 Time sequence of the concentration at L=3.52 (Δpp=2 mm) and Str=2.64 (f=8Hz), Re=0.5.

4.2.6 Improving the macromixer

The results of the macromixer with four opposite pairs of synthetic jets discussed above are very promising for enhancing mixing liquids at low Reynolds numbers (Re<1). We have demonstrated numerically that the synthetic jet principle significantly enhances the mixing of liquids at Re=0.5. The relatively short distance downstream required to mix effectively the liquid samples was one of the most interesting features of the macromixer design. Moreover, the asymmetric synthetic jet cavity also played an important role in enhancing mixing due to the variation in the strength of the liquid jets. This effect considerably stretched and folded the fluid interface, which enhanced the mixing degree significantly. All these characteristics make

this mixer design a potential alternative for mixing liquids at low Reynolds numbers, particularly at Re<1.

However, if this macromixer design is intended to be fabricated in a microscale, the relatively large volume could be a concern for microfluidic devices. Another difficulty could be the complicated geometry of such a macromixer design, which may increase its cost if it is manufactured. These issues could be overcome if the macromixer geometry is simplified by reducing the number of synthetic jets and the cavities size. Therefore, in the next section, a macromixer with two pairs of opposite synthetic jets and shorter cavities is investigated numerically.

4.3 Mixer with two pairs of opposite orifices

After analysing a mixer with four opposite synthetic jets and finding that it is possible to mix liquids at Reynolds numbers of 0.5, we now wish to know if it is possible to design a mixer with just two pairs of synthetic jets but maintaining the excellent mixing performance of the previous design.

4.3.1 Definition of the problem

Consider the macromixer configuration shown in Figure 4.11. The mixer is composed of two pair of synthetic jets opposite to each other and one pair of symmetric synthetic jet cavities. The rest of the dimensions and features of the macromixer design were kept the same as the previous macromixer. The configuration of this macromixer and its dimensions are displayed in Figure 4.11.

It is important to mention that for a better comparison between the previous macromixer and the present macromixer, we considered keeping the same operating conditions such as the actuation amplitude, frequency, the diffusivity value of the species to mix ($D=10^{-10}$ m^2/s) and Re=0.5.

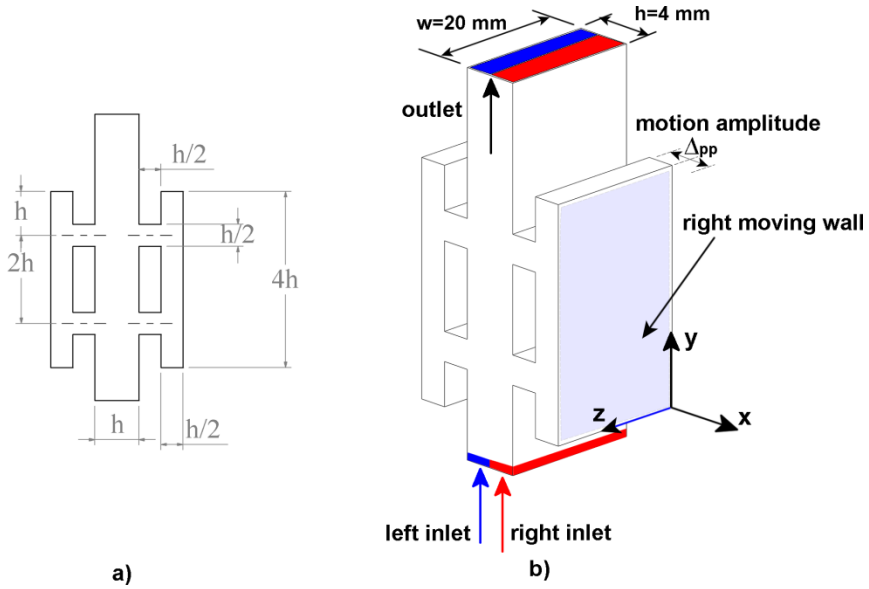

Figure 4.11 Mixer with two pairs of opposite jets. a) Lateral view and dimensions, b) Isometric view of the mixer with its inlet configuration.

To investigate the performance of the present mixer, we propose to analyse it in the same way as before, varying the actuation displacement from 0.5 to 2.0 mm in

steps of 0.5 and the actuation frequencies from 1 to 10 Hz in steps of 1 Hz. The independent variation produced different values for the stroke length and Strouhal numbers because of the reduced cavity size implemented in the present macromixer.

The stroke length will be the first independent variation considered to analyse this macromixer. Table 4.3 shows the range of stroke lengths while keeping the Strouhal number constant.

Table 4.3 Stroke length study keeping the Strouhal number constant.

Displacement Δ_{pp} (mm)	**Stroke length (L)**	**Strouhal number (Str)**
0.5	0.25	1.33 (f=1 Hz)
1.0	0.50	1.33
1.5	0.75	1.33
2.0	1.0	1.33

A similar approach was considered as in the previous mixer regarding the Strouhal number study. The Strouhal number was varied from 1.33 to 13.33 in steps of 1.33, as shown in Table 4.4, while the stroke length was kept constant to 0.25.

Table 4.4 Strouhal number study keeping the stroke length constant to its minimum value tested.

Strouhal number (Str)	**Stroke Length (L)**
1.33 (f=1 Hz)	0.25 (Δ=0.5 mm)
2.66 (f=2 Hz)	0.25
4.0 (f=3 Hz)	0.25
5.33 (f=4 Hz)	0.25
6.66 (f=5 Hz)	0.25
7.98 (f=6 Hz)	0.25
9.33 (f=7 Hz)	0.25
10.66 (f=8 Hz)	0.25
12.0 (f=9 Hz)	0.25
13.33 (f=10 Hz)	0.25

4.3.2 The effect of the stroke length on mixing

To show the stroke length effect on the mixing of the macromixer with two opposite synthetic jets, the corresponding numerical simulations were performed. The concentration contours are shown in Figure 4.12 after 6 seconds of mixing time. It

shows that increasing the stroke length significantly improves the segmentation of the fluid interface, which enhanced mixing. Notice that the fluid interface was enlarged considerably when the stroke length was L=1.0 (Δ_{pp}=1.0 mm). Interestingly, the apparent mixing only took place along the main channel and not within the synthetic jet cavities. This feature may be due to the low values of the stroke length, in other words, to the weakness of the liquid jets at this operation condition. Overall, we conclude that increasing the stroke length of the liquid jets helped to improve the mixing of the two liquid samples in this macromixer.

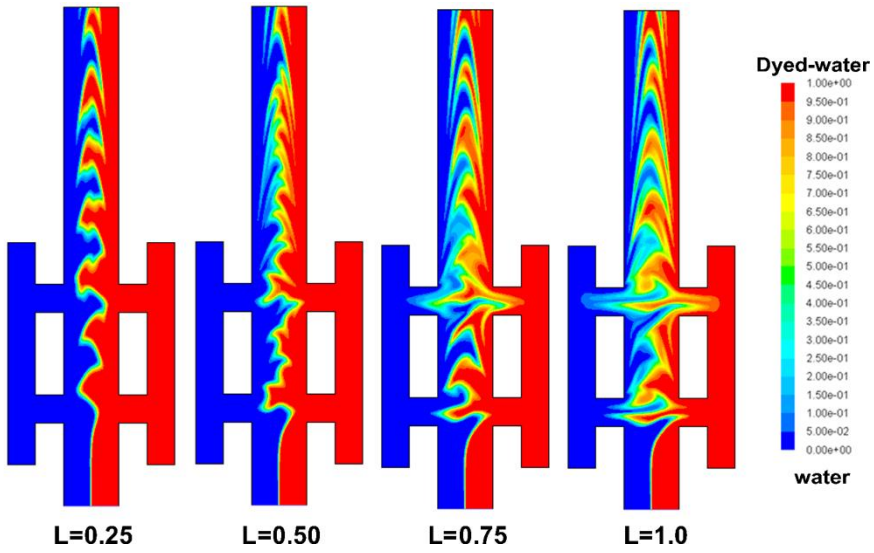

Figure 4.12 Stroke length study at Str=1.33 (f=1 Hz), Re=0.5, t=6 seconds.

4.3.3 The effect of the Strouhal number on mixing

In order to investigate the effect that the Strouhal number has on the mixing of the liquids, the numerical simulations mentioned in Table 4.4 were carried out. The Strouhal number was varied from 1.33 to 13.33 in steps of 1.33 while the stroke length was kept constant (L=0.25). Overall, the concentration gradients of the mixture suggest that increasing the Strouhal number has a significant effect on improving mixing. Mixing seems to increase along the main channel when increasing the actuation frequency of the synthetic jets. Interestingly, an unexpected result was found at Str=1.33 (f=1 Hz), where the fluid interface was remarkably stretched and folded by the jet liquids. This segmented fluid interface is attributed to the low actuation frequency. However, mixing is not uniform as in the rest of the cases considered.

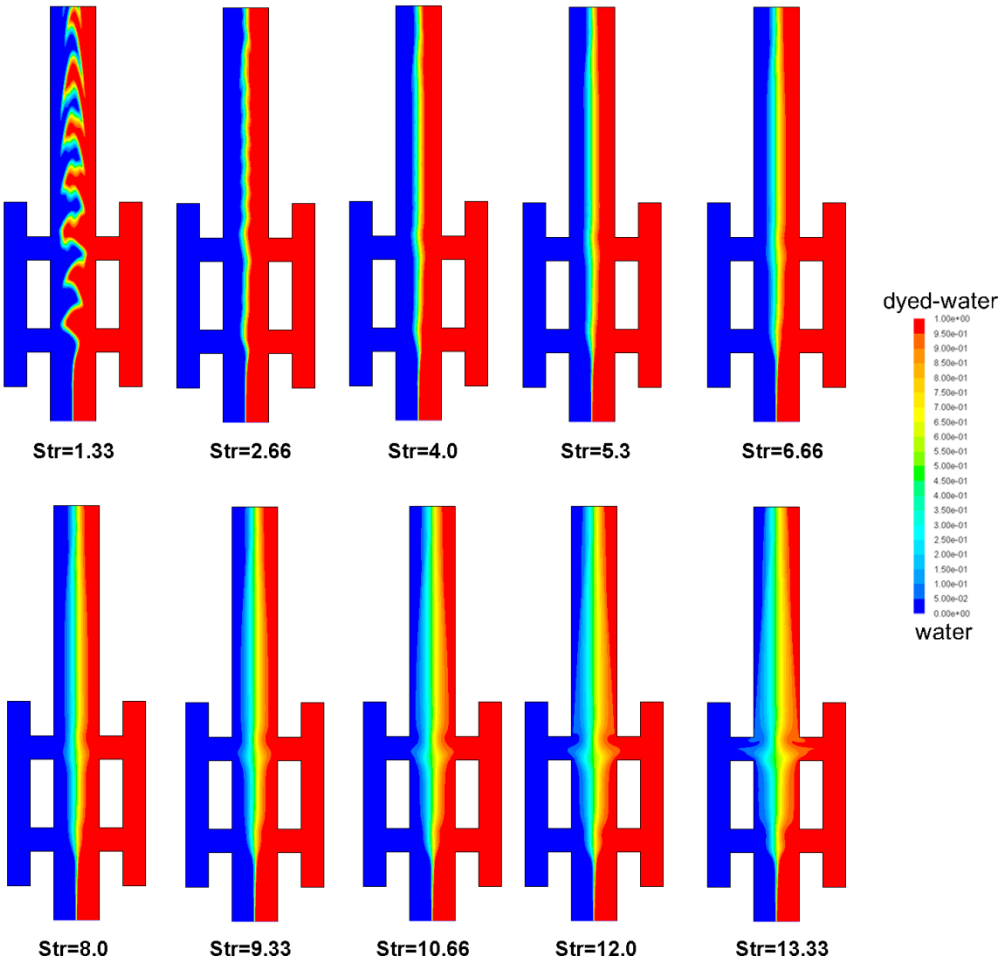

Figure 4.13 Strouhal number study at L=0.25 (Δ=0.5 mm), Re=0.5, t=6 seconds.

4.3.4 Mixing quantification while varying the stroke length

In order to know the degree of mixing when the stroke length was varied from 0.25 to 1.0, we proceeded to quantify the mixing degree of the mixture. To get a closer comparison of the mixing performance between the two mixers, we calculated the mixing degree at the same location as in the previous macromixer; one h downstream from the last synthetic jet orifice, see Figure 4.6. Moreover, the time-average technique was also considered here to quantify the mixing degree. Six images were selected within the 6-7 seconds of mixing time.

The mixing degree quantification as a function of the stroke length is displayed in Figure 4.14. In this graph, it is clear that increasing the stroke improves the mixing degree of the mixture. The improvement was about 5% for the stroke lengths between 0.5 and 1.0. However, at the lowest stroke length tested (L=0.25), an unexpected mixing

degree was found. The mixing degree seemed to be larger than when operating the mixer with a higher stroke length, for example at L=0.5 (Δ_{pp}=1.0 mm). The apparent "good" mixing was mainly due to the highly segmented fluid interface, see Figure 4.12. This effect occurred because the fluid interface was in a horizontal position when the mixing quantification was measured, giving a higher mixing degree than at the next stroke length.

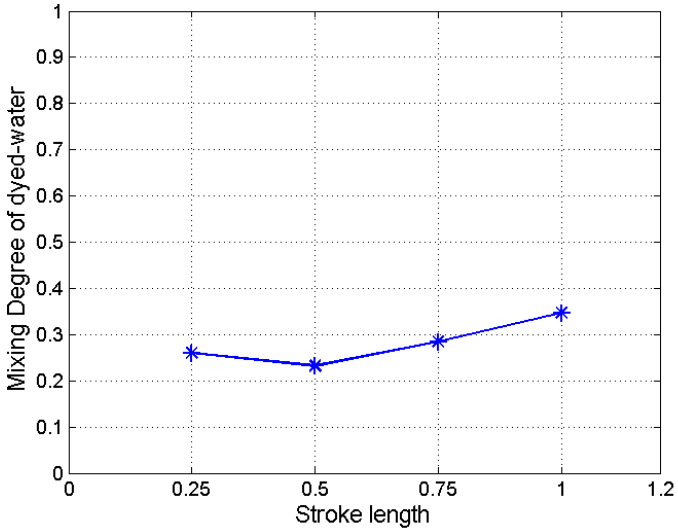

Figure 4.14 Time-averaged mixing degree for the four stroke lengths tested, Str=1.33, Re=0.5, t=6-7 seconds.

4.3.5 Mixing quantification while varying the Strouhal number

To find the effect that the Strouhal number has on the mixing degree, the quantification of the mixture was also carried out at the same time frame and location as the previous macromixer. This is taken into account to make a mixing comparison between the two macromixers designed until now. Figure 4.15 shows the mixing degree tendency for the Strouhal numbers considered. Notice that the mixing behaviour was very similar to the case of the mixer with four opposite jets, see Figure 4.8. In the case of the macromixer with two opposite synthetic jets, the mixing degree improves steadily while increasing the Strouhal number. A mixing degree of about 0.33 was the maximum value determined which also corresponds to the maximum Strouhal number tested (Str=13.33, f=10 Hz).

An interesting finding was that at Strouhal number of 1.33 (f=1 Hz), the mixing degree seemed to be better than for the next five Strouhal numbers tested. However, if we look at the concentration contours in Figure 4.13, the extent of mixing visually indicates that the mixing degree is not that high. This unrealistic mixing degree was determined because the fluid interface was highly segmented along the main channel. This means that at some moments in time, the fluid interface had a horizontal section that coincided with the time and place when the mixing degree was quantified. Hence, the mixing degree quantified at Str=1.33 did not represent the real mixing degree of the mixture and it should be discarded.

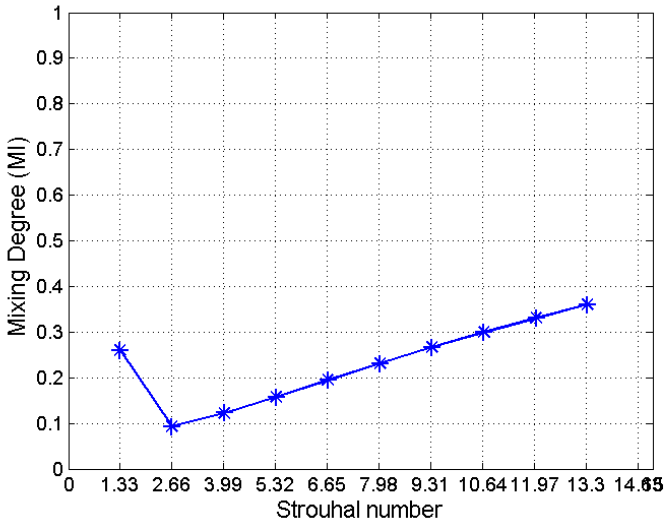

Figure 4.15 Time averaged of the mixing degree varying the Strouhal number, L=0.25 (Δpp=0.5 mm), Re=0.5, t=6-7 seconds.

4.3.6 The optimal operating condition

To find the optimal operating condition, the stroke length and the Strouhal number were varied as in the previous macromixer. The stroke length was varied from 0.5 to 1.0 in steps of 0.5, while the Strouhal number was varied from 2.66 (f=2 Hz) and 21.28 (f=16 Hz) in steps of 2.66 (f=2 Hz). The mixing degree trend of this variation is shown in Figure 4.16.

Looking at the mixing degree shown in Figure 4.16 can help us to find the best operating condition taking the power consumption as the criterion. For example, consider that the mixer requires one unit of energy every time the Strouhal number (frequency) or the stroke length (piston displacement) is increased. Hence, from Figure

4.16, we can see that the optimal operation condition should be between Str=10.66 (f=8 Hz) and Str=15.96 (f=12 Hz). Making the corresponding calculations of energy units required at those operating conditions, it was found that to reach a 90% mixing degree, the mixer should operate with a stroke length of 1.0 (Δ_{pp}=2 mm) and a Strouhal number of 10.66 (f=8 Hz). At this working condition, the mixer requires 12 units of energy to reach 90% mixture quality.

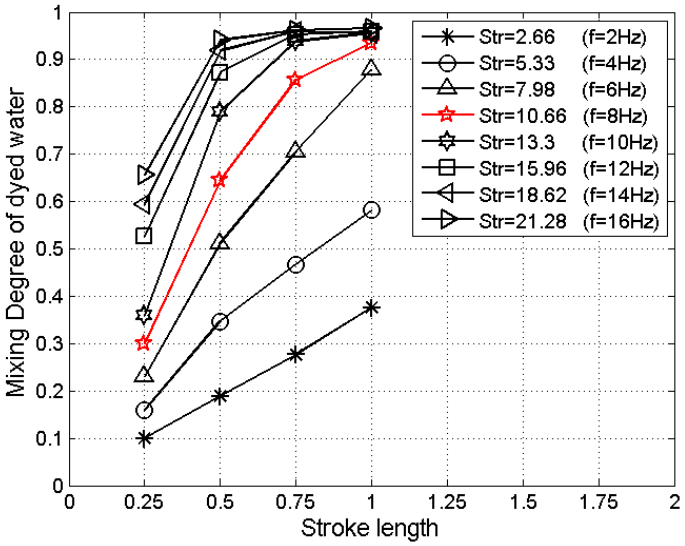

Figure 4.16 Time averaged of the mixing degree varying both the Strouhal number and the stroke length, Re=0.5, t=6-7 seconds.

4.3.7 Time sequence of the optimal mixing condition

To investigate how the mixing process took place in the mixer at the best operation conditions, we looked at a time sequence of the concentration contours. Figure 4.17 shows the time sequence of the concentration contours of the macromixer at four moments in time. It is interesting to see that the fluid interface stretched and folded with the piston-like motion of the cavities in a symmetric trend at t=0.1 s and t=0.15 s.

The effect of the enlargement of the fluid interface on mixing seemed more evident at t=0.25 s, which was indicated by the green-yellow colour of the concentration. The two pairs of opposite synthetic jets showed that the fluid interface was stretched and folded with a similar flow pattern. This effect was mainly due to the symmetric cavities. The advantage of having two pairs of orifices was that the fluids mixed when they tried to cross the two pair of orifices. For instance, when the fluids

passed the first pair of orifices, they tryed to rearrange in a parabolic velocity profile (not good for mixing enhancement). However, that behaviour was avoided with the second pair of orifices because they fluids were stretched and folded a second time for enhancing mixing further.

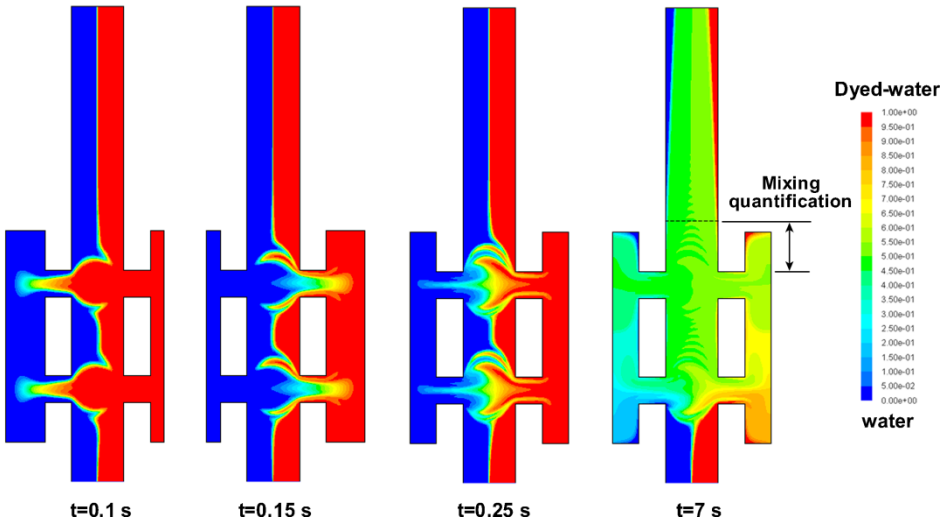

Figure 4.17 Time sequence of the mixing process at the best operating conditions: L=1.0 (Δ_{pp}=2 mm), Str=10.66 (f=8 Hz), Re=0.5.

We have stated that 90% mixing quality was achieved at L=1.0 (Δ_{pp}=2 mm), Str=10.66 (f=8 Hz) and after 6-7 seconds of mixing. Nevertheless, to give further evidence of this, the concentration contours of the fluids at these operating conditions are also displayed in Figure 4.17.

These concentration contours were reached when the mixed liquids flowed downstream. Due to the laminar flow of the liquids, they developed a parabolic velocity profile, Figure 4.18. This flow behaviour continued until it reached the channel outlet (Figure 4.17). Interestingly, some unmixed liquid remained attached to the walls of the channel. This occurred due to the low Re involved but also because the velocity on the walls was set as zero in the boundary conditions. Nevertheless, this attachment of the unmixed liquids to the channel walls could be solved if the whole domain is initialised as a fully mixed fluid, following the injection of the liquids to be mixed and the actuation of the synthetic jets. It is important to mention that those unmixed traces did not indicate the separation of the already mixed liquids.

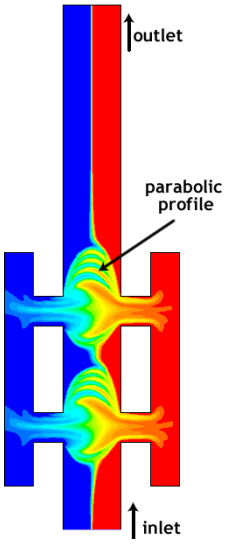

Figure 4.18 Mixture flowing downstream in a parabolic velocity profile.

Regarding the mixing performance of the mixer with two pairs of synthetic jets, we can say that it was able to achieve a fairly homogeneous concentration at the location where the mixing degree was determined. This indicated its potential for mixing effectively two liquids at Re=0.5.

4.3.8 Mixer improvements

We have shown numerically that it is possible to mix effectively two liquid samples at Re=0.5, using a macromixer with two pairs of synthetic jets. Nevertheless, this mixer configuration is very similar to the macromixer with four synthetic jets. This means that the difficulties to manufacture it remained unchanged. Furthermore, the visualisation of the mixing process, mentioned in Chapter 3, section 3.5, is the main concern with this macromixer design if is intended to be manufactured.

Therefore, with the experience acquired in the design, manufacturing and assembly of the previous macromixer with four pairs of synthetic jets, an alternative macromixer design is proposed not only to address the visualisation issue but also to simplify its fabrication, assembly and control system.

4.4 Mixer with one opposite pair of synthetic jets

The macromixer consists of just one single pair of synthetic jets. The synthetic jets in this macromixer are located at the lateral position of the main channel. With this macromixer modification, the construction and operation of macromixer is largely simplified. Another advantage of this mixer is that the design will allow the visualisation of the mixing process, which was the main concern with the two previous macromixers.

Before knowing the final dimensions and the configuration of the macromixer design, several numerical simulations were carried out to be more certain of its effectiveness in mixing at Re=0.5. Once the macromixer configuration was optimized with the aid of numerical simulations, a test rig was fabricated to perform the experiments.

4.4.1 Definition of the problem

Consider the macromixer shown in Figure 4.19b. It is composed of a rectangular channel and two cavities. The main improvement of this macromixer is in the way that the channel inlets are implemented and also the location of the synthetic jet cavities. The macromixer modification is considered because that is a closer representation of a micromixer used in microfluidic applications, see Figure 4.19a [4], [63], [78], [86], [87], [90], [93], [44], [97], [98]. One of the main advantages of this micromixer configuration allows the visualisation of the mixing process. Using this macromixer arrangement, we want to investigate its mixing performance at the same Reynolds number as the two previous macromixers (Re=0.5) and also the best operation condition to reach 90% mixture quality.

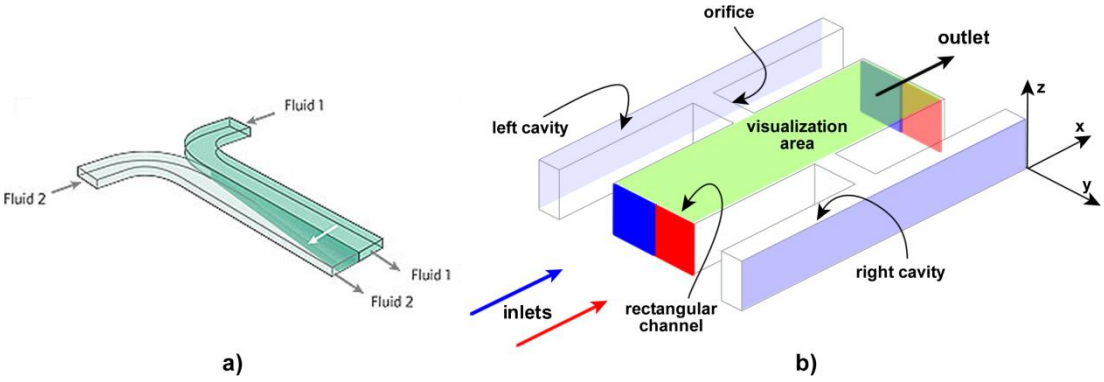

Figure 4.19 a) Micromixer configuration [4] and b) Macromixer configuration with one pair of synthetic jets.

Before defining the dimensions of the macromixer under discussion, several numerical simulations were carried out to have confidence that the mixing performance of 90% was fulfilled and then we proceeded to manufacture it. The dimensions for the final macromixer design are the following: channel width of 10 mm with a height of 5 mm, leading to an aspect ratio of 2. The depth and width of the synthetic jet orifice are h and h/2 respectively. The length of the synthetic jet cavity is 7h and its depth h/2.

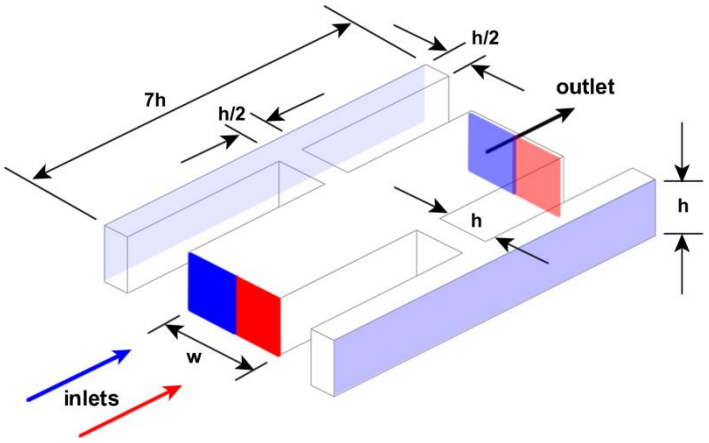

Figure 4.20 Dimensions of the macromixer with one pair of opposite synthetic jets.

- **Boundary conditions**

In order to simulate the macromixer with one pair of synthetic jets, appropriate boundary conditions have to be selected. A parabolic velocity profile was defined at the mixer inlet by means of a User-defined Function (UDF), see Appendix B. The outflow condition was selected for the channel outlet, the non-slip boundary condition was selected for the channel walls, while a sinusoidal motion was implemented to actuate the moving walls using a UDF. Finally, the initialization of the working fluids was also set with a UDF.

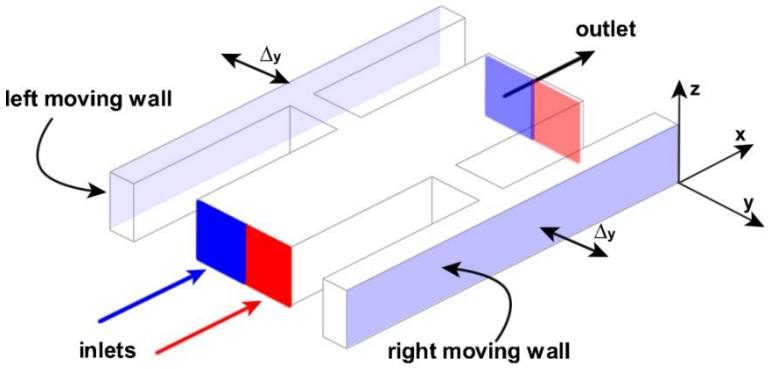

Figure 4.21 Boundary conditions of the macromixer.

4.4.2 Approach to studying the macromixer

In order to evaluate the mixing performance of this mixer design, we need to analyse it somehow. One way is using the critical dimensionless numbers involved in the mixer design. Hence, the two critical dimensionless numbers, the stroke length and the Strouhal number, are systematically varied as follows:

- The stroke length will be varied from 0.7 to 2.8 in increments of 0.7 (Δ_{pp}=0.5 mm), while keeping the Strouhal number constant to its minimum value Str= 0.83 (f=1 Hz), see Table 4.5.
- The Strouhal number will be varied from Str=0.83 to Str=8.33 by steps of 0.83 (f=1 Hz), while the stroke length is kept constant to its minimum value of L=0.7 (Δ=0.5 mm), see Table 4.6.

It is important to state that the analysis of the macromixer with one pair of synthetic jets will be from the experimental and numerical point of view.

Table 4.5 Stroke length study keeping the Strouhal number constant.

Stroke Length (L)	**Strouhal number (Str)**
0.7 (Δ=0.5 mm)	0.83 (f=1 Hz)
1.4 (Δ=1.0 mm)	0.83
2.1 (Δ=1.5 mm)	0.83
2.8 (Δ=2.0 mm)	0.83

Table 4.6 Strouhal number study keeping the stroke length constant.

Strouhal number (Str)	**Stroke Length (L)**
0.83 (f=1 Hz)	0.7
1.66 (f=2 Hz)	0.7
2.50 (f=3 Hz)	0.7
3.33 (f=4Hz)	0.7
4.16 (f=5 Hz)	0.7
5.0 (f=6 Hz)	0.7
5.83 (f=7 Hz)	0.7
6.66 (f=8 Hz)	0.7
7.50 (f=9 Hz)	0.7
8.33 (f=10 Hz)	0.7

4.4.3 Settings to match the experiments and the simulations

Before performing the experiments and the numerical simulations of the macromixer in this section, one important aspect has to be considered: the diffusivity of the fluids to be mixed.

In the previous two macromixers, (macromixers with four and two pairs of synthetic jets), the value of the diffusivity constant considered was one of the typical diffusivities found in microfluidic devices, which is $D=10^{-10}$ m^2/s. However, as two commercial paints are used to investigate mixing in the experiments, (see Chapter 3, section 3.6), their diffusivity value is not provided by the manufacturer. This value has to be determined somehow to set it in the numerical simulations. Fulfilling this consideration, it is more likely to have a closer match of the concentration contours in the experiments and the numerical simulations.

Therefore, to investigate the value of the diffusivity of the commercial paints selected the mixer was simulated with five different values of diffusivity, which are shown in Table 4.7.

Table 4.7 Diffusivity values considered to find the diffusivity of the commercial paints.

Case	Diffusivity
a)	$D=2.23x10^{-6}$ m^2/s
b)	$D=2.23x10^{-7}$ m^2/s
c)	$D=2.23x10^{-8}$ m^2/s
d)	$D=2.23x10^{-9}$ m^2/s
e)	$D=2.23x10^{-10}$ m^2/s

To have a concentration reference, an experiment was performed at Str=0.83 (f=1 Hz), L=0.7 (Δ=0.5 mm) and Re=0.5 using the commercial paints. The results are shown in Figure 4.22.

Figure 4.22 Experimental results of the concentration of the two commercial paints.

After this, five numerical simulations with the same operating conditions but with the diffusivities shown in Table 4.7 were carried out. The simulation results are shown in Figure 4.23 displaying all the diffusivities tested. A qualitative assessment of the concentration contours of the five numerical simulations suggests that case b) from Figure 4.23 is the one which most closely matches the experiment. Therefore, a diffusivity of 2.23×10^{-7} m^2/s will be used in the numerical simulations of this particular macromixer.

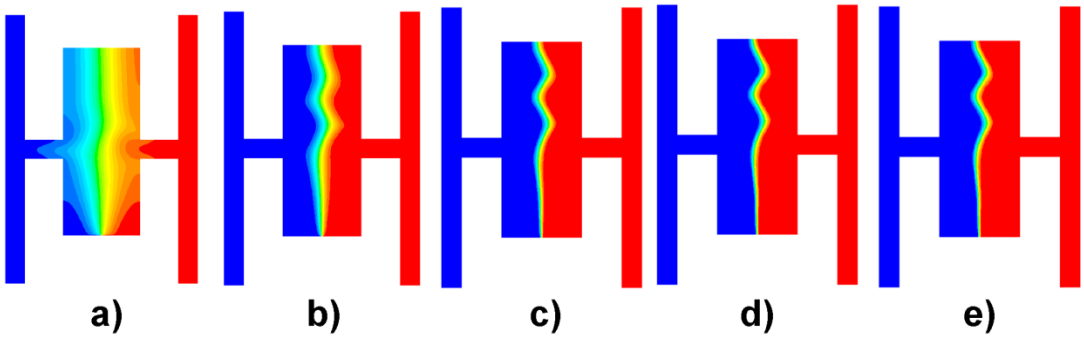

Figure 4.23 Simulation results of the five diffusivities tested.

4.4.4 Poor mixing at Re=0.5

To verify that poor mixing takes place when two fluids flow along each other in a channel at Re=0.5, an experiment was performed. To do this, we used the macromixer design with one pair of synthetic jets, see Appendix C. The experiment consisted of pumping two liquid samples through a main channel, as shown in Figure 4.24. The concentration gradients of the two fluids to be mixed showed that poor mixing takes place while they are flowing alongside each other. It is worth mentioning that not even the change of direction of the flow in the T-zone improved significantly

the mixing of the fluids. Furthermore, this gives evidence that mixing with pure molecular diffusion is a very slow mixing process at low Reynolds numbers.

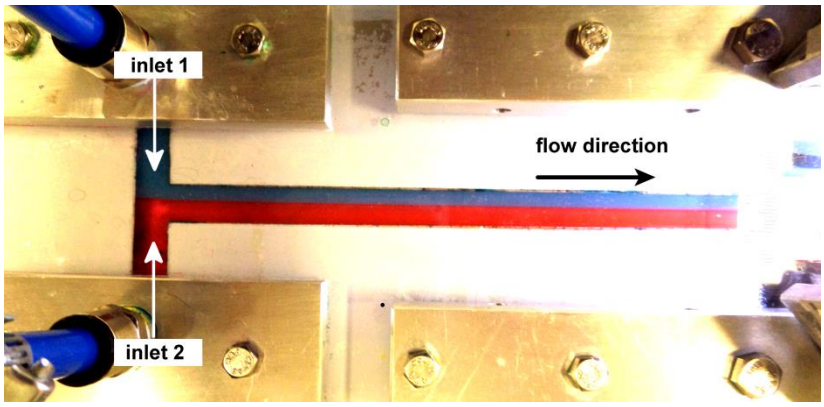

Figure 4.24 Poor mixing of the two liquid samples at Re=0.5.

4.4.5 The effect of the stroke length on mixing

First, we will investigate with both experiments and numerical simulations how the stroke length affects the mixing process of the liquids when is varied from L=0.7 to L=2.8 in steps of 0.7, see Table 4.5. The experimental and numerical results are presented in Figure 4.25. The upper images correspond to the experiments and the lower images to the simulations. It is important to mention that all images are the top view of the macromixer. From Figure 4.25, we observe that when L=0 the liquids flow along each other showing mixing just at the fluid interface. The extent of mixing is more evident in the image from the experiments due to the fact that the liquids were put into contact a considerable distance upstream, see Figure 4.24.

However, when the synthetic jets were actuated according to Table 4.5, the mixing of the fluids started to have significant improvement. This actuation led to the stretching and folding of the fluid interface, which also increased the surface area to allow molecular diffusion to take place. Increasing the stroke length from 0.7 to 2.8 has a significant effect on improving the mixing of the fluids. Interestingly, the mixing process only takes place along the main channel downstream and not inside the synthetic jet cavities in all the four cases tested.

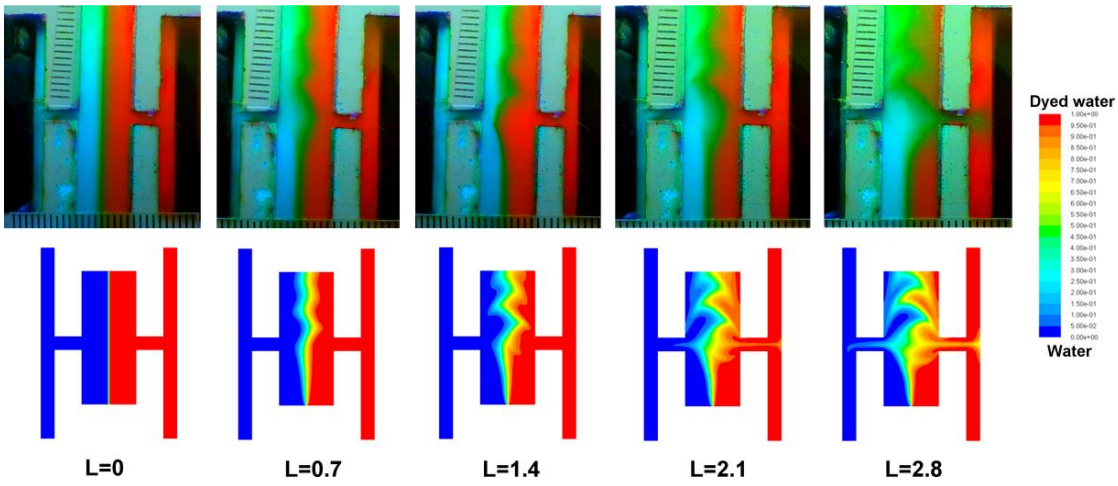

Figure 4.25 Concentration contours of the liquids to mix at different stroke lengths keeping the Strouhal number constant at 0.83 (f=1 Hz), Re=0.5.

4.4.6 The effect of the Strouhal number on mixing

In order to investigate the influenced of the Strouhal number, we performed the set of experiments and numerical simulations shown in Table 4.6. The results of this study are displayed in Figure 4.26 and Figure 4.27. A qualitative examination of the concentration of the fluids suggests that mixing is enhanced in a great extent when the Strouhal number is increased.

Interestingly, the only experimental case where the fluid interface displayed an undulated shape downstream at Str=1.66 (f=1 Hz). The apparent good mixing observed downstream is due to the fact that the fluids have enough time to diffuse between each other before the next fluid perturbation occurs. In contrast, when the Strouhal is increased to higher values than 1.66, the fluid interface seems to rearrange to its original position.

Another interesting finding was the formation of a mixing area before the synthetic jet orifice, which became evident in the numerical simulations at Str=3.3. Moreover, such effects become evident in the experimental images at Str=7.50 and Str=8.33. The mixing area in question may be an indication of the formation of vortical structures caused by the velocity of the liquid jets.

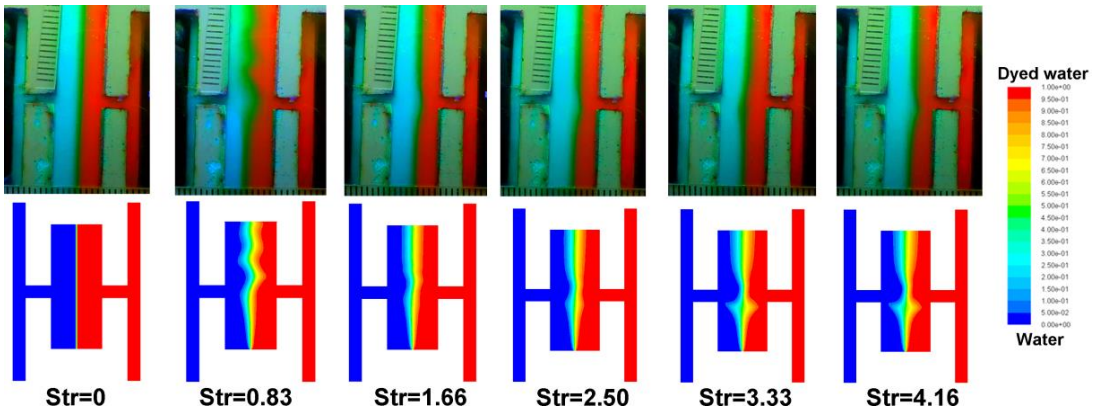

Figure 4.26 Concentration of the liquid during the Strouhal number study, keeping the stroke length constant to 0.70 (Δ=0.5 mm), Re=0.5.

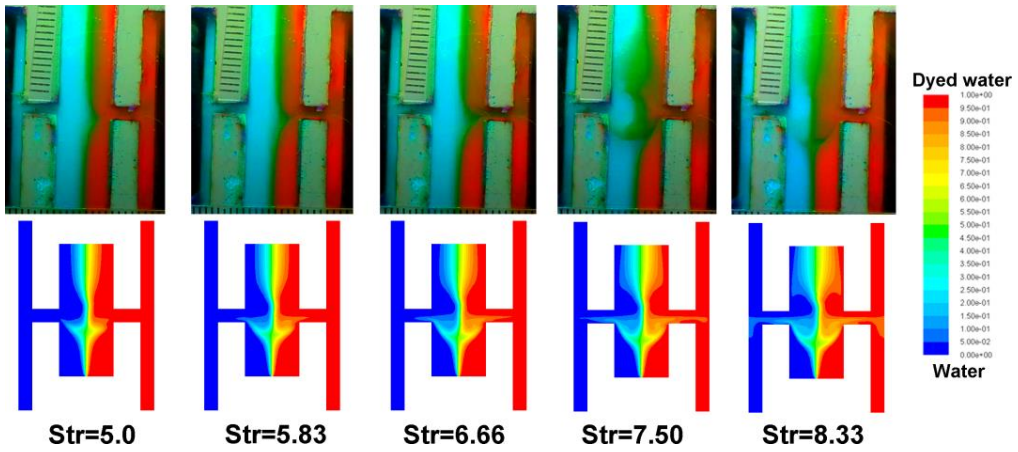

Figure 4.27 Concentration of the liquid during the Strouhal number study keeping the stroke length constant to 0.70 (Δ=0.5 mm), Re=0.5.

In summary, we can state qualitatively that increasing the Strouhal number enhances significantly the mixing of the liquids in the synthetic jet macromixer with one pair of synthetic jets at Re=0.5. However, to know the extent of this mixing, the quantification of the mixing degree of the mixture is discussed next.

4.4.7 Mixing quantification

The method to quantify the mixing degree of the mixture was as mentioned in Chapter 3. In the case of the experimental results, it consisted of determining the colour intensity of the pixels using a programme written in Matlab. The colour intensity of the pixels was normalized to convert it to a 0 to 1 value, which indicates the mixing degree of the mixture. The total number of pixels across the channel section was 152.

The location at which the mixing quantification was determined was just one channel width downstream from the synthetic jet orifice, as shown in Figure 4.28. It is important to mention that the mixing degree of each experimental and simulated case was determined using a time-averaged technique of 6 images. Additionally, these images were taken within the fourth oscillating cycle of the synthetic jets.

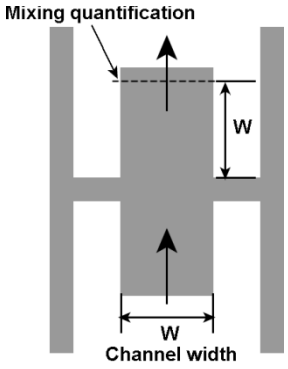

Figure 4.28 Quantification location of the mixing degree.

To illustrate the mixing technique, the concentration contours of an experimental image were plotted at the initial conditions (L=0 and Str=0) and are shown in Figure 4.29. The concentration profile experienced a sudden change in the middle of the channel due to the fact that half of the channel is filled with water and the other half with dyed water, which indicates a value of 0 or 1 respectively. The mixing degree of the mixture was determined using the average concentration of six different images taken within one oscillating cycle.

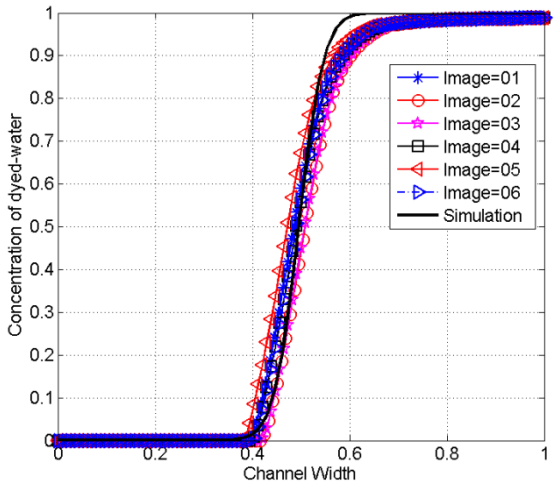

Figure 4.29 Time-average of the concentration contours of dyed water at L=0, Str=0, Re=0.5.

4.4.7.1 Mixing quantification varying the stroke length

As mentioned above, the mixing quantification was determined using a time-average of the concentration of 6 images for both the experiments and the numerical simulations. All the concentration values were obtained within the fourth oscillating cycle of the synthetic jet and this was decided to allow the flow field develop a periodic behaviour before making the quantification of the mixing degree. Figure 4.30 shows the mixing degree trend while increasing the stroke length.

In general, the mixing degree improved steadily when increasing the stroke length. The maximum mixing degree values were determined at the highest stroke length tested (L=2.8, Δ_{pp}=2.0 mm) in both the experiment and numerical simulation. The maximum mixing degree quantified was about 40% and the difference between the numerical simulations and the experimental results was about 3-4% in most of the cases tested. This mixing difference was considered to be sufficienly accurate for future numerical simulations.

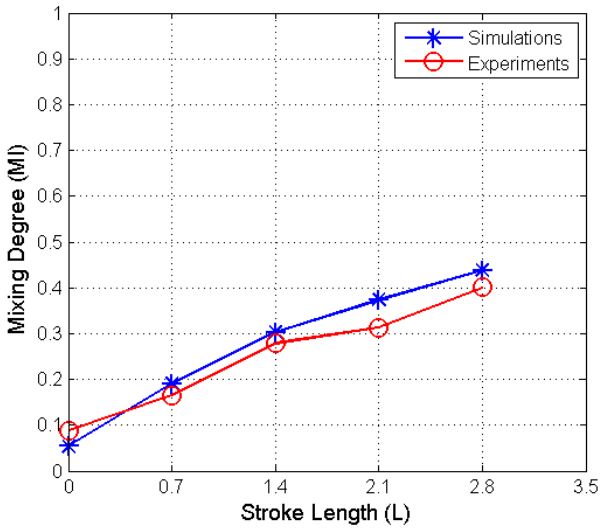

Figure 4.30 Mixing degree behaviour when the stroke length is increased from 0.7 to 2.8 in steps of 0.7, Re=0.5.

4.4.7.2 Mixing quantification varying the Strouhal number

We will now quantify the mixing degree while the Strouhal number is increased from 0.83 to 8.33 in steps of 0.83. The mixing degree of the experimental and numerical simulations is displayed in Figure 4.31. The results showed that the mixing degree also improved when increasing the Strouhal number. The most significant improvement

started to be after Str=4.16 (f=5 Hz). The maximum mixing degree calculated was 0.40, which corresponded to the maximum Strouhal number tested (Str=8.33). Interestingly, the mixing degree remained at about 0.2 when the Strouhal number was between 0 and 4.16.

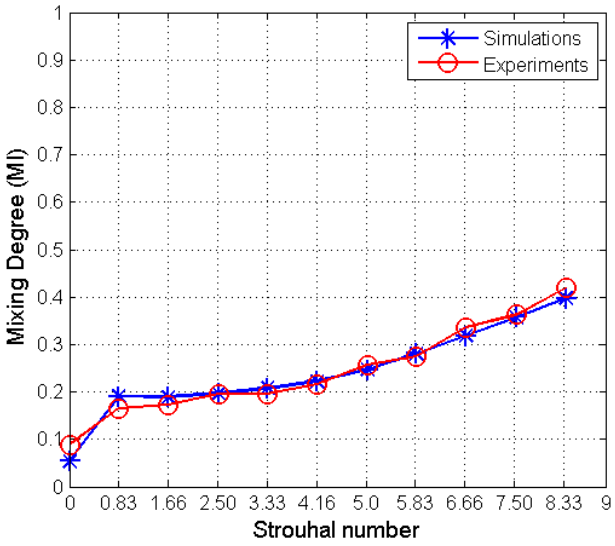

Figure 4.31 Mixing degree varying the Strouhal number, Re=0.5.

4.4.8 Power consumption

The power consumption is an important parameter to consider in the macromixer with synthetic jets. As we have mentioned in the previous section, enhancing the mixing degree of a fluid mixture could be done in two different ways: 1) increasing the stroke length, 2) increasing the Strouhal number. Nevertheless, when these parameters are increased to higher values, the power consumption of the actuating device also increases. If this is the case, the mixer will be less efficient.

To address this issue, we will investigate how the power consumption affects the mixing quality of the mixture. However, before this, we will discuss the way power consumption of the actuator was determined.

The power of a system can be expressed as:

$$Power = \frac{F \cdot d}{t} \tag{4.1}$$

where F is the actuation force, d the peak-to-peak distance that the actuator travels in each oscillating cycle, and t is the time required to travel such a distance [170]. Regarding

the force that the electromagnetic actuator used in the experiments, it was 50 Newtons. The distance that the actuator rod travelled was variable and it went from 0.5 mm to 2.0 mm in steps of 0.5 mm, as shown in the stroke length study, see Table 4.5. In this case, the time that one oscillation cycle lasted was constant because the actuation frequency was set to 1 Hz. With these data, we determined the power consumed for every synthetic jet actuation.

First, we will analyse the power required to actuate the synthetic jets for the four different stroke lengths tested. The power consumption calculations are presented in the form of a graph in Figure 4.32. Overall, we can state that the mixing degree is enhanced while the power is increased to higher values. As we expected, high power consumption of the system means reaching better mixing degree. In most cases, the mixing degree improvement was about 10%, except when the power went from 50 to 75%. At this interval, the mixing enhancement was just about 3 to 4%.

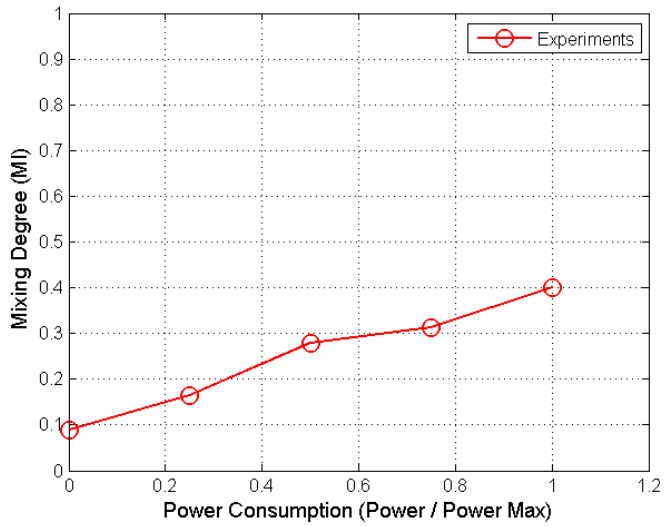

Figure 4.32 Mixing degree versus the power consumption of the electromagnetic actuator for the stroke length study.

We will now investigate how the mixing degree is affected in terms of power consumption in the Strouhal number study. The results of the power consumption to enhance mixing are shown in Figure 4.33. We can see that the maximum mixing degree reached by the mixer was when the actuator worked at the maximum power tested, (f=10 Hz). If we take into account that the mixing degree was about 10% without any actuation of the synthetic jets, the total mixing degree improvement was just 30% when actuating the synthetic jets with the highest frequency (f=10 Hz).

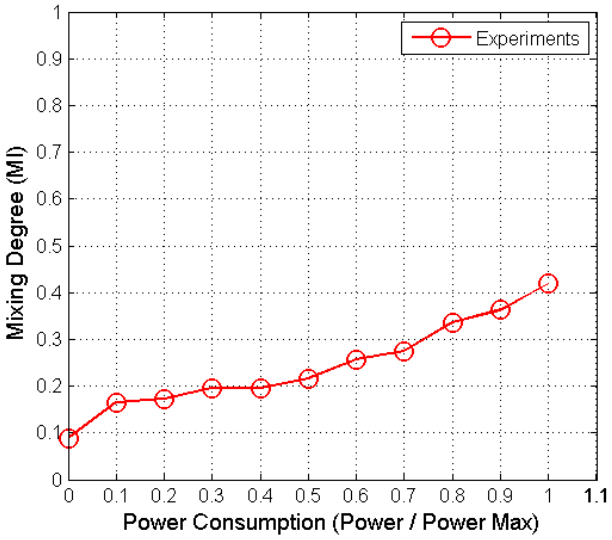

Figure 4.33 Mixing degree versus the power consumption of the electromagnetic actuator for the Strouhal number study.

4.4.9 The optimal operating condition

The previous analysis of the stroke length and the Strouhal number only showed how the mixing enhancement of the fluids evolved when they were independently varied. However, this analysis did not tell us at which operating condition we should operate the synthetic jet mixer to reach a mixing degree of 90%.

In order to find the optimal operating condition, we carried out several numerical simulations, where not only the stroke length but also the Strouhal number in the range stated in Table 4.5 and Table 4.6 were varied. The mixing results increasing the Strouhal number and the stroke length are displayed in Figure 4.34. The results showed that there were several operating conditions at which the mixer can reach a mixing degree of 90%. However, considering that the power is an important parameter which influences the efficiency of the mixing device, we will select the operating condition at which the mixer requires the minimum energy consumption to mix the liquid samples effectively.

Therefore, after the corresponding calculation related to power consumption, the best operating condition was at stroke length of 2.1 (Δ_{pp}=1.5 mm) and a Strouhal number of 6.66 (f=8 Hz).

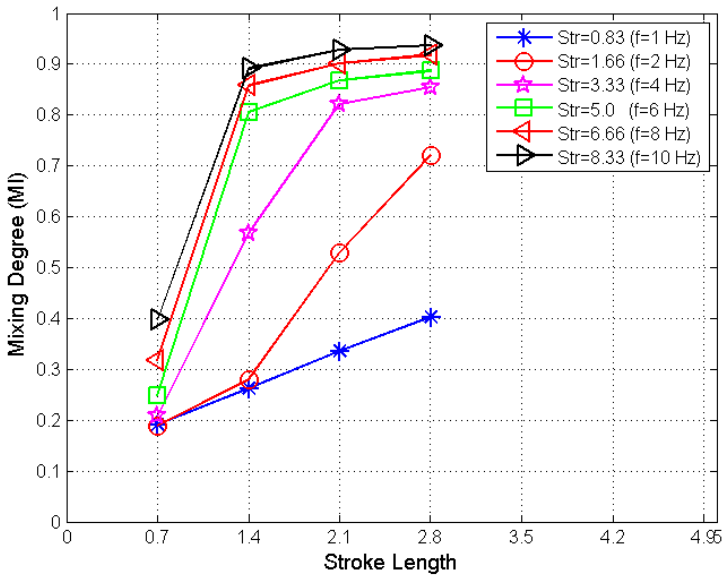

Figure 4.34 Mixing degree varying the stroke length and the Strouhal number within the fourth oscillation cycle of the synthetic jets, Re=0.5.

- **Time sequence of the best operating condition**

To investigate how the mixing process took place in the macromixer at the best operating condition, we looked at a time sequence of the concentration contours. The purpose of doing this was to show how the liquid jets were developed in the mixer while time progresses.

A sequence of images were selected at different instants in time and they are shown in Figure 4.35. The fluid interface was significant stretched and folded in the main channel at t=0.1 s. The enlargement of the fluid interface seemed to enhance the mixing of the liquid samples. At the next time sequence, where t=0.15 s, the fluid interface was enlarged to a greater extent, leading to a further mixing improvement. Moreover, at t=0.20 s, the fluid interface started to be less evident because the concentration of the liquids became uniform in the main channel.

The constant stretching and folding of the fluid interface improved significantly the mixing of the liquid samples after just 4 seconds, as shown Figure 4.35. The uniformity of the concentration of the fluids in the main channel and cavities of the macromixer was the evidence of the 90% mixing quality quantified in the previous section.

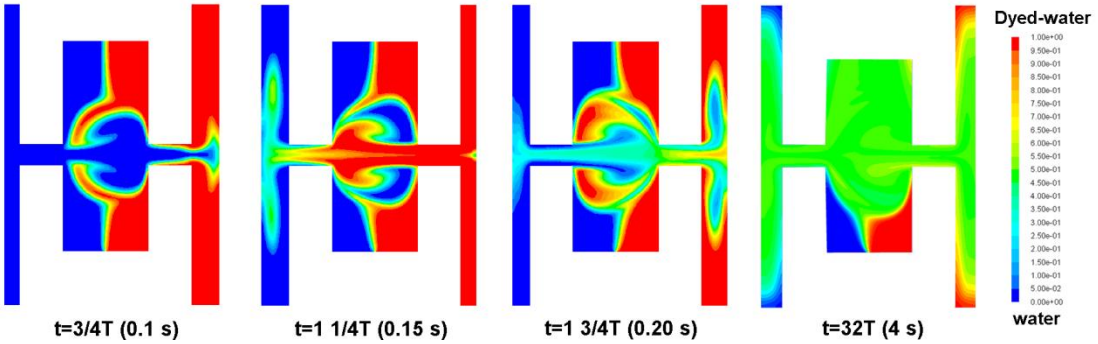

Figure 4.35 Time sequence for the best operating conditions of the macromixer, L=2.1 (Δ_{pp}=1.5 mm), Str=6.66 (f=8 Hz) Re=0.5.

To validate the mixing performance predicted in the numerical simulations at L=2.1 (Δ_{pp}=1.5 mm), Str=6.66 (f=8 Hz) and t=4 s, the corresponding experiment was carried out. The concentration contours at this operating condition are shown in Figure 4.36. Overall, the concentration of the two liquid samples seemed to be fairly homogeneous inside the main channel and in the two cavities. The stretching of the fluid interface in the channel inlet of the macromixer looked quite similar to the one predicted by the numerical simulation, Figure 4.35, t=4 s.

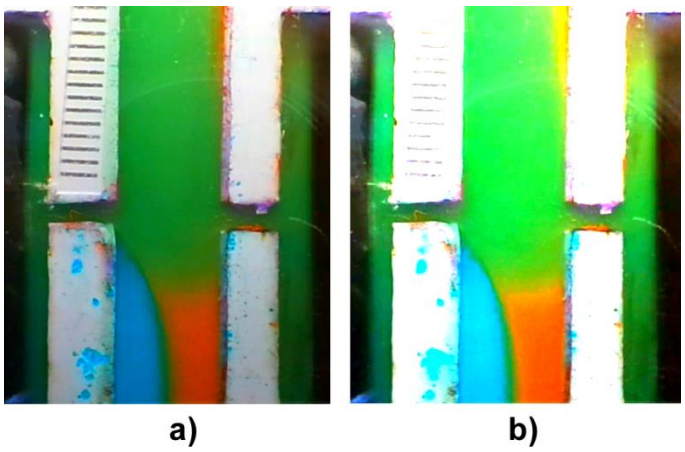

Figure 4.36 Concentration contours of the liquids to be mixed obtained from the experimental test of the synthetic jet mixer at L=2.1(Δ_{pp}=1.5 mm), Str=6.66 (f=8 Hz), Re=0.5, t=4 s. a) Plain image and b) Adjusted colour.

To make a quantitative comparison between the numerical and experimental results, we determined the mixing degree of the mixture at approximately the same location as in the numerical simulation (one channel width from the orifice). The quantification of the mixing degree was 0.92, which was about 2-3% more than in the numerical simulations. Therefore, we can state that the numerical simulations and the experimental results are sufficiently close for our mixing purpose.

- **Concentration of dyed-water downstream**

After determining the mixing degree of the mixture, we were also interested in looking at the concentration profile across the main channel at the optimal operating condition. This is important to verify if the concentration profile was close to 0.5 which indicate a fully mix condition. Two locations were selected downstream: one at half the channel width (w/2) and a second one at one channel width (w) downstream (see Figure 4.37b). The concentration profiles at such locations are shown in Figure 4.37a, which confirmed the tendency to reach a concentration of 0.5.

Out of the two locations measured, the concentration profile that is at a distance of w/2 downstream was close to the value of 0.5 across the microchannel, which suggested that mixing was almost complete. However, the concentration profile at channel width (w) downstream showed a different trend, particularly at the two extremities of the channel. This concentration profile provided further evidence to the 92.01% mixing quality shown in Figure 4.34.

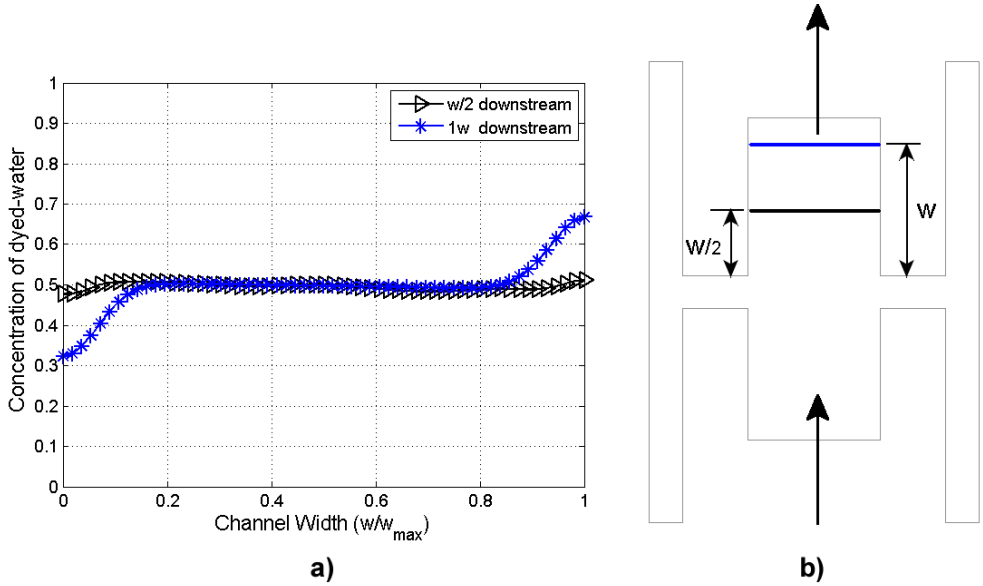

Figure 4.37 Concentration profile of dyed water at two different locations of the channel downstream, L=2.1, Str=6.66, Re=0.5, t=4 s.

- **Velocity streamlines**

To visually examine the flow pattern created by the synthetic jets, we display the velocity streamlines of the flow are displayed in Figure 4.38. The formation of vortical structures, before and after the synthetic jet orifices, are clearly evident. The streamlines path suggested that the fluid experienced a three dimensional behaviour

caused by the synthetic jets, as shown in Figure 4.38b. The fluid trajectories suggest that the mixing of the fluids was improved largely due to the recirculation areas in the main channel.

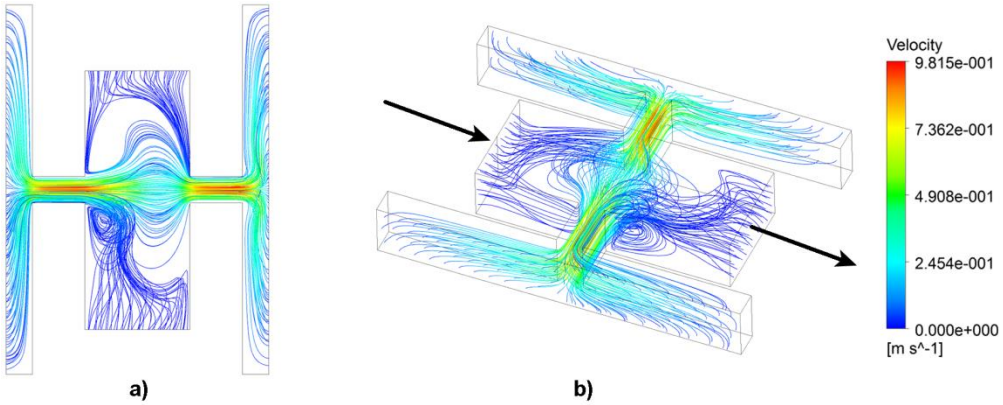

Figure 4.38 Streamlines of the velocity for the best operating conditions L=2.1 and Str=6.66, Re=0.5.

- **Vortical structures produced by the synthetic jets**

One of the motives for using synthetic jets for mixing enhancement at low Reynolds numbers was to take advantage of the vortical structure that they can generate. We wanted to use those vortical structures to enhance the mixing quality of viscous liquids. To find out if such desired vortical structures were formed in the macromixer, the velocity vectors and the concentration of the two fluids to mix are shown in Figure 4.39. Interestingly, two vortices are formed within the main channel; one vortex structure before the synthetic jet orifice and another one after it, which were separated by a liquid jet (synthetic jet) coming from the respective cavity.

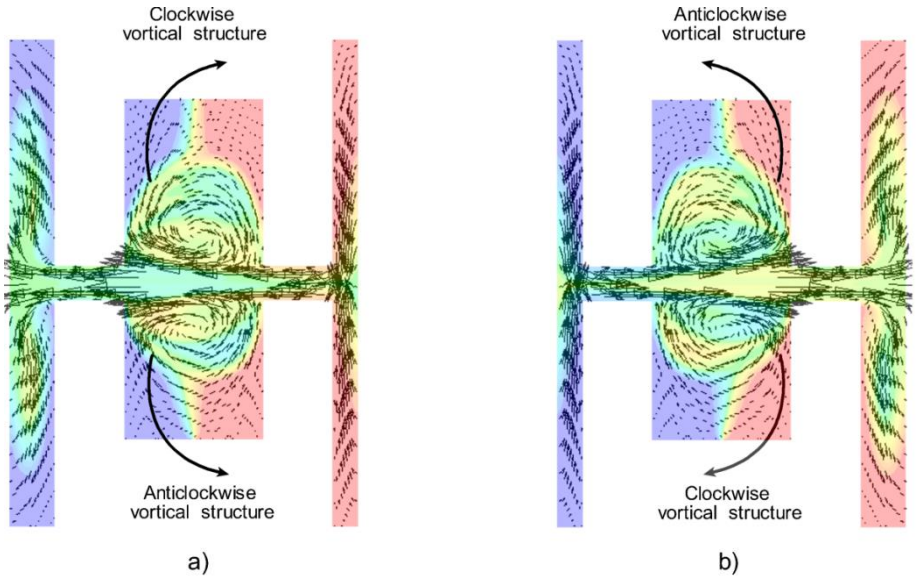

Figure 4.39 Vortical structures generated by the synthetic jets at the best operating condition, a) cavity actuation from right to left, b) cavity actuation from left to right.

Interestingly, the flow circulated in opposite directions in each vortical structure. For example, in Figure 4.39a the vortex structure located before the synthetic jet orifice showed an anticlockwise fluid circulation while in the other vortical structure the fluid circulated in a clockwise direction. Moreover, when the opposite synthetic jet cavity was actuated, as shown in Figure 4.39b, the vortical structures changed their direction.

The direction indicated by the velocity vectors in the two vortical structures was clear evidence of the mixing mechanism behind the synthetic jet mixer. The effect due to the alternative stirring in those recirculating structures was beneficial for enhancing mixing. The high degree of stretching and folding of the fluids produced by those vortices had a remarkable impact for enhancing mixing, which confirms the excellent mixing quality reached at this operating condition.

- **Velocity ratio**

We should remember that in the present synthetic jet, mixing happens in a cross-flow setting. The first flow corresponds to the main flow velocity in the channel and the second flow corresponds to the flow velocity of the synthetic jet. The ratio between these two flow velocities is known as the velocity ratio.

In the last section, we have looked at the vortical structures that were formed in the mixing channel by the synthetic jets, but we did not mention the ratio of the fluid

velocities to produce those recirculating patterns. The velocity ratio computed in the macromixer is shown in Figure 4.40. As we can see from this figure, the velocity ratio should be above 200 to reach a mixing degree of 90%. In other words, the velocity of the liquid jet coming out from the synthetic jet cavities should be 200 times higher than the velocity of the fluid flowing in the main channel. These result suggested that a high velocity ratio is required to achieve 90% mixing quality.

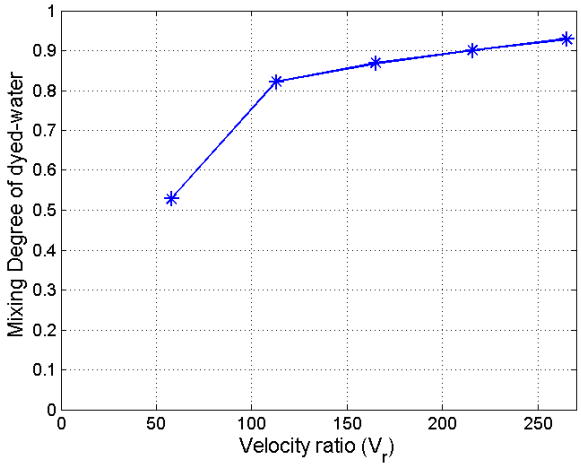

Figure 4.40 Velocity ratio keeping stroke length constant to 2.1 and varying the Strouhal number from 1.66 (f=2 Hz) to 8.33 (f=10 Hz) in steps of 1.66 (f=2 Hz), Re=0.5, t=0.4 s.

- **Mixing time**

The time that a mixing device takes to mix liquid samples is often a very important parameter which is related to the mixing efficiency. Efficient mixers are those which can mix liquid samples in the shortest time possible and with the minimum energy consumption. In many scenarios, mixing should take place very rapidly. For example, in a chemical reaction occurring in a microreactor [4], [5]. Therefore, to investigate how the present mixer performs in this domain, we quantified the mixing degree of the mixture during four seconds. This was plotted versus the mixing degree of the mixture in Figure 4.41. The location at which it was evaluated was at one channel width downstream from the synthetic jet orifice (w=10 mm). The mixing degree was significantly improved when time progressed, particularly within the first two seconds. The mixing improvement continued for the next two seconds although at a lower rate. Figure 4.41 also shows that to achieve a mixing degree of 90%, the mixer requires four seconds at L=2.1, Str=6.66.

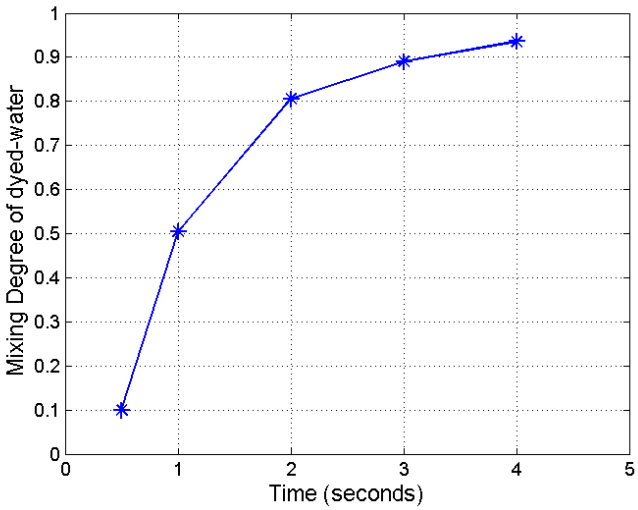

Figure 4.41 Mixing degree during the first four seconds of mixing at L=2.1 (Δpp=1.5 mm), Str=6.66 (f=8 Hz), Re=0.5.

4.5 Scaling down of the macromixer

As we are interested in the design of a micromixer with synthetic jets, in this section we scaled down the macromixer with one pair of synthetic jets. This was considered to investigate its performance at a microscale. The criterion to scale down the mixer was based on the microchannel size of one commercial micromixer available in the market [169]. The dimensions of the cross-section of the main microchannel were 350 μm wide and 150 μm depth, leading to an aspect ratio of 2, as shown in Figure 4.42. The reduction in size of the macromixer was by a factor of 28.

It is worth mentioning that the microchannel cross-section of the micromixer, comercialized by Dolomite [169], is not completely rectangular. However, in our study, we considered a fully rectangular cross-section of the microchannel.

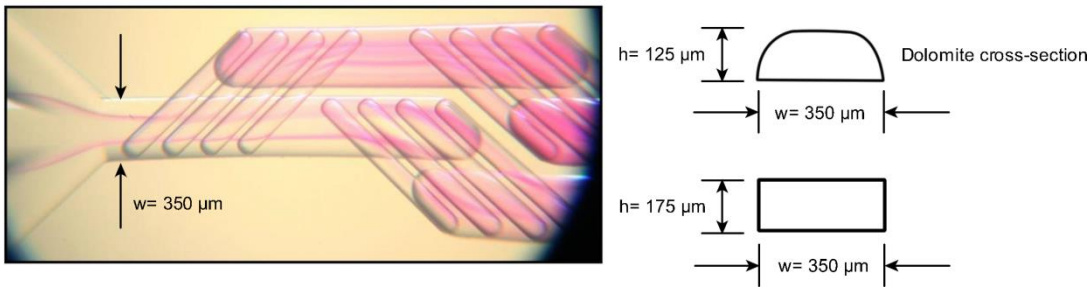

Figure 4.42 Cross-section considered for the numerical simulation of the scaled down micromixer [169].

- **Diffusivity in microdevices**

In the macromixer with one pair of synthetic jets, the mixing process was carried out using the diffusivity of commercial paint with a diffusivity of 2.23×10^{-7} m^2/s. However, in microfluidic devices, typical diffusivities are two or three orders of magnitude lower, which are between 10^{-10} and 10^{-12} m^2/s [49], [71], [157], [113]. Therefore, the diffusivity value considered to simulate the micromixer was $D=10^{-11}$ m^2/s. With this adjustment, the mixing performance of the micromixer will be closer to a real scenario.

- **The best operating condition**

In order to make a comparison in performance between the macromixer and the micromixer, the micromixer will be operated with the proportional actuation conditions: $\Delta pp = 3w/4$ (262.5 μm) and f=8 Hz; given a constant Re (Re=0.5).

The mixing performance of the scaled down mixer is shown in Figure 4.43 using the same time sequence as in its macromixer counterpart. A qualitative assessment indicated that the micromixer did not completely mix the liquid samples. Although the stretching and folding of the fluids interface occurred in the main channel, it was not enough to significantly enhance the mixing of the samples as found in the macromixer.

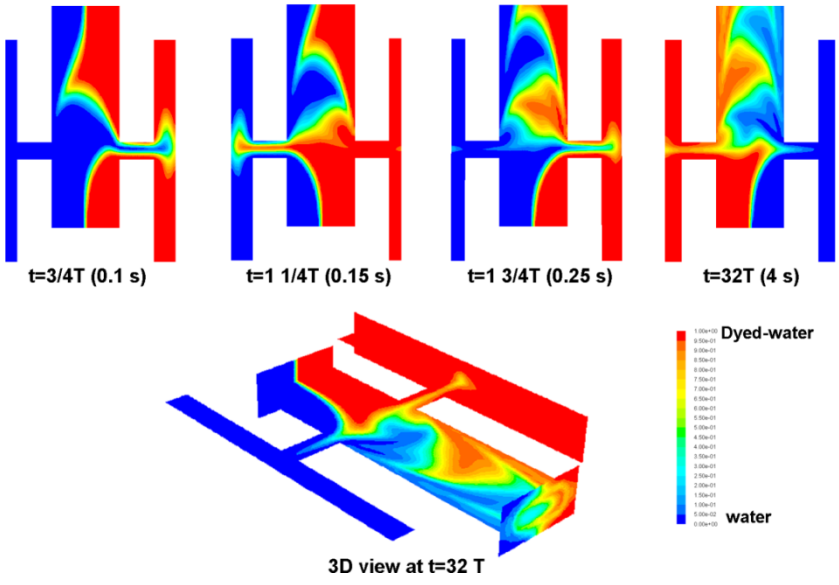

Figure 4.43 Time sequence of the micromixer at the best operating conditions: (Δpp=3w/4 or 262.5 μm) and (f=8 Hz), Re=0.5.

In terms of the mixing degree, it was calculated at the same location and time, and it was about 32%. If a comparison is made between this mixing degree and the one

measured in the macromixer, it gave a 58% difference or 58% less mixing in the case of the micromixer. This is a significant difference regarding mixing performance, which suggested that studying a micromixer from its macroscale point of view was not valid..

4.5.1 Possible causes of the poor mixing

- **Low diffusivity**

The fact that the liquid samples in the micromixer had a much lower diffusivity value than the one used in the macromixer seemed to make mixing more difficult.

- **Actuation amplitude**

The peak-to-peak displacement was not to be sufficiently enough to stir up the fluids and promote mixing. The stretching and folding of the fluid interface appeared to be shorter in the micromixer than in its macromixer counterpart. This effect caused a shorter fluid interface for the mixing of the fluids. Therefore, we inferred from the stroke length study that increasing the peak-to-peak displacement (stroke length) could improve mixing in the micromixer.

- **Velocity ratio**

The velocity ratio could be another cause of the poor mixing in the micromixer configuration. From the time sequences of the mixer shown in Figure 4.43 we did not observed any clear evidence of vortical structures like those seen in the macromixer. Furthermore, the calculations of the velocity ratio for both mixers showed that the velocity ratio was 204 times bigger in the macromixer than in the micromixer. Hence, increasing the velocity ratio could create the vortical structures to enhance mixing.

- **Surface-volume ratio**

The surface-volume ratio may also be one cause of the poor mixing performance of the micromixer. This feature rules micromixers due to the large fluid confinement in a microchannel.

4.6 Optimization of the micromixer with synthetic jets

The mixing degree quantified in section 4.5 suggested that we cannot obtain the same mixing performance when scaling down a macromixer. Although the scaled down micromixer significantly segmented the fluids to mix, its mixture quality was not close to 90%. Therefore, a modification of the cavity and orifice of the micromixer is proposed in an attempt to increase the velocity ratio of the fluids to mix.

The mixing performance and the mixing quantification will be determined as in previous sections using the critical dimensionless numbers. The mixing investigation of this improved design was also carried out using numerical simulations.

4.6.1 Definition of the problem

To define our problem, consider the micromixer shown in Figure 4.44. In an attempt to improve the mixing performance of the previous micromixer, the micromixer geometry was slightly modified. The orifice width was reduced from w/2 to w/4, and the cavity length was increased from 7h to 7w, as shown in Figure 4.44. We should remember that the dimension of the channel width (w) was 350 μm and its depth (h) 175 μm.

The reason for making such a modifications in the synthetic jet orifices and cavities was to increase the velocity ratio between the mean flow and the synthetic jets. This modification could lead to circulating regions of the working fluid in the main microchannel as in the macromixer, which could be beneficial for enhancing mixing.

Therefore, we want to investigate if such a micromixer can effectively mix the liquid samples at an even lower Reynolds numbers. In the previous micromixer, the Reynolds number considered was 0.5, which is still a typical Reynolds number in microfluidics. However, in this section the modified micromixer will be tested mixing at Re=0.25.

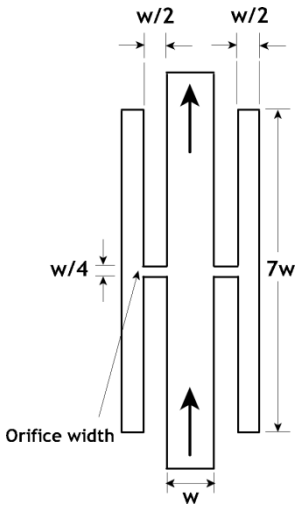

Figure 4.44 Top view of the modified micromixer.

- **Numerical method**

To perform the 3D numerical simulations of the improved micromixer, we selected the same numerical model (see Chapter 3): the species-transport model without a chemical reaction. However, in an attempt to determine if the flow displays chaotic advection, the discrete phase model [171] was also used. The discrete phase model consists of seeding inert particles in the main flow, making the assumption that those particles are passive particles which only follow the path of the flow stream and do not interfere with the flow. The discrete phase model is also useful as a visualisation tool to show the particle distribution which can be related to mixing. The results of the discrete phase model will allow us to visually assess the particle distribution and to obtain Poincaré maps which are used as a qualitative tool to visually determine unmixed zones in the micromixer [14], [53], [54], [55], [56].

Mixing will be investigated, as in previous macromixers by varying the stroke length and the Strouhal number. Regarding the stroke length, it will be performed as shown in Table 4.8. The stroke length is directly related to the channel width of the micromixer. Hence, the channel width was divided into four equally spaced parts to obtain the peak-to-peak displacement to calculate the stroke length.

Table 4.8 Stroke lengths study keeping the Strouhal number constant.

Stroke Length (L)	Strouhal number (Str)
3.5 (Δ=w/4)	0.0875 (f=1 Hz)
7.0 (Δ=w/2)	0.0875
10.5 (Δ=3w/4)	0.0875
14.0 (Δ=w)	0.0875

Next, the Strouhal number will also be varied independently, as shown in Table 4.9. The only variable that will be varied to increase the Strouhal number will be the actuation frequency increased from 1 to 10 Hz in steps of 1 Hz. The stroke length was kept constant to its minimum value (Δ=w/4) in all the simulating cases.

Table 4.9 Strouhal number study keeping the stroke length constant.

Strouhal number (Str)	Stroke Length (L)
0.0875 (f=1 Hz)	3.5 (Δ=w/4)
0.175 (f=2 Hz)	3.5
0.2625 (f=3 Hz)	3.5
0.35 (f=4 Hz)	3.5
0.4375 (f=5 Hz)	3.5
0.525 (f=6 Hz)	3.5
0.6125 (f=7 Hz)	3.5
0.7 (f=8 Hz)	3.5
0.7875 (f=9 Hz)	3.5
0.875 (f=10 Hz)	3.5

4.6.2 The effect of the stroke length on mixing

To visually examine the effect that the stroke length had on the mixing degree of the two fluids, a series of sequential images are presented in Figure 4.45. The stroke length was varied from L=3.5 to 14.0 in steps of 3.5 and the concentration contours of dyed water were taken after 4.0 seconds of simulation time. The stroke length study shows that the stretching and folding of the fluid interface was slightly enlarged when it was augmented from 3.5 to 14.0. Such an increase of the fluid interface seemed to be beneficial for mixing enhancement. This effect can be seen mainly along the main microchannel. In general, we can state that increasing the value of the stroke length

from 3.5 to 14.0 to increase the mixing of the two streams. However, at this moment, we cannot say how much the mixing degree improved in each case.

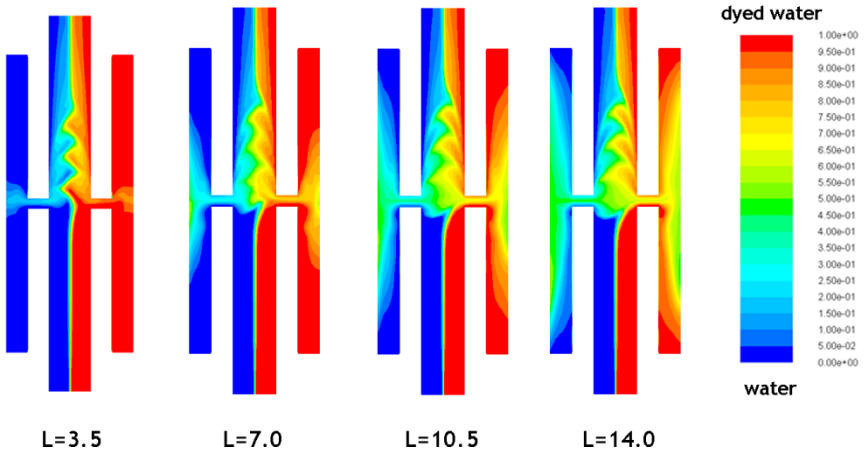

Figure 4.45 Concentration contours of the stroke length study, Str=0.0875 (f=1 Hz), Re=0.25, t=4 s.

4.6.3 The effect of the Strouhal number on mixing

The concentration of the fluids while varying the Strouhal numbers is shown in Figure 4.46. Overall, mixing improved considerably as the Strouhal number was increased. In most of the cases, the mixture seemed to be fairly homogeneous along the mixing channel.

The particular case at which the Strouhal number is 0.0875 (f=1 Hz), the fluid interface was still noticeable where the fluid was stretched and folded downstream. Interestingly, the segmented fluid interface was no longer visible in further Strouhal numbers because of the higher segmentation rate of the fluids.

A visual examination of the concentration of the liquids in the micromixer suggested that mixing enhancement was clearly evident when the Strouhal number was increased from 0.0875 (f=1 Hz) to 0.875 (f=10 Hz).

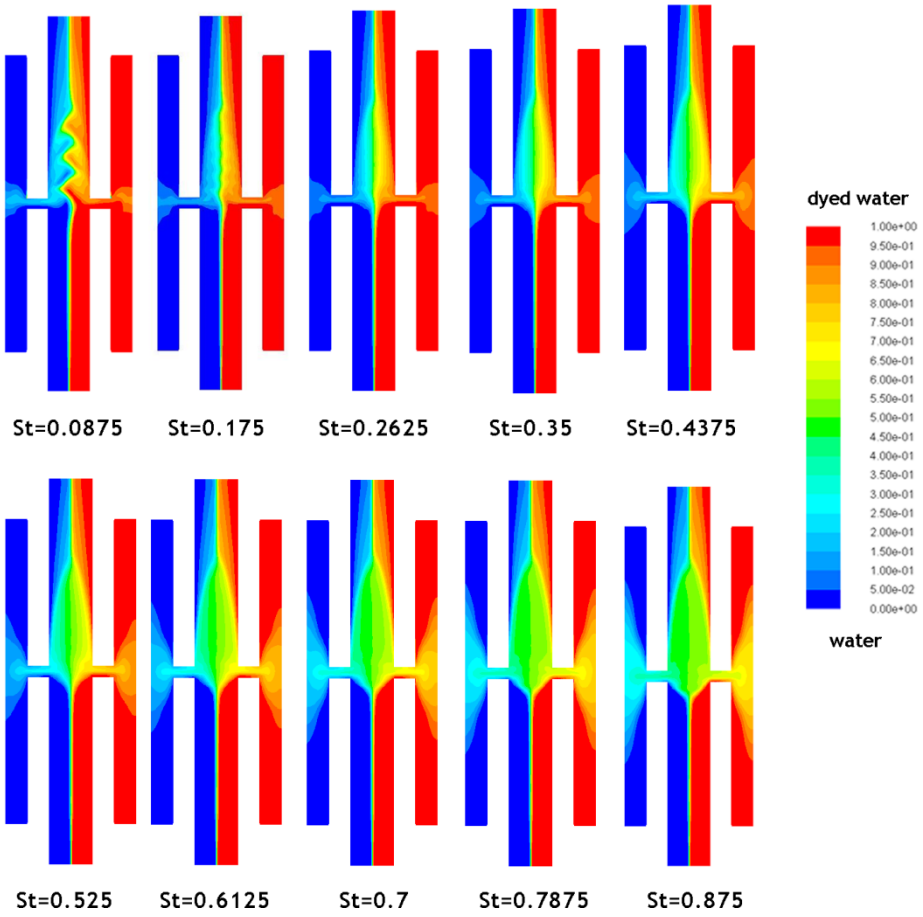

Figure 4.46 Concentration contours of the Strouhal number study, L=3.5 (Δpp=w/4), Re=0.25, t=4 s.

4.6.4 Quantification of the mixing degree of the mixture

To evaluate the mixing degree of the mixture, it was determined in the same technique of time average and at the same location as in the previous mixer: one channel width from the orifice downstream.

4.6.4.1 Mixing degree while varying the stroke length

The mixing degree quantification of the mixture corresponding to the stroke length study is shown in Figure 4.47. The lowest mixing degree of the mixture was obtained when the stroke length was at its minimum (L=3.5). A mixing degree of 0.46 was quantified at such an operating condition. However, when the stroke length was increased to 7.0 the mixing improvement was about 10% more than in the previous case. The improvement continued reaching a mixing quality of 60% at L=10.5. Interestingly, the mixing degree was not significantly enhanced when the stroke length

was varied beyond 10.5. The mixing remained constant, for example at stroke length of 14.0. Overall, we can say that increasing the stroke length had an important effect on enhancing the mixing degree of the mixture but not sufficient to obtain our desired 90% mixing quality.

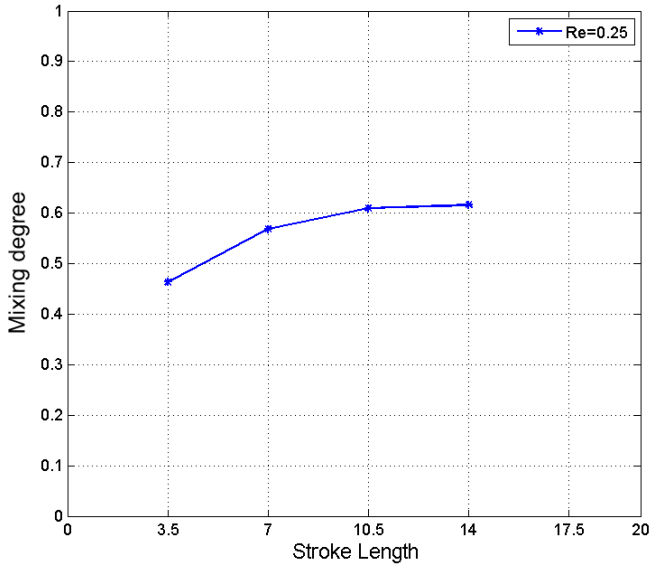

Figure 4.47 Mixing degree while varying the stroke length.

4.6.4.2 Mixing degree varying the Strouhal number

Now, the mixing degree of the mixture was quantified when the Strouhal number was varied from 0.0875 to 0.875 (f=1-10 Hz) and its effect on the mixing degree is shown in Figure 4.48. In general, the mixing degree improved almost steadily when the Strouhal number was increased. The most significant improvement of the mixing degree was between Str=0.2625 (f=3 Hz) and Str=0.7 (f=8 Hz). A mixing degree of 0.9, which is the mixing target, was achieved at the last two Strouhal numbers tested (Str=0.7875 and Str=0.875).

On the other hand, notice that the lowest mixing degree was determined at Str=0.175 (f=2 Hz) and not at Str=0.0875 (f=1 Hz). The higher mixing degree at Str=0.175 was attributed to the highly segmented interface, which changed while time progressed.

Overall, we can state that the mixing degree was significantly enhanced when the Strouhal number was increased from 0.0875 to 0.875 (f=1-10 Hz) in the modified micromixer design.

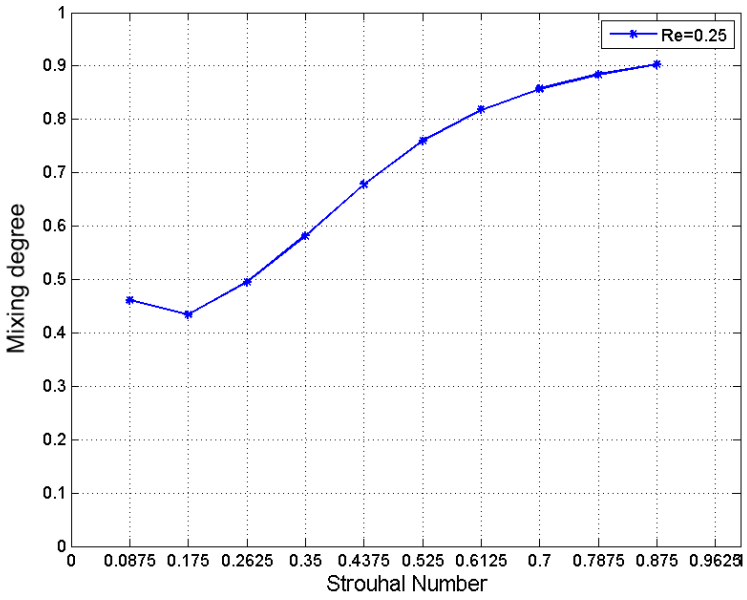

Figure 4.48 Mixing degree while varying the Strouhal number.

4.6.5 Best operating condition

In order to find the best operating condition, we performed additional numerical simulations. They consisted of selecting several Strouhal numbers and the four stroke length previously considered (see Table 4.8). The results of this study are reported in Figure 4.49. It shows that the mixing degree of the mixture improved significantly when the stroke length and the Strouhal number were increased. As we were interested in the best operation condition, and considering the criterion of low energy consumption and 90% mixing quality, the micromixer should operate with a stroke length of 10.5 (Δ_{pp}=3w/4) and a Strouhal number of 0.525 (f=6 Hz).

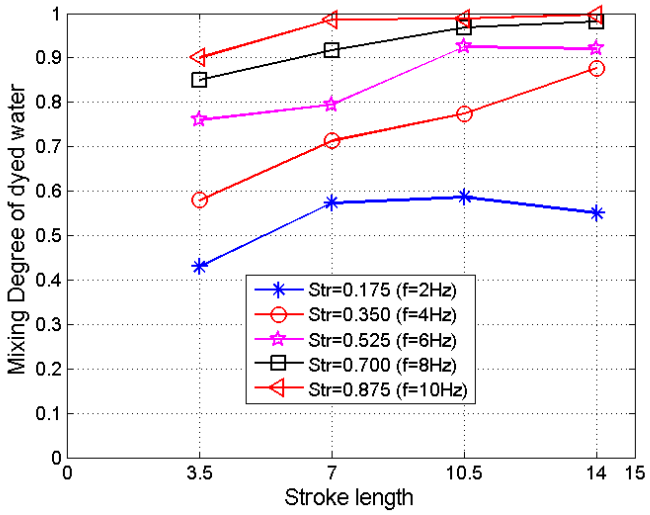

Figure 4.49 Mixing degree varying both the Strouhal numbers and the stroke length, Re=0.25, t=3-4 s.

To visually evaluate the mixing degree of the selected operating condition, the concentration contours of the liquids are shown in Figure 4.50. It shows that the numerical plane at which the mixing degree was quantified displays, qualitatively, an average concentration close to 0.5. Such a concentration distribution of the liquids, not only on the numerical plane but also along the main microchannel downstream, suggested that the synthetic jet micromixer can reach a mixing performance of 90% in just four seconds of mixing.

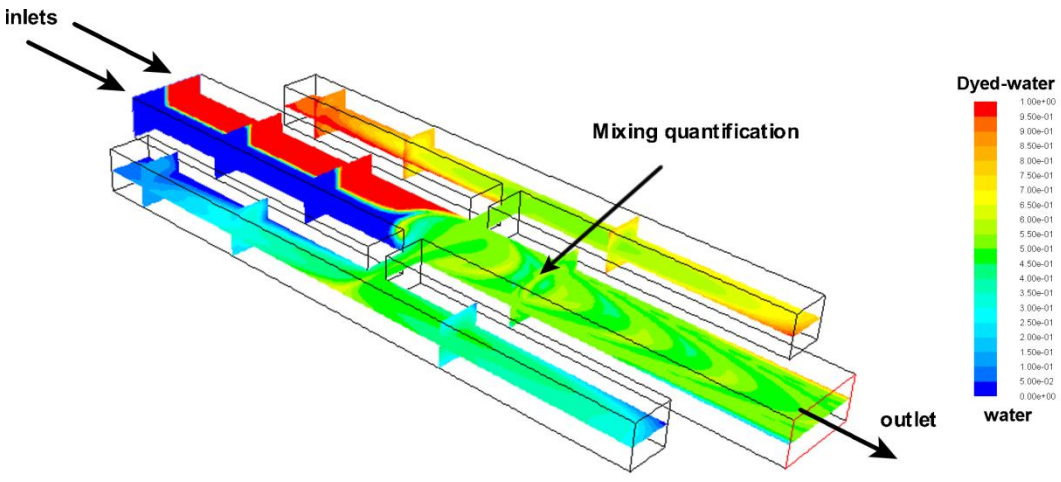

Figure 4.50 Concentration contours and numerical plane of the micromixer at which the mixing degree was determined, L=10.5 (Δpp=3w/4), Str=0.525 (f=6 Hz) Re=0.25, t=3-4 s.

4.6.6 Poincaré maps

An alternative technique to visually determine the mixing quality of a mixture is using a particle distribution technique with the aid of Poincaré maps [14], [53], [54], [55], [56]. This visualization technique is based on introducing small particles in the fluid stream to observe their path while they are driven by the main flow. In our case, the seeding of particles will be at the inlets of the synthetic jet micromixer and their trajectory of each particle was tracked to display their distribution in the synthetic jet micromixer.

To perform such visualisation, the micromixer was numerically simulated using the best operating condition (L=10.5 (Δpp=3w/4), Str=0.525 (f=6 Hz)). Hence, the distribution of the seeded particles after 4 seconds of mixing is shown in Figure 4.51. The particle distribution was fairly homogeneous along the main microchannel downstream. Interestingly, the particles representing dyed water and water did not mix while they flowed along the micromixer inlet. The particles initiate their mixing when they approached the synthetic jet orifice due to the alternative synthetic jet perturbations. Overall, an excellent distribution of the particles along the micromixer outlet is achieved, which gave further evidence of the 90% mixing quality quantified in the previous section.

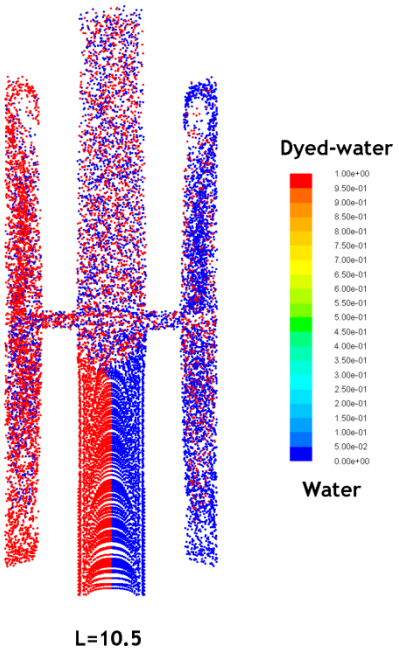

Figure 4.51 Particle distribution in the micromixer at L=10.5 (Δpp=3w/4), Str=0.525 (f=6 Hz), Re=0.25, t=4 s.

4.6.7 Mixing time

Another important parameter in microfluidics is the mixing time. In many applications, a fast mixing is often desirable. For example, in microchemical reactions the mixing time has to be in the order of a few milliseconds [4], [5]. Although the mixing time depends on the application; it is often required to be within a few seconds. For example, in DNA analysis [172].

To show how fast the synthetic jet micromixer can mix the liquid samples and achieve a 90% of mixing quality, the mixing degree of the mixture as a function of mixing time is shown in Figure 4.52. The graph shows that the mixing degree increased exponentially at early times and then it approached the asymptotic limit of unity. Therefore, present micromixer reached the mixing degree target of 90% after 2.5 seconds of mixing for a Re=0.25.

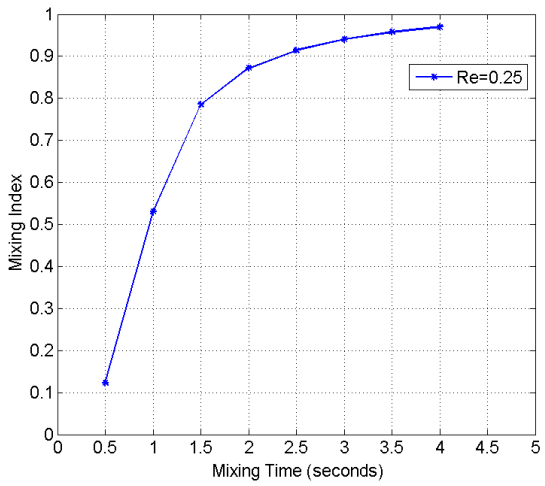

Figure 4.52 Mixing degree as a function of time of the synthetic jet micromixer, L=10.5 (Δpp=3w/4), Str=0.525 (f=6 Hz), Re=0.25.

4.6.8 Lyapunov exponent

To determine if the flow field in the micromixer was chaotic, we made use of the Lyapunov exponent. The Lyapunov exponent is often utilised to calculate the divergence of the flow in respect to its initial conditions [21], [24], and it is defined as:

$$\sigma_i\left(X, M_i\right) \equiv \lim_{\substack{t\to\infty \\ |dX|\to 0}} \left[\frac{1}{t}\ln\left(\frac{|dx|}{|dX|}\right)\right] \tag{4.2}$$

where $|dX|$ is the vector length at the initial condition of a particle, $|dx|$ represents the length of such a vector at time t and M_i is the corresponding orientation of the vector. An interesting fact of equation (4.2) is that if the initial condition $|dX|$ and the "final" condition $|dx|$ have the same value; the Lyapunov is 0. On the other hand, positive values indicate a chaotic behaviour whilst zero values indicate non-chaotic flow behaviour.

To determine the Lyapunov exponent in the micromixer, we displayed first the streamlines in the micromixer to visualise their pattern (see Figure 4.53).

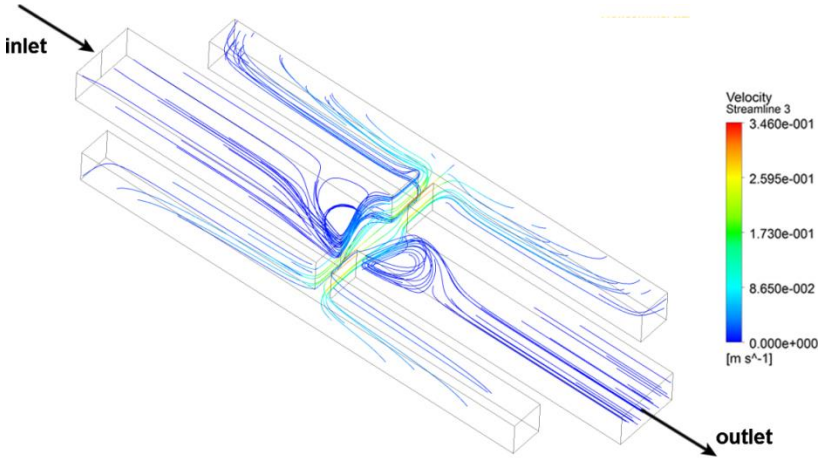

Figure 4.53 Velocity streamlines in the synthetic jet micromixer

To calculate the Lyapunov exponent, the path of a single particle was considered as shown in Figure 4.54. The Lyapunov exponent was calculated considering the change of the y co-ordinate of the particle. It is worth mentioning that the particle positions were selected at locations where the divergence of the flow is large with respect to the y co-ordinate. Then, with such co-ordinate values, the Lyapunov exponent was determined.

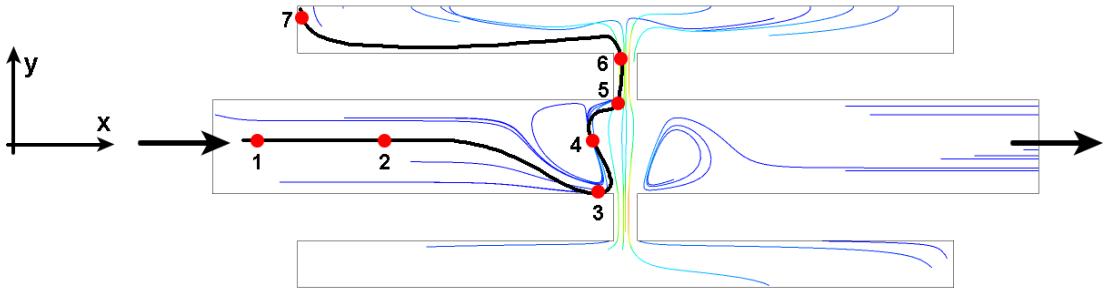

Figure 4.54 Particle trajectory to determine the Lyapunov exponent.

Figure 4.55 shows the calculated Lyapunov exponents at the seven different positions of the particle considered. Overall, the positive values of the Lyapunov exponent suggest that the particle experiences chaotic behaviour. When the particle moves from position two to three, for example, the Lyapunov exponent increases to a value of about 2.2, which means that the particle path is chaotic. The particle continues displaying chaotic behaviour when it displaces towards position four, five, six and seven (see Figure 4.54). Interestingly, when the particle goes from position three to four, the Lyapunov exponent is zero. This is due to the fact that the particle returned to its initial position (position 1) with respect to the y co-ordinate.

In addition, when the particle displaces from position one to two, the Lyapunov exponent is zero. This indicates that the path of the particle was not chaotic, as seen in Figure 4.55. Notice that the particle trajectory was along the x co-ordinate and did not diverged from it leading to zero value of the Lyapunov exponent.

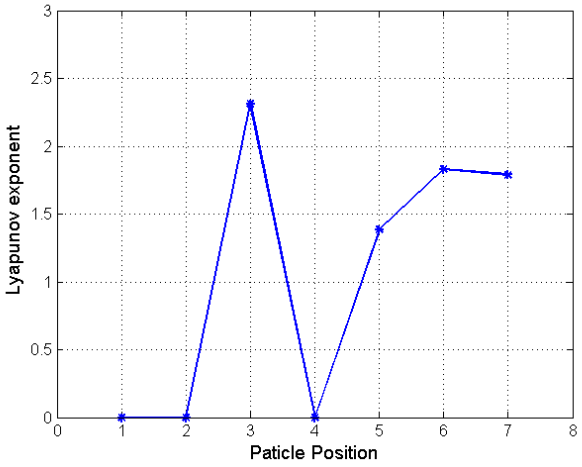

Figure 4.55 Lyapunov exponent of the trajectory of a single particle in the micromixer.

4.6.9 Practical application of the synthetic jet micromixer

The good mixing performance of the optimized micromixer with synthetic jets is promising for mixing enhancement in microchannels but its practical application may not be very promising. The reason for this is due to the challenging task of finding an actuator in the current market. The actuator should meet some requirements like small size, easy control, low power consumption, high actuation force and low heat release.

The more promising actuators are the ones based on the piezoelectric principle. However, the force that they can deliver is proportional to their size. Moreover, even if an available piezoelectric actuator meets the force requirements, it often does not fulfil the peak-to-peak displacement to operate a synthetic jet micromixer. Another possible inconvenience is the fact that a piezoactuator generates a considerable amount of heat due to the power supply needed to operate them. Temperature increases are not a desirable variable in most of microfluidics processes, especially in processes involving living cells or organic samples applications [7], [109].

Therefore, at the time this thesis was written, these disadvantages of the micromixer with synthetic jets limit its implementation in practice. Hence, we should find an alternative way to address the mixing issue in microdevices. Keeping in mind all those concerns and difficulties, in the next chapter we proposed a new micromixer design which does not require any sort of mechanical actuation to promote mixing.

4.7 Concluding remarks

In this chapter, we investigated mixing enhancement with synthetic jets at two typical Reynolds numbers found in microdevices (Re=0.5, 0.25). Several mixer designs were proposed in order to develop a simple but effective micromixer with synthetic jets. The conclusions of such a process are as follows:

- **Macromixer with four and two pairs of synthetic jets**

The chapter started with the study of a macromixer design proposed for mixing enhancement at Re=0.5. This approach was taken due to the difficulties encountered to manufacture a micromixer. The configuration of the first macromixer consisted of four pairs of opposite synthetic jets. The quantification of the quality of the mixture showed that increasing either the stroke length or the Strouhal number significantly improved the mixing of the liquids samples. To reach the mixing quality target of 90%, the synthetic jets had to be operated with an actuation displacement of 2.0 mm and a frequency of 8 Hz.

Considering that the mixing volume was considerably large in the mixing area of the previous macromixer, an improvement was proposed which consisted in reducing such a mixing volume. The modification consisted mainly in the reduction of the number of synthetic jet pairs and the cavity size. In terms of the mixing performance of the improved macromixer, it was shown that it was possible to mix two liquid samples at Re=0.5 with just two pairs of opposite jets with a reduced and symmetric cavity size. The quantification of the mixture indicated that a 90% mixing quality was also possible to achieve with the modified macromixer. Interestingly, the operation conditions to reach that mixing degree were the same as for the macromixer with four pairs of opposite jets: an actuation displacement of 2.0 mm and frequency of 8 Hz. Although these parameters coincided in both macromixers, the stroke length and Strouhal number did not. The reason for this was due to the difference in the cavity size.

- **Macromixer with one pair of synthetic jets**

Due to the good mixing performance achieved with the macromixer with four and two synthetic jets, an additional macromixer with one pair of synthetic jets was proposed in order to further simplify the previous macromixers. The main

improvements consisted in simplifying the channel geometry, the moving frame and the channel inlet configuration.

The mixing degree was also improved significantly when increasing the stroke length and the Strouhal number. The best operating condition to reach 90%mixing quality was very close to the operating conditions found in the macromixers with four and two pairs of synthetic jets. It was reached by actuating the synthetic jets with a peak-to-peak displacement of 1.5 mm and frequency of 6 Hz which meant 2 Hz and 0.5 mm lower than the previous macromixers. The selection of this operating condition was based on the criterion of using the minimum energy consumption of the electromagnetic actuator.

In order to have a better understanding of the mixing process taking place in the micromixer at the best operating conditions, we looked further into the fluid pattern inside it. The streamlines and the velocity vectors suggested the formation of vortical structures in the main channel, which were attributed to the actuation of the synthetic jets. Such vortical structures played a crucial role in enhancing mixing due to the alternative recirculation of the fluids that they produced.

The main objective of this chapter was to study a micromixer from the macroscale point of view. This was proposed to find the optimal and simplest geometry and the operating conditions to reach 90% mixing quality. Once the macroscale mixer was optimised, we proceeded to scale it down to have a micromixer. The results of the scaled micromixer showed that the mixing performance of the macro and micro mixers were dramatically different. The difference was about 58% less mixing degree for the micromixer. Therefore, we conclude that it is not possible to study a micromixer from a macroscale point of view.

- **Optimised micromixer**

To address the poor mixing performance of the scaled down micromixer, two minor modifications were made to the geometry. Synthetic jet cavities were enlarged 7 times the channel width and the synthetic jet orifice size was reduced to a quarter of the microchannel width. With the geometry changes, the mixing performance of the micromixer was enough to reached 90% mixing quality, operating it at L=10.5 (Δ_{pp}=3w/4) and Str=0.7 (f=8 Hz).

Such a mixing performance was also qualitatively verified with Poincaré maps to visualise the distribution of small particles in the flow and verify possible unmixed zones. The good distribution of the particles confirmed the 90% mixing quality. Additionally, the Lyapunov exponent was also calculated to verify if the flow inside the synthetic jet micromixer was chaotic. The positive Lyapunov exponents, determined for a single particle, indicated that the flow inside the micromixer is chaotic. This is another factor that contributes to the good mixing performance of the synthetic jet micromixer.

Chapter 5

Micromixer: A multiphase approach

5.1 Introduction

In the previous Chapter, we have demonstrated that it is possible to mix liquids in microchannels using a micromixer with synthetic jets. Although the outcome regarding mixing enhancement is very promising with such a micromixer design, it has several limitations. For example, the difficulty of finding a suitable actuator to produce the synthetic jets.

In an attempt to address the limitations of the synthetic jet micromixer and simplify its design, we introduce another approach for mixing enhancement in this chapter. It consists of making use of a multiphase flow and the surface tension that takes place between miscible and immiscible phases to enhance mixing. With this new mixing technique, we intend to show that it is possible to mix highly viscous liquids ($Re<1$) by having a simple microchannel geometry and without using any external source of energy to mix the liquid samples effectively. Another feature of this method is that a control system is not required at all.

In regards to mixing enhancement, the aim of this chapter is directly related with the main goal of this thesis, which is to design a simple but effective micromixer with a view to practical application in numerous disciplines. The way we intend to achieve this aim is by designing a micromixer which can mix liquid samples in a microchannel with a simple design. Therefore, we propose a micromixing device where

two liquid samples flow alongside each other while they mix. The mixing principle of the multiphase micromixer takes advantage of the geometry configuration and the surface tension, acting on the liquid-gas interface. The study was performed entirely by using numerical simulations, which were validated as discussed in Chapter 3. The excellent mixing performance achieved with this micromixer, with a mixing degree above 90%, is very promising and a follow-up experimental study would be beneficial.

5.2 Definition of the problem

The main problem in a micromixer is the poor mixing performance at low Reynolds numbers (Re<1). A new approach is proposed in this section to address this. First, we need to define what the desirable characteristics of an "*ideal*" micromixer are. The first desirable feature is that it has to be easy to control and manufacture. The second characteristic is that the micromixer has to be effective and efficient to mix liquid samples.

Keeping in mind the aforementioned features, we propose a micromixer with a simple geometry, shown in Figure 5.1. It consists of a main rectangular microchannel with two cavities at each side of it, which are connected by a transverse microchannel.

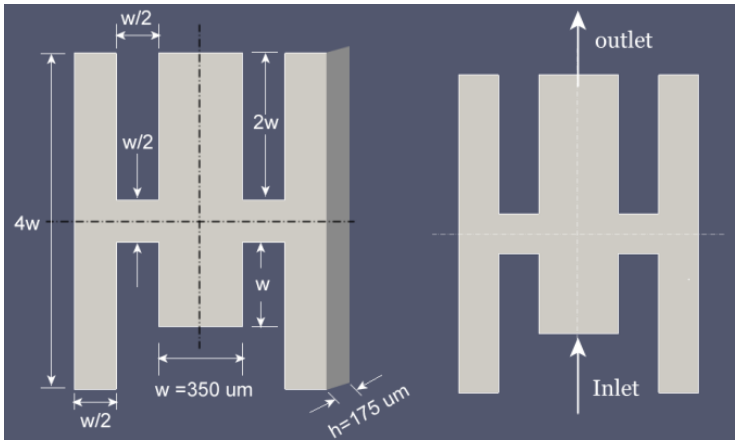

Figure 5.1 Geometry of the multiphase micromixer.

The micromixer consists of a geometry similar to the one used in the synthetic jet micromixer, but with several changes to the dimensions. The difference in dimensions is mainly on the synthetic jet orifices and cavities. In the multiphase micromixer, the orifice is slightly larger than in the optimised micromixer with synthetic jets, which is w/2 rather than w/4. Meanwhile, the cavity length was reduced from 7w

to 4w. The dimensions of the main cross-section of the microchannel were not changed; the microchannels width (w) and height (h) were kept 350 μm and 175 μm respectively, see Figure 5.1.

In order to achieve the desired Re of the fluids that will be mixed in the microdevice, only two parameters could be varied: the dynamic viscosity, μ and the mean velocity U_{mean} of the fluid. For simplicity, only one parameter was varied: the main fluid velocity.

In terms of the working fluid, water is selected in all the numerical simulations with the following properties:

- Dynamic viscosity = 0.001003 Pa·s
- Density = 1000 kg/m^3
- Surface tension between water and air = 0.072 N/m^2
- Diffusivity of the miscible phases = 2.23x10^{-11} m^2/s

As previously discussed in Chapter 4, the typical diffusivity values of liquid samples in microfluidics are D=10^{-10} and D=10^{-12} m^2/s [49], [71], [157], [113]. Therefore, in order to test the multiphase micromixer, a mean value of this diffusivity range was chosen, which was D=2.23x10^{-11} m^2/s.

- Another fluid property of considerable importance is the surface tension coefficient. As we are considering the fluid phases of water and air, the value of the surface tension of the interface of such phases is 0.072 N/m at 20 °C [173], [174], which is also set in the numerical simulations.

5.3 Numerical method

To investigate the mixing performance of the multiphase micromixer, a systematic number of numerical simulations are required. Due to the nature of this new micromixer design, the previous software used (ANSYS Fluent 14.0 [166]) does not fulfil the requirements for carrying out this sort of numerical simulation. The issue with such software is that it does not have a solver to simulate the mixing process in a multiphase setting. After an exhaustive search for a suitable Computational Fluid Dynamics (CFD) software that fulfils the previous requirements, the open source

software called OpenFOAM 2.3.1 was selected because it has a suitable solver for carrying out the numerical simulations of the proposed multiphase micromixer.

The numerical solver used to simulate the micromixer is the *interMixingFoam* from OpenFOAM 2.3.1. This solver is suitable to simulate three incompressible fluids, two of them miscible and the third one immiscible. The volume of fluid method (VOF) is also coded in this solver to capture and track the fluid interface between the miscible and the immiscible fluids [175]. Hence, the solver *interMixingFoam* from OpenFOAM 2.3.1 is used to investigate the mixing performance of the multiphase micromixer.

5.4 Fluid domain

To be able to simulate the proposed micromixer numerically, it is essential to define the numerical fluid domain. The whole fluid domain of the micromixer arrangement includes two separated channel inlets, the confluence section, the mixing zone and the microchannel outlet. All of these components of the micromixer are included in a real case. Nevertheless, the simulation of the whole fluid domain would be computationally expensive and time consuming. Therefore, only the section of interest will be simulated, which is shown in Figure 5.2.

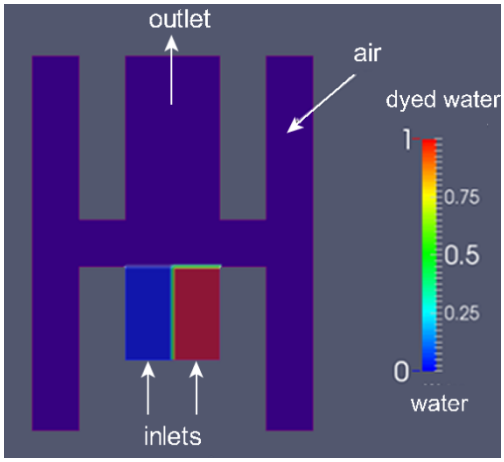

Figure 5.2 Initialisation of the fluid phases within the fluid domain.

In order to simulate the micromixer, the correct boundary conditions have to be set for the fluid domain which are:

- A non-slip-boundary condition and a constant contact angle of 60° on all the walls of the fluid domain are defined.

- A constant flow velocity is set at the channel inlet.
- The *inletOutlet* boundary condition is selected at the channel outlet. The reason for this is because air is taken in and expelled in the main microchannel when the working fluid flows through the microchannel.

The fluid initialisation is another important setting required before performing the numerical simulation. In other words, the fluids inside the fluid domain have to be defined. Considering that the multiphase flow simulations require a considerable amount of computational time, the fluid in the micromixer is defined as shown in Figure 5.2. Dyed water and water are initialised along the microchannel inlets. Meanwhile, air is defined in the rest of the fluid domain. To execute the fluid initialisation in OpenFOAM, the *setFields* library was used.

5.5 Contact angle

In an attempt to simulate the liquid and gas phases within the microchannel as close as possible to reality, a contact angle value between the liquid-solid-gas interfaces is required. In this work, it is assumed that the micromixer is fabricated using ordinary glass. Therefore, the dynamic contact angle formed by the liquid phase (water) and the gas phase (air) on such material is 60° [176]; this contact angle value is included on all the boundary conditions denoted as walls in the numerical simulations.

5.6 The effect of gravity in the micromixer

To verify if the force of gravity can be neglected or not in the numerical simulations of the multiphase micromixer, we will determine the Bond number (Bo). The Bond number indicates the relative importance of the force of gravity of the working fluid of a microfluidic device and it can be neglected if $Bo \leq 10^{-3}$ [177]. The Bond number is determined as:

$$Bo \equiv \frac{L^2}{ls^2} \tag{5.1}$$

where L^2 is the characteristic length, in our case it is the diameter of a droplet which is approximately 350 μm and ls^2 is the characteristic length scale of the microchannel, which is calculated as follows:

$$ls^2 = \sqrt{\frac{\gamma}{\rho g}} \tag{5.2}$$

where γ is the surface tension of the liquid phase (water), ρ is its density and g is the acceleration due to gravity. Considering that the working fluid is water, the value of the surface tension is 0.073 N/m [173], [174], the water density as 1000 kg/m^3 and the acceleration of gravity g equal to 9.81 m/s^2, giving a characteristic length scale 2.68 mm. Substituting this value in equation (5.1) gives a Bond number of 0.0169. This calculated Bond number of the multiphase micromixer is higher than a value of 0.001, which suggests that the force of gravity has to be considered in all the numerical simulations.

5.7 Mixing performance of the multiphase micromixer

To evaluate the mixing performance of the multiphase micromixer at the typical Reynolds numbers found in microfluidics devices (Re<1), three scenarios are proposed: Re=1.0, 0.5 and 0.1 (see Table 5.1). These three cases are considered in an attempt to cover the range of Re found in microfluidic devices (Re<1).

Table 5.1 Reynolds numbers to evaluate the mixing performance of the multiphase micromixer.

Case	Reynolds number
1	1.0
2	0.5
3	0.1

5.7.1 Concentration contours

In order to demonstrate the effectiveness of the multiphase micromixer, we display the concentration contours of the three cases in Figure 5.3. For simplicity, only

the top view of the micromixer is shown. The green colour, observed in the form of a droplet downstream, indicates a concentration value of about 0.5. In other words, the fluid in the droplet is made up of approximately 50% dyed-water and 50% water, which suggests that the miscible phase is fully mixed.

If a comparison is made between the three Reynolds numbers shown in Figure 5.3, we can observe that a larger droplet is formed when Re=1.0. This result is due to the fact that the liquid phase has a larger velocity in such a case when compared to the other two cases. Another interesting finding is that the fluids seem to pre-mix before crossing the transverse microchannel, particularly at Re=0.1.

This qualitative assessment suggests that a very good mixing of the liquids is achieved at the three Reynolds numbers tested. In a later section, the mixing degree will be quantitatively determined to know how effective this micromixer is in terms of mixing enhancement at Re<1.0.

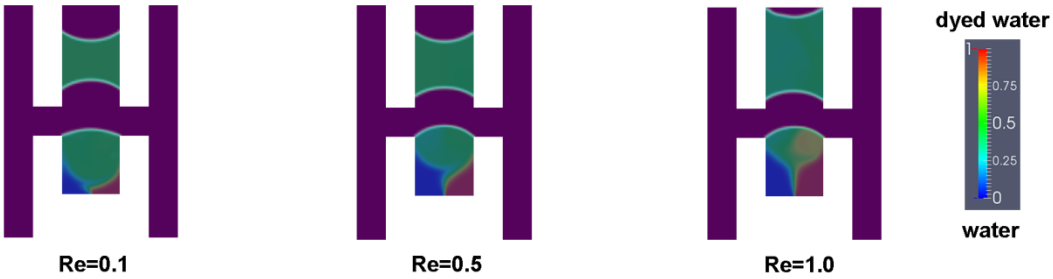

Figure 5.3 Concentration contours of the fluids, Re=0.1, 0.5, 1.0.

5.7.2 Time sequence of the concentration contours at Re=0.5

To have a better understanding of the mixing process inside the microchannel, a time sequence of images is shown in Figure 5.4. At a time of 0.100 seconds, the fluids to be mixed start to form a droplet when they reach the transverse orifice. While they are forming this droplet, the liquids appear to stir up, which enhances mixing indicated by the change in concentration. When the time progresses to 0.120 s, the fluids try to fill the right cavity. This fluid displacement occurred suddenly due to the surface tension force and the capillary effect taking place in the microchannel. During this time frame, the fluid interface stretches and folds allowing the mixing enhancement of the fluids.

At t=0.150 s, the liquids are displaced to the opposite cavity due to the increase of pressure in the right cavity causing the stretching and folding of the fluids. Notice that at this stage, some liquid has crossed the transverse channel and it is there, where the liquid starts its segmentation to form a droplet. In the next image, at a time of 0.160 s, the segmentation of the fluids starts to become more evident and the fluid interface is stretched in the transverse channel due to the motion of the droplet downstream. Interestingly, the segmentation of the liquids seems to enhance mixing, to a great extent, due to the continuous stretching and folding of the fluid interface (liquid-gas). Finally, at t=0.170 s, the miscible phase is segmented while another droplet starts to be formed in the transverse microchannel. This process then starts all over again.

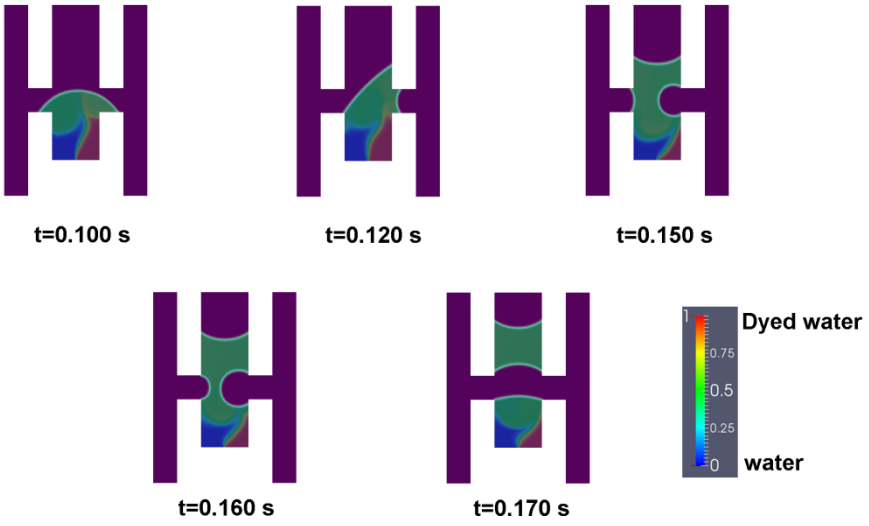

Figure 5.4 Time sequences showing the concentration contours of dyed water, Re=0.50.

5.7.3 Velocity vectors

To have a better understanding of the behaviour of the fluid interface formed by the gas-liquid phases, we now look at the fluid concentration and the velocity vectors in the micromixer. These are shown in Figure 5.5 at t=0.160 s. The magnitude of the velocity vectors suggests that the gas phase experiences higher velocity rather than the liquid phase.

Considering the gas phase, the velocity vectors show two recirculating zones close to the liquid-gas-solid interface (Figure 5.5b). That is why the velocity vectors are oriented in all directions. It is important to mention that the velocity vectors seem to go through the walls of the micromixer. However, that is not the case because they are only

indicating that the velocity of the fluid is significantly high at that very location. They do not suggest that the gas phase crosses the walls. Moreover, the recirculating zones are generated due to the fact that the liquid phase tends to keep its shape (meniscus) while it is moving downstream. This constant motion leads to the stirring of the liquid phase that improves the mixing of the liquid samples as a consequence.

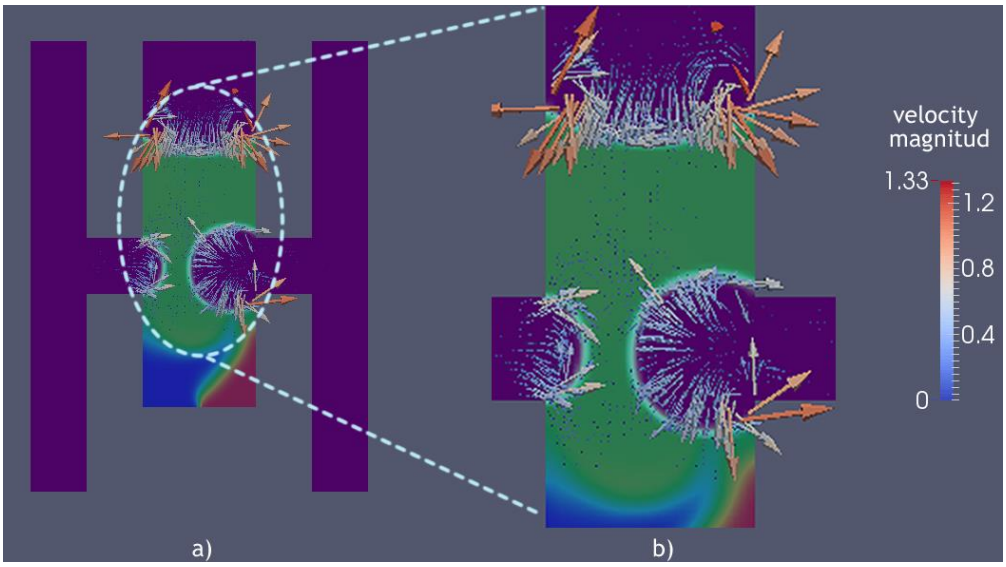

Figure 5.5 Velocity vectors close to the liquid-solid-gas interface, Re=0.5, t=0.16 s.

5.7.4 Pressure contours

To investigate the pressure change inside the microchannel due to the motion of the liquid phase, the pressure contours of the 3D micromixer domain are shown in Figure 5.6 at three different moments in time. Since we are working with a multiphase flow, the liquid phase is represented with a blue colour and the gas-phase is indicated in red. It is important to specify that the representation of the pressure in OpenFOAM 2.3.1 is not the total pressure but the pressure over the density of the respective fluid phase and is measured from a reference pressure value of zero.

From Figure 5.6a, the pressure contours show that the right cavity presents the highest pressure in the micromixer, reaching a pressure value of about 360 Pa at t=0.15 s. The increase in pressure of the right cavity is due to the attempt of the fluid to fill it. Interestingly, when time progresses to 0.16 seconds (Figure 5.6b) the maximum pressure takes place in the left cavity (opposite cavity). This occurs because the higher pressure of the gas phase from the right cavity pushes the liquid phase towards the left cavity. This

change in the pressure of the cavities stretches and folds the fluid interface considerably, which leads to mixing enhancement, as we have already discussed.

However, when the simulation progresses to 0.17 seconds, the liquid phase flows downstream with a higher velocity than the fluid at the inlet, which produces its segmentation. This segmentation leads to the formation of a liquid droplet with a well-defined meniscus up and downstream. This segmentation effect allows the gas phase to occupy the two cavities without being blocked by the liquid phase, leading to a lower pressure value. The process is repeated when the next droplet is formed.

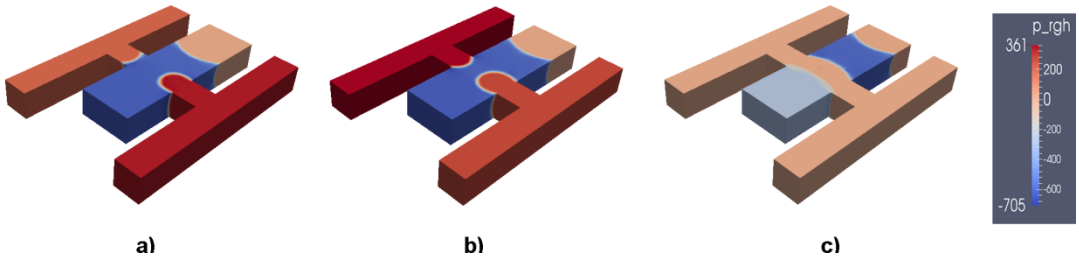

Figure 5.6 Pressure contours of the air-phase and liquid-phase at three instants in time, a) t=0.15 s, b) t=0.16 s and c) t=0.17 s, Re=0.5.

5.7.5 Mixing quantification

The quantification of the mixing degree is determined using the concentration of dye-water taken across a plane in the main microchannel. The distance of the quantification was just 350 μm from the transverse channel downstream (see Figure 5.7a). The mixing degree as a function of the Reynolds numbers tested, are shown in Figure 5.8. Remembering that a mixing degree of 0.9 represents complete mixing, it is clear that this mixing degree is achieved at Reynolds numbers 0.1 and 0.5 for the first droplet formed in the microchannel. At Re=1.0 the mixing degree was about 0.87, which is below the 0.9 mixing target. This slightly lower mixing degree is attributed to the main flow velocity of the liquid samples due to the higher Reynolds number. Nevertheless, this apparent poor mixing was improved in the second droplet where the mixing degree of approximately 0.95 was measured in the three cases considered.

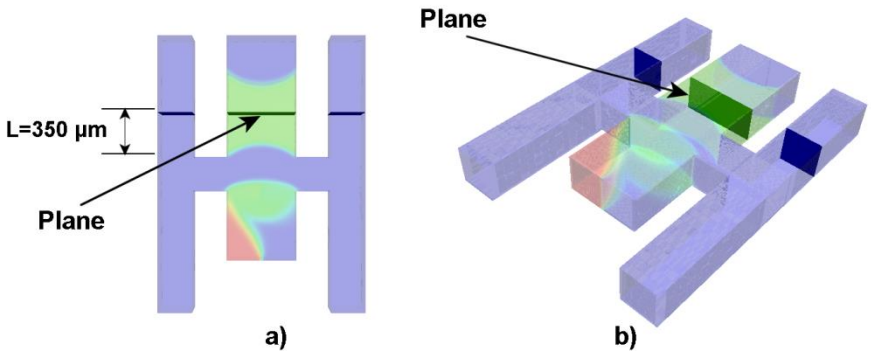

Figure 5.7 Plane at which the mixing degree was quantified: a) top view and b) isometric view of the micromixer.

Additionally, the lower mixing degree quantified in the first droplet is mainly due to the fact that the liquids to be mixed were initialized just before the transverse microchannel (see Figure 5.2). This assumption did not accurately represent the fact that when the liquids approach the transverse channel, they are partially pre-mixed while trying to flow through the main channel. This pre-mixing further improves the mixing degree from 0.92 to 0.95 in the second droplet, as shown in Figure 5.8.

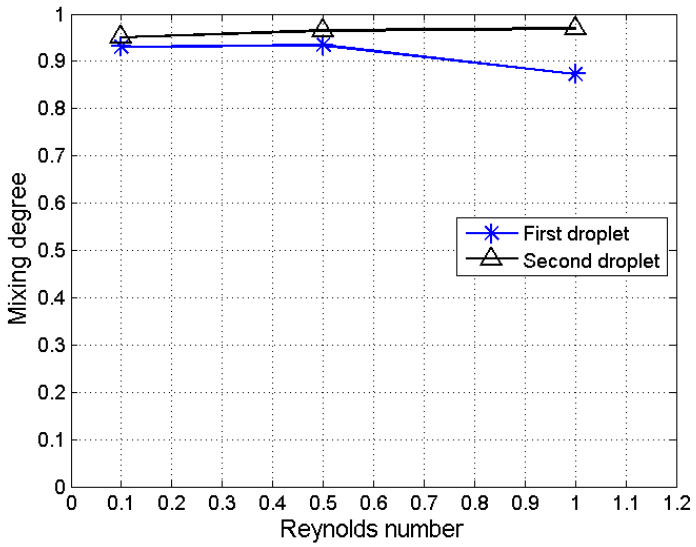

Figure 5.8 Mixing degree as a function of the Reynolds numbers.

5.7.6 Concentration contours across the microchannel

The concentration of dyed water across the cross-section of the formed droplets is displayed in Figure 5.9. At the initial conditions (no mixing), a step up in the concentration in the middle of the channel is shown, meaning that half of the

microchannel is occupied by dyed water $(c_i = 1.0)$ and the other half by water $(c_i = 0.0)$.

However, as mixing takes place the concentration tends to reach a value of 0.5 across the microchannel. It is worth mentioning that with each case, these concentration profiles were obtained across the droplets formed downstream. Therefore, the concentration profiles give evidence of the excellent mixing quality of the final mixture.

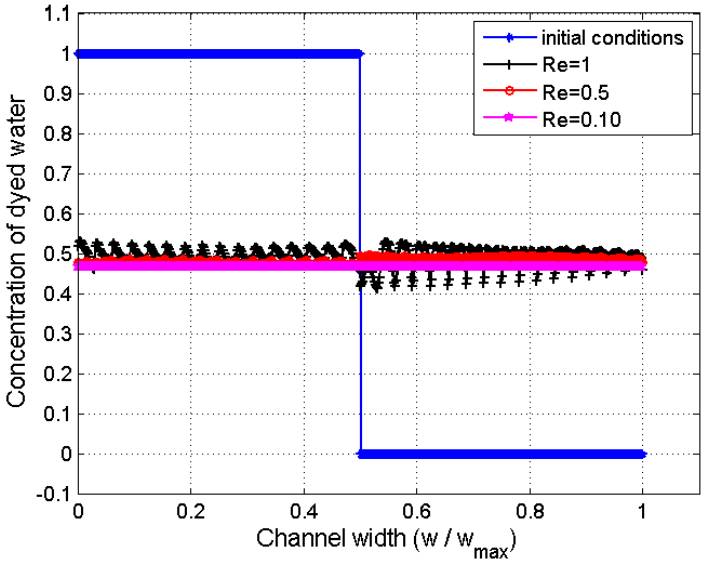

Figure 5.9 Concentration profiles across the microchannel at one channel width from the orifice downstream, Re=1.0. 0.5, 0.1.

5.7.7 Mixing length and mixing time

As we have stated in previous chapters, the mixing time and distance are crucial parameters in a micromixer device. This is because of the limited availability of the liquid samples, which suggests that mixing should take place at short distances and within a time range of a few seconds.

Regarding the mixing distance of the multiphase micromixer, the multiphase micromixer mixed effectively the liquid samples within one channel width (w=350 μm) from the transverse channel downstream. On the other hand, the mixing time is also an important variable when mixing in microdevices. The mixing time required to mix efficiently in the multiphase micromixer was just 0.170 seconds for the first droplet at Re=1.0. This significant fast mixing suggests that the multiphase micromixer has potential for applications where rapid mixing is needed.

5.8 The flow segmentation issue

As we have discussed in section 5.7 of this chapter, the working principle of the multiphase micromixer is based on segmenting the fluids to mix into droplets. We have seen that they are produced by forcing the fluids through two opposite cavities, leading to the stretching and folding of the fluid interface which significantly enhances mixing. When the first droplet moves towards the channel outlet, another droplet starts to be produced in the cavities area. When the second droplet forms, it also flows downstream and the process continues over and over again.

However, the segmentation of the fluid might not be desirable in microfluidic applications, where a continuous flow is often required to perform analysis. The microfluidic user needs a continuous flow of the already mixed fluids and not a segmented flow in the form of droplets. Therefore, in an attempt to fulfil this requirement, the segmentation issue is addressed by making a very simple modification at the channel outlet of the micromixer.

The micromixer modification consists of adding an additional outlet to the current micromixer design, as shown in Figure 5.10. Notice that the second microchannel outlet (outlet 2) is connected to the original outlet (outlet 1) downstream to avoid any interference in the mixing area. The remarkable feature of this solution is that there is no need to use any external energy source to pump the liquids (droplets) towards outlet 2. The fluids are pumped simply by taking advantage of the capillarity phenomenon [2].

It is worth mentioning that the boundary condition set in outlet 2 is the same as the one set in outlet 1: the *inletOutlet* boundary condition. This setting allows, as we already mentioned in section 5.4, the gas phase (air) to be ingested and expelled when the liquid phase is in motion inside the micromixer, just as in a real scenario.

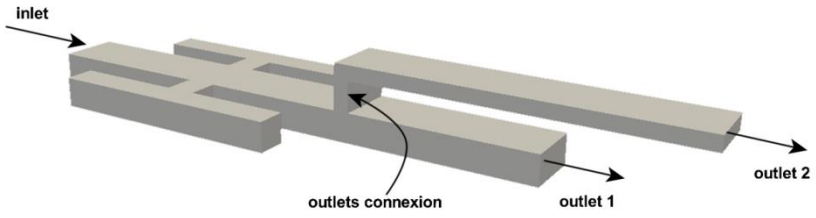

Figure 5.10 Modification of the multiphase micromixer to solve the segmentation issue.

To demonstrate that the flow segmentation issue is solved with an additional channel outlet, a time sequence of images of the evolution of the miscible and immiscible phases in the micromixer are shown next. Figure 5.11, for example, shows a droplet approaching the intersection between the two channel outlets and starts to flow upwards by capillarity. Notice that the liquid adjusts its shape to fill the vertical microchannel. This effect also stretches and folds the fluids interface which may cause further mixing to the already mixed droplet.

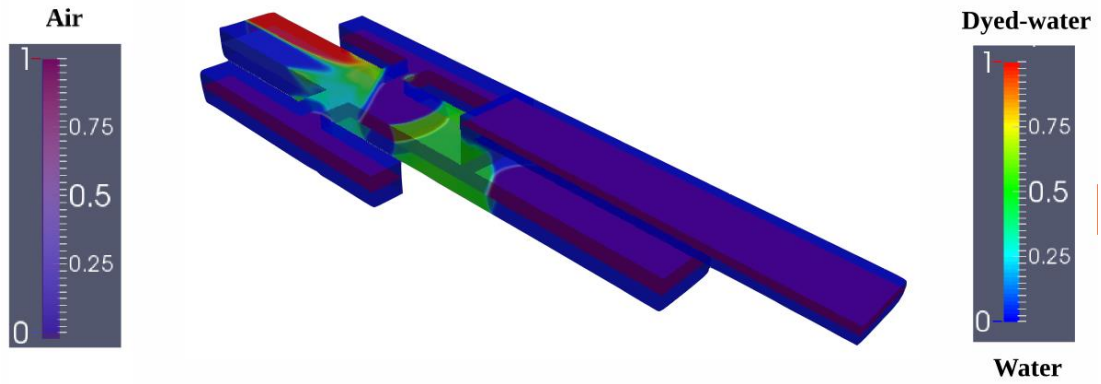

Figure 5.11 The first droplet approaching the vertical microchannel, t=0.21 s, Re=1.0.

In the next time sequence shown in Figure 5.12, almost half of the droplet is pumped towards outlet 2. The stretching of the droplet is fairly large and it occupies both channel outlets at this moment in time (t=0.22 s). Interestingly, the miscible phase is attached to one side of the upper channel in its attempt to fill it. The stretching effect continues for another 0.03 seconds until the droplet completely fills the upper channel, as seen in Figure 5.13. The miscible phase remains in this position until the next droplet is also pumped, as shown in Figure 5.14.

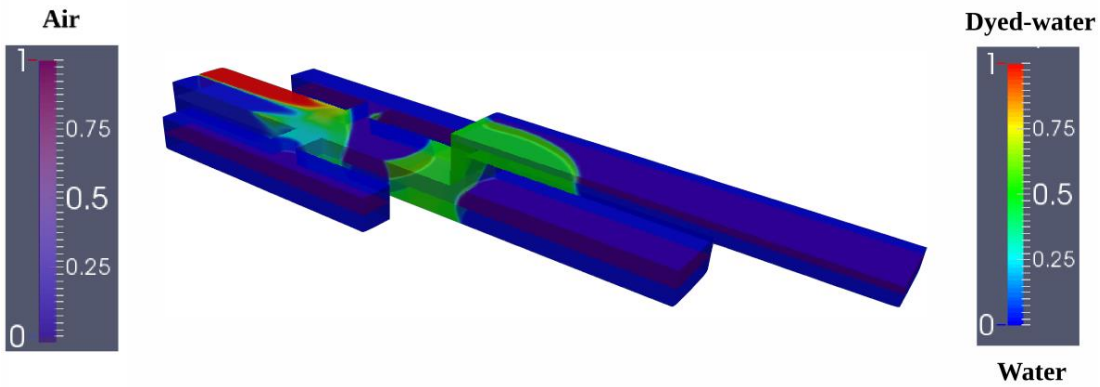

Figure 5.12 Pumping of the droplet by capillarity action at t=0.22 s, Re=1.0

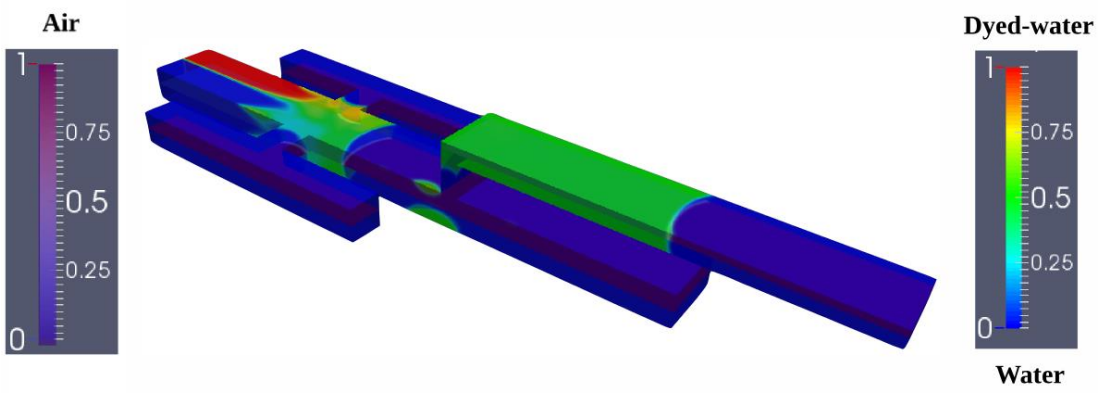

Figure 5.13 Droplet pumped to the channel outlet 2, t=0.25 s, Re=1.0.

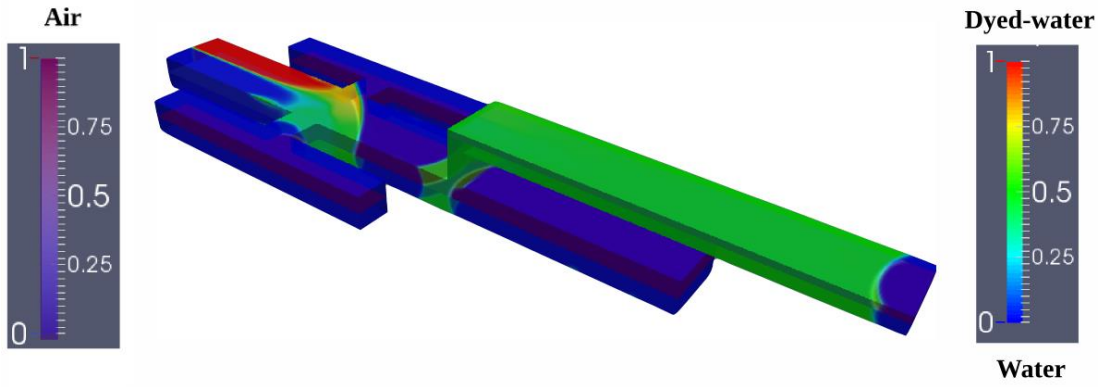

Figure 5.14 Merging of the two liquid droplets, t=0.355 s, Re=1.0.

One interesting point is that the pumping of the miscible phase is considerably fast. It takes only 0.05 seconds to completely pump one droplet from one channel outlet to the other. Additionally, the amount of time for pumping and merging two droplets is about 0.355 seconds in the multiphase micromixer.

In order to verify if the mixing of the two merged droplets improved when pumping them from one channel outlet to the other, the quantification of the mixing degree was computed. A mixing degree of 0.9943 was determined at the middle length of the channel outlet 2. This excellent mixing quality indicates that the pumping effect not only merges the segmented flow, but also improves the mixing degree by approximately 4-5% of the already mixed droplets, reaching 99% mixing quality.

The remarkable fast mixing and high mixing degree quantified in the multiphase micromixer make it an efficient micromixer with promising practical applications in most microfluidic devices.

5.9 Limitations of the multiphase micromixer

The mixing performance of the multiphase micromixer is very effective at Reynolds numbers below one. However, very specific microfluidics applications may require mixing above this Re range. For example, in electrokinetic applications, the Reynolds numbers are in the range of 1 to 10 [178], [179]. Hence, in order to investigate the mixing performance of the multiphase micromixer for Reynolds numbers above one, two cases were numerically simulated with Reynolds numbers at 2.0 and 5.0.

It is worth mentioning that the numerical simulation to perform this test on the multiphase micromixer only considers the fluid domain without the modification discussed in the previous section. This is because we are interested on evaluating mixing in the main mixing zone and not at the channel outlets.

The results of the concentration of the fluids at Re=2.0 for the first and second droplet produced in the micromixer are shown in Figure 5.15. Notice that a larger droplet forms due to the increase in the Reynolds number. A visual assessment suggests that the flow segmentation seems to be reduced due to the higher velocity of the liquid phase. In terms of the mixing quality, a qualitative evaluation indicates that mixing is not homogenous in both droplets as in the case of Re<1. It is evident that there are still unmixed liquid in both droplets. This is confirmed when the quantification of the mixing degree of the mixture is performed, giving 0.83 and 0.76 for the first and second droplet respectively. These results lead us to conclude that the effectiveness of the multiphase micromixer slightly decreases at a Reynolds number of 2.

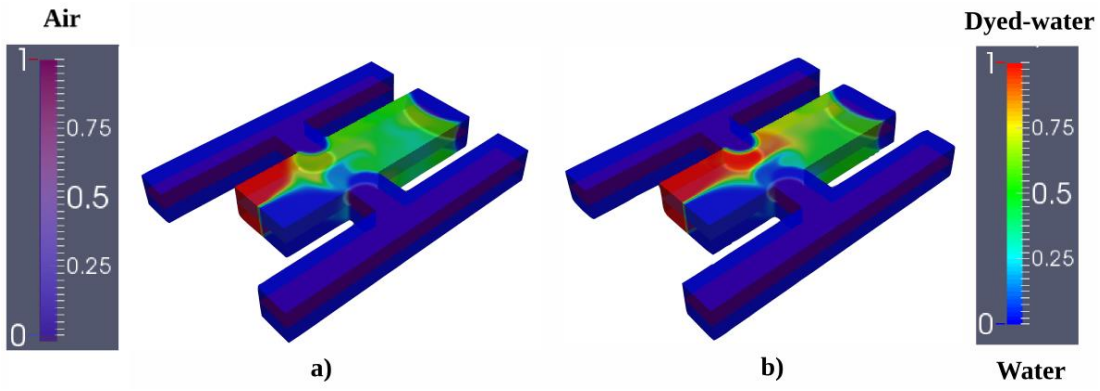

Figure 5.15 Concentration contours in the multiphase micromixer for a) first droplet and b) second droplet, Re=2.0.

The concentration contours of the first and second droplets are displayed in Figure 5.16 for the second case investigated, where Re=5.0. In this case, the decrease segmentation rate of the fluid is more evident than in the previous case. The formation of droplets starts to be more difficult due to the increment in the velocity of the liquid phase. In Figure 5.16a, for example, the miscible phase flows through the transverse microchannel without any apparent segmentation. A similar behaviour occurs with the second droplet, Figure 5.16b, where it is also evident that unmixed liquid traces pass through the transverse microchannel, leading to poor mixing downstream.

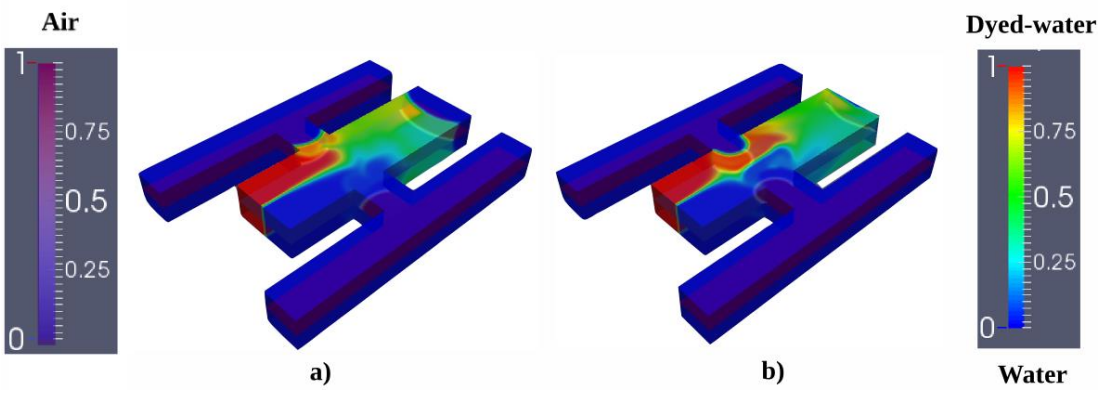

Figure 5.16 Concentration contours in the multiphase micromixer for a) a first droplet and b) a second droplet, Re=5.0.

To be certain of the mixing degree of the multiphase micromixer at Re=5.0, the mixing degree quantification was performed at the same location as in previous case s (350 μm). The results give a mixing degree of 0.56 and 0.40 for the first and second droplets respectively. This confirms that a dramatic reduction in the mixing degree takes places when the Reynolds number is increased to 5.0.

The main issue with the multiphase micromixer lies with the fact that at higher Reynolds numbers, the average velocity of the flow increases. This increment affects the capacity of the micromixer to segment the flow into liquid droplets. The liquid phase tends to form a kind of "bridge" through the transverse microchannel, which diminishes the flow instabilities that take place at Reynolds numbers below 1, causing poor mixing.

An alternative micromixer design is proposed in the next chapter to overcome the poor mixing performance of the multiphase micromixer at Re>1.

5.10 Concluding remarks

In this Chapter we have investigated numerically the mixing performance of a micromixer design based on the multiphase flow for mixing enhancement at Reynolds numbers below one using the open source code OpenFOAM 2.3.1.

The geometry of the multiphase micromixer is very similar to the synthetic jet micromixer and plays an important role in enhancing the miscible phase. In this particular micromixer design, the liquid phase stretches and folds while passing through the microchannel arrangement. This effect leads to a remarkable mixing enhancement, above 90%. Furthermore, the excellent mixing performance of the micromixer device is maintained even at Reynolds numbers as low as 0.1.

The high mixing degrees of the mixture, reached with this micromixer design, were within a very short period of time; in the order of milliseconds. Another interesting result is the one related with the distance required to mix the liquids inside the micromixer; it was just one microchannel width (w=350 μm).

The advantages of the multiphase micromixer over the synthetic jet micromixer and other micromixers reported in the literature, [13], [73], [86], [91], [95], [44], [101], [103], [130], [137], [140], are the following:

1. Simple geometry.
2. Not needing any simple or complex control system to enhance mixing.
3. Not requiring any external energy source supply.
4. No moving parts needed to operate the micromixer.
5. Short mixing time (0.17 s) and distance (350 μm) to achieve 95% mixing quality.

All the previous advantages of the multiphase micromixer fulfil the mini-aims stated in the introduction of this thesis: short mixing time, simple design, minimum energy consumption, mixing degree above 90% and a simple control system.

The excellent mixing degree delivered by the multiphase micromixer makes it a very attractive option for numerous practical applications in the area of microfluidics.

Chapter 6

Spinning Disk Micromixer

6.1 Introduction

In the previous chapter, we studied the possibility of using a multiphase flow approach for mixing in microdevices. The outcome of the study suggests that it is possible to mix two liquid samples effectively at Re<2. The quality of the mixture was above 90%, which is considered a complete mixture. Many micromixer designs were also presented which makes the multiphase micromixer a potential solution for mixing enhancement in microfluidic applications. Nevertheless, the multiphase micromixer has some limitations; one of them is that it cannot mix effectively at Re>2.

In this Chapter, we will investigate another micromixer design as an alternative for mixing liquid samples, with a broader range of Reynolds numbers found in microfluidic devices. Typical Reynolds numbers in microfluidics are between 10^{-6} and 1.0 [38], [1], [39]. However, there are other applications where the Re is higher. For example, in electrokinetic studies, the Reynolds number varies between 0.1 and 10. Mixing is also required in electrokinetic applications for enhancing the mixing of solutions [178], [179].

The chapter starts with the description of the working principle behind the spinning micromixer design as well as the numerical method and boundary conditions needed to simulate it. In order to demonstrate that poor mixing takes place in a straight microchannel, numerical simulations are carried out first. After this, the spinning disk

component of the micromixer is activated to investigate its effects on the mixing of two liquid samples. The concentration of the liquids as well as the velocity streamlines and vectors are shown in order to determine the flow pattern in the micromixer. The chapter continues with the numerical investigation of the mixing of the liquids samples while they fill the microchannel. Then, the quantification of the mixing degree is performed showing that the actuation of the spinning disk increases significantly the mixing quality of the mixture, reaching values above 90% for the range of Reynolds number considered (0.1<Re<10). The chapter concludes highlighting the applicability of the spinning disk micromixer.

6.1 Definition of the problem

In an attempt to design a micromixer that can mix liquid samples with a broad range of Reynolds numbers, we designed the spinning disk micromixer. It is worth mentioning that, during the design process, our main goal was to design a micromixer with the simplest configuration possible. To fulfil this requirement, we designed a micromixer that consists of just one straight rectangular microchannel and a spinning disk placed at the bottom of it, as shown in Figure 6.1. The spinning disk could be located at the top or at the bottom of the microchannel wall. We decided to implement it at the bottom wall because in this way, in a practical test, it allows the micromixer user to observe the mixing process while it takes place.

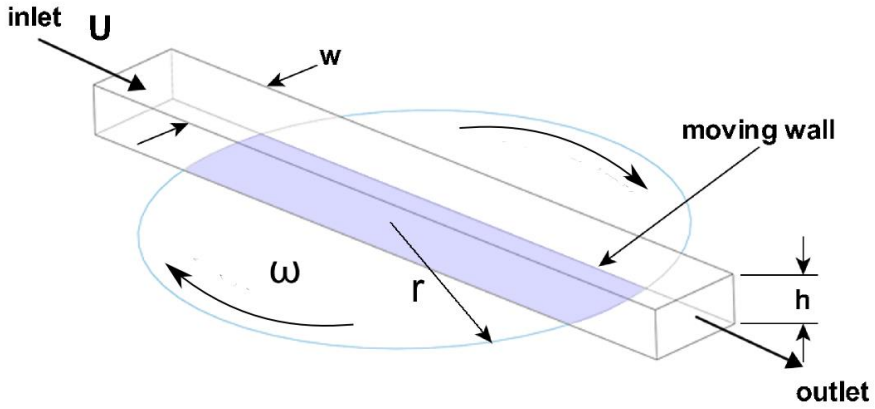

Figure 6.1 Diagram of the spinning disk micromixer.

The main characteristic of this micromixer is the spinning disk located at the bottom wall of the rectangular microchannel, with which we expect to promote the mixing of two liquid samples.

Regarding the size of the micromixer, it has the same dimensions as the micromixer mentioned in Chapter 4. The microchannel width (w) and height (h) are 350 μm and 0.175 μm, respectively. The radius of the spinning disk is four times the microchannel width and its centre is located at the geometrical centre of the microchannel.

The spinning disk micromixer design can be considered to be an active micromixer. The reason for this is that in order to stir the fluid and enhance mixing an external energy source is required. The energy source to spin the disk could be provided by a little DC motor or by an external magnetic field.

The aim of the spinning disk micromixer is to investigate the possibility of enhancing mixing at $0.1<Re<10$.

6.1.1 Numerical solver

In order to simulate the spinning disk micromixer numerically, we make use of the same numerical solver from the open source software, OpenFOAM 2.3.1, as in Chapter 5. Hence, the *interMixingFoam* solver is used to perform the 3D numerical simulations in this chapter.

A very important parameter that was taken into account in all the numerical simulations was the Courant-Friedrichs-Lewy number (CFL). It can be defined as the number of numerical cells that the working fluid crosses during one time step. The recommendation is to keep it below a value of 1. Doing this, the working fluid is forced to cross one, or less than one, numerical cell within one time step. This consideration is paramount for reducing numerical errors (numerical diffusion) while the numerical simulations are executed. Therefore, the CFL was kept at about 0.5 in all the numerical simulations performed in this chapter. In addition, it is worth mentioning that beside the CLF, a mesh sensitivity study was also carried out to make the case independent of its mesh density. These two considerations were included in the numerical simulations in an attempt to diminish possible numerical errors.

6.1.2 Boundary conditions

In order to simulate the mixing process in a microchannel, several boundary conditions need to be defined (see Figure 6.2). The basic boundary conditions used for the numerical simulation of the spinning disk micromixer are the following:

- **Inlets**. The two fluids to be mixed were defined using the boundary condition of *fixedValue* for the flow velocity. The velocity of the fluid was specified with a constant value. Furthermore, the concentration of each fluid to be mixed was also defined within these boundaries. For the fluid defined as dyed-water, the concentration value was set as 1.0, and for the fluid named water; a concentration of 0 was considered.
- **Outlet**. The boundary condition of *zeroGradient* was set at the microchannel outlet. This condition considers that the fluid velocity, normal to its surface, has a zero gradient.
- **Walls**. For the non-moving walls of the microchannel, the *nonslip* boundary condition and the contact angle formed by the liquid-solid phases were considered. A dynamic constant contact angle of 60° was specified on all the walls.
- **Moving wall.** The boundary condition of *rotatingWallVelocity* was used to define the motion of the spinning wall of the micromixer. Within this boundary condition, the speed of the spinning disk (angular velocity) and the direction of rotation can be easily modified.

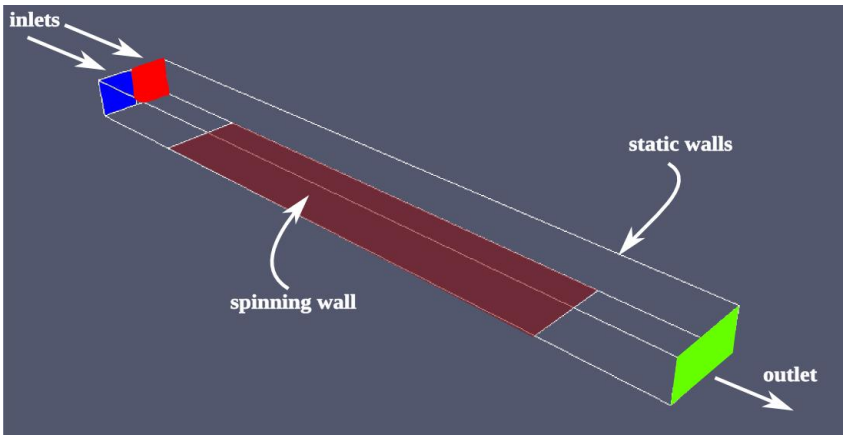

Figure 6.2 Boundary conditions of the spinning disk micromixer

6.2 The filling process of the micromixer

The filling process in microchannels is very important in many applications. In a practical scenario, for example, the users of microfluidic devices, like micromixers, may wish to mix their liquid samples as they are pumped through the microchannel. The reason for this is because the liquid samples may be restrictively expensive or not available in large amounts.

To visualise the filling process and to find out if poor mixing takes place when the two liquids flow alongside each other within the straight microchannel, we performed the corresponding numerical simulations. It is worth mentioning that the spinning wall was not put into motion and the Reynolds number was equal to 1.0 during the filling study.

A time sequence showing the filling process of the microchannel is presented in Figure 6.3. The direction of the flow is from the bottom to the top of the microchannel. Notice that a meniscus forms at the liquid-solid-gas interface, while the liquids flow alongside each other. The contact angle was approximately 60° as can be observed in Figure 6.4. The filling of the microchannel with the liquid samples took place as time progressed. Initially, the fluid domain was defined by three phases (dyed-water, water and air) but when the liquid samples started to flow along the microchannel, they forced the air out of the domain. This seems to be like those found in nature.

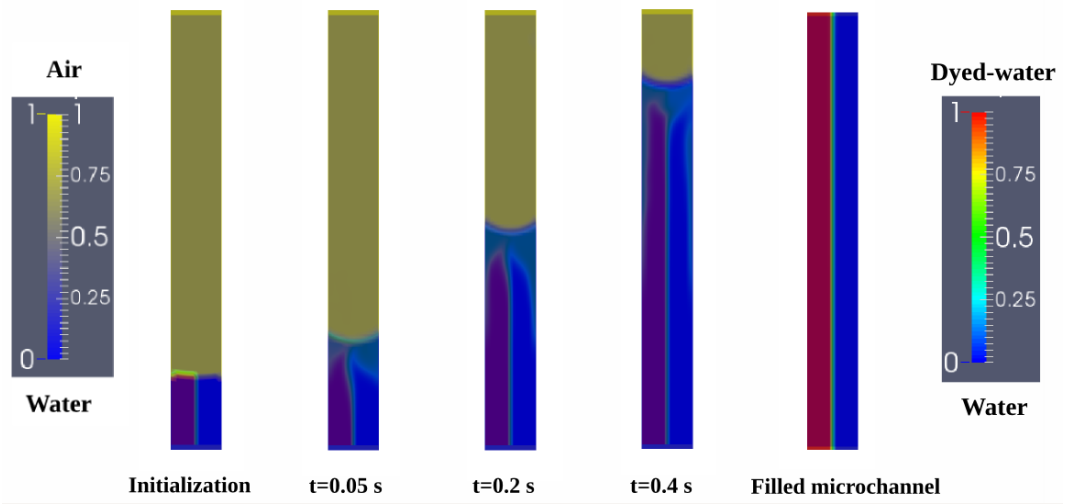

Figure 6.3 Concentration gradients of the air, dyed-water and water phases at different times of the filling process in a rectangular microchannel, Re=1.

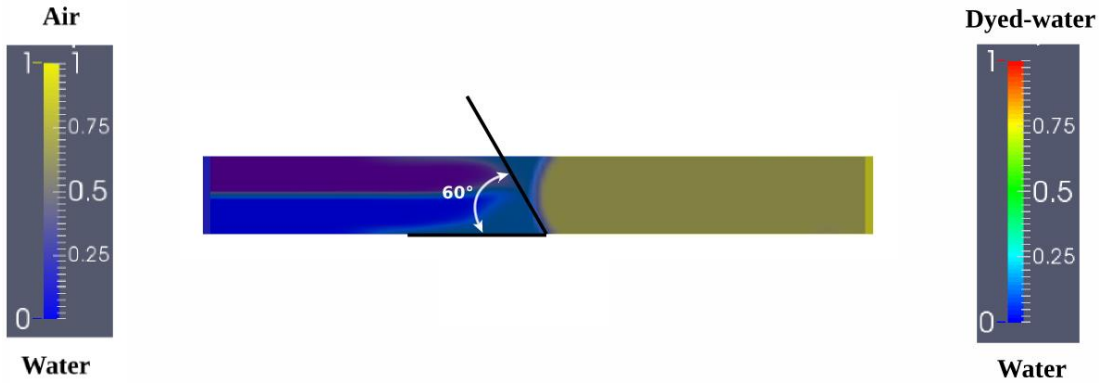

Figure 6.4 Contact angle formed by the liquid-solid phases in the microchannel, Re=1, t=0.2 s.

Interestingly, when the two liquids finally filled the microchannel, they did not significantly mix with each other. The action of just pumping the liquids through the microchannel did not seem to enhance mixing, as seen in Figure 6.5. The only apparent mixing occurred at the liquid interface, which can be attributed to molecular diffusion. The concentration of the two liquid samples was clearly distinguished from each other. Therefore, an alternative method for enhancing the mixing of the liquid samples should be implemented.

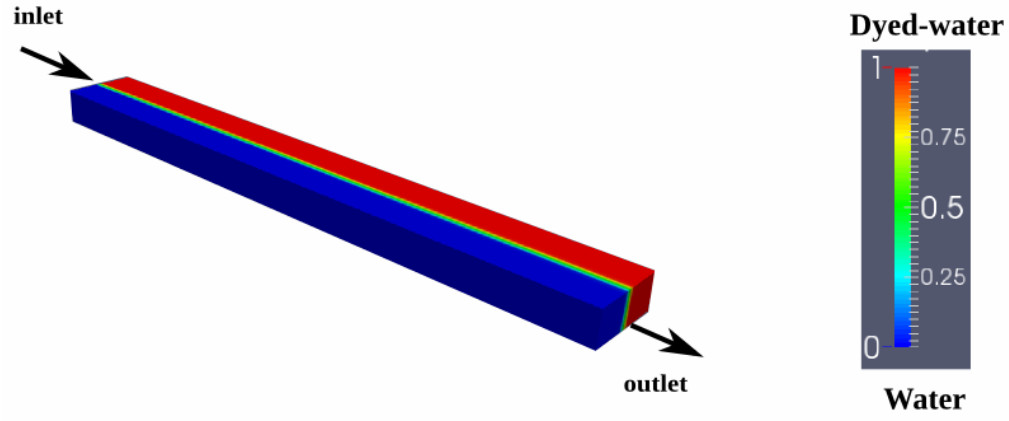

Figure 6.5 Isometric view of the filled microchannel showing the concentration gradients of the dyed-water and water phases at Re=1.

6.3 Micromixer actuation

As we have seen in the previous section, during the filling process of the microchannel, molecular diffusion is not enough for mixing effectively the two liquid samples in a straight microchannel. Therefore, we proceeded to perturb the parallel streams by means of the activation of the spinning disk (wall). Two different scenarios

were considered when activating the disk: 1) after the two liquids completely filled the microchannel and 2) before the two liquids passed through the spinning disk area or filled the microchannel.

We used the first scenario, as an excellent way of visualising how the fluids were mixed inside the microchannel when the spinning disk started its motion. We should make it clear that this condition is not likely to happen in reality. However, it was useful to show the fluid pattern that the liquids followed when the spinning disk was put into motion.

The second scenario is what most microfluidics users desire to happen; they wish to mix their liquid samples while the liquids are pumped through a microchannel. Therefore, to fulfil this requirement, the spinning disk of the micromixer was put into motion before the fluid passed over it.

6.3.1 Actuation after the filling of the microchannel

We demonstrated in the previous section that just pumping the liquid samples through a microchannel poor mixing occurred. In order to enhance mixing we put into motion the spinning disk located at the bottom wall of the microchannel, see Figure 6.1. The findings for the case of Reynolds number equal to 1.0 and an angular velocity of 12 rad/s (f=2 Hz) are presented next.

6.3.1.1 Concentration contours

The mixing process we are dealing with is time dependent and to be able to show how the mixing progresses with time, we opted for presenting it in a time sequence of images. Four instantaneous images of the concentration of the liquids were selected within the first second of mixing to show the mixing process as shown in Figure 6.6. The first feature we noticed was that the fluids stretched and folded when the spinning disk was activated. We should remember that the direction of the spinning disk was clockwise. Due to the motion and position of the spinning disk, the fluids to mix are stirred in an anti-clockwise direction as shown in Figure 6.6. This effect will be address in a later section with the help of streamlines and velocity vectors.

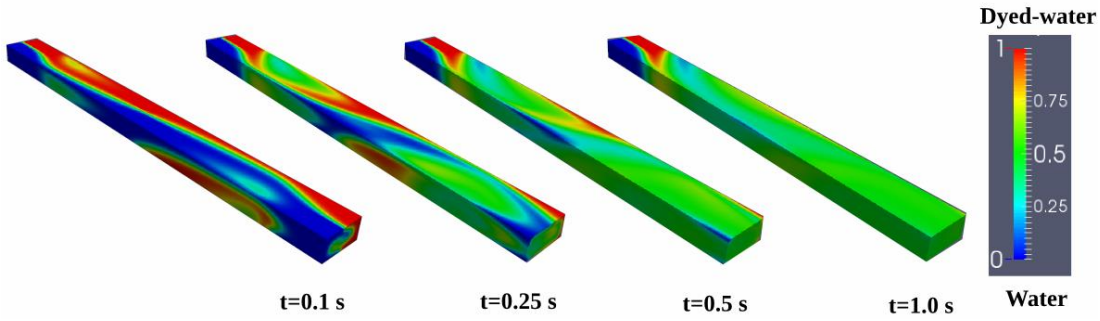

Figure 6.6 Time sequence of the spinning micromixer after the microchannel was completely filled with dyed-water and water, Re=1 and rotation of disk ↻.

In terms of mixing performance, we can qualitatively see that after half a second of activating the spinning disk, the mixture quality at the channel outlet looked quite uniform. The homogeneous concentration, which appears to be close to a value of 0.5, gives us an idea that the liquids were fully mixed. In addition, when we compared the two mixing conditions at t=0.5 s and t=1.0 s, we observed that some traces of unmixed fluid in the middle of the microchannel were still present at t=0.5 s. In contrast, those unmixed traces of fluid were not evident when the mixing time was 1.0 s.

The reason for the unmixed fluids at the centre of the microchannel was attributed to the tangential velocity of the spinning disk. We should remember that the tangential velocity of the spinning disk varies with its radius. Hence, the centre of the spinning disk should be lower than at its perimeter. However, the unmixed fluids were fully mixed when they approached to the perimeter of the spinning disk. This was mainly due to the high tangential velocity of the spinning disk.

6.3.1.2 Streamlines along the microchannel

In the previous section, we have seen how the concentration contours evolved while activating the moving disk. Nevertheless, to have a better understanding of what happens with the fluid inside the microchannel, the streamlines and several planes across the microchannel are shown in Figure 6.7. The stretching and folding of the streamlines indicate that the fluids recirculate inside the microchannel. It is not surprising that the most intense stretching and folding of the streamlines seemed to be at the perimeter of the moving disk because that is where the maximum tangential velocity of the spinning disk is concentrated. To verify this, we will look at the velocity vectors in the next section.

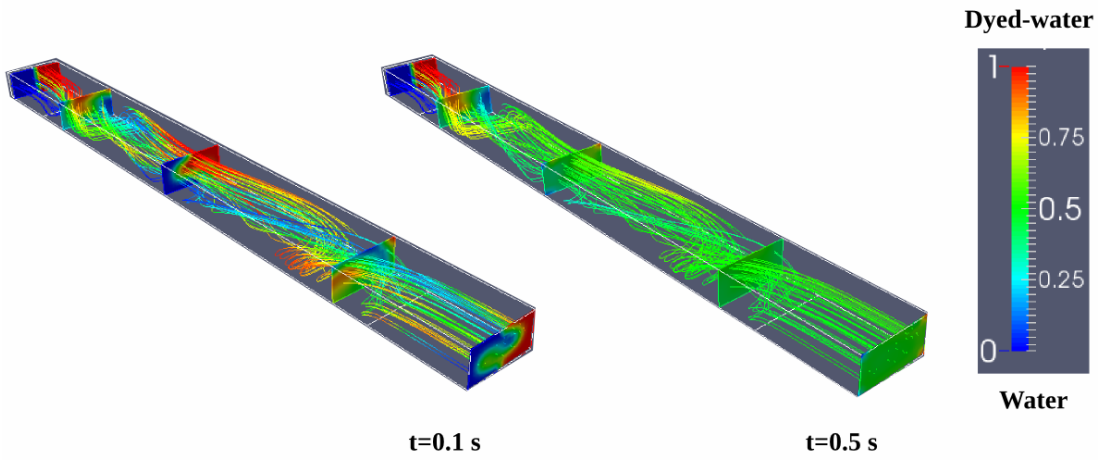

Figure 6.7 Time sequence of streamlines along the microchannel, Re=1 and rotation of disk ↻.

6.3.1.3 Velocity vectors

The velocity vectors of the flow pattern are useful in showing the direction of the flow. In our case, we will display them to know the direction of the liquids when the spinning disk is activated. A top and an isometric view of the microchannel showing the velocity vectors are displayed in Figure 6.8. From the top view, we observe that the velocity vectors have a clockwise direction as we specified previously. This simple clockwise rotation of the disk produced the stretching of the fluid interface as seen on the concentration planes across the microchannel at t=0.05 s and this effect continues as long as the spinning disk is in motion.

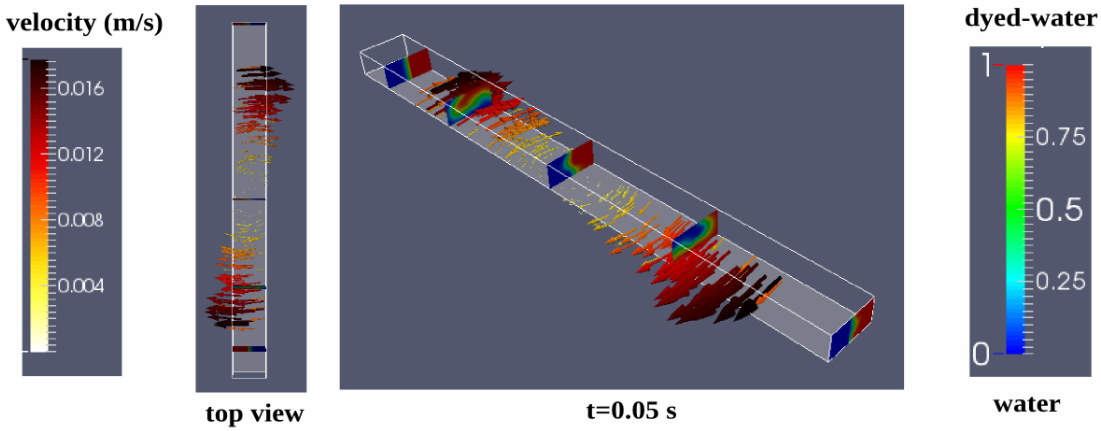

Figure 6.8 Velocity vectors on the rotating disk of the microchannel, Re=1 and rotation of disk ↻.

6.3.1.4 Recirculating flow

To look further into the effect that the moving disk has on the flow, we display the velocity vectors on several planes across the microchannel, as shown in Figure 6.9. On the planes across the microchannel inlet, the two liquids to be mixed recirculate from left to right due to the spinning disk. We should remember that the direction of the spinning disk is defined as clockwise. We can also see from a closer view of the microchannel inlet (left side) that, being close to the spinning wall, the velocity vectors had a higher magnitude than at any other location along the crossing plane. Furthermore, the streamlines showed the trajectory that the fluid followed downstream. It is interesting that the fluids tend to rearrange to a parabolic velocity profile when they approach to the centre of the spinning disk. However, when they approach to the perimeter of the opposite side of the spinning disk, they start to be stretched and folded once more, but in an opposite direction. The change of the circulation direction can be seen in the upper right image of Figure 6.9.

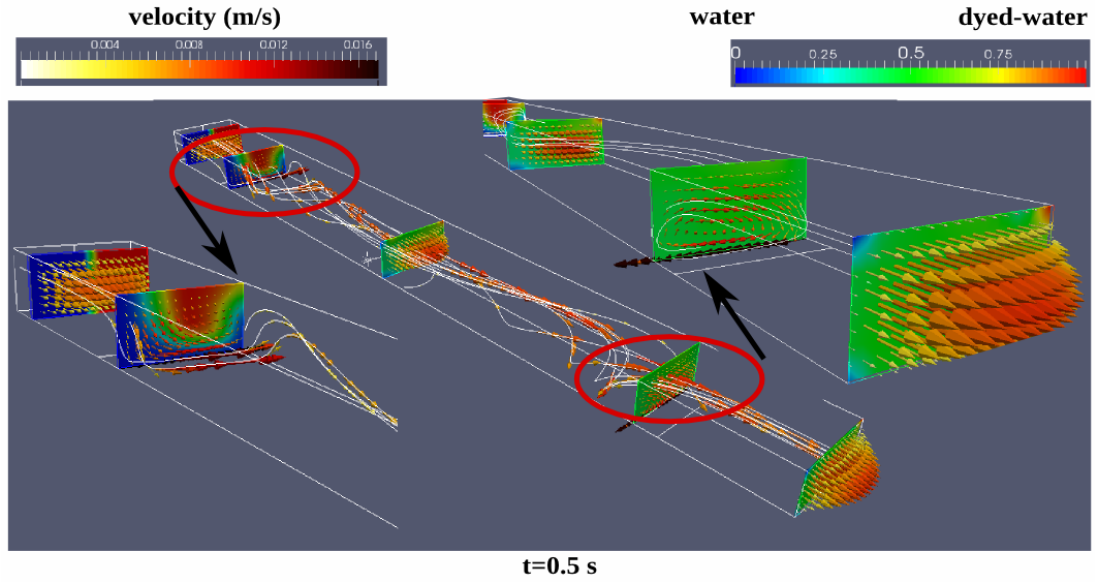

Figure 6.9 Flow recirculation at some specific planes across the microchannel, Re=1 and rotation of disk ↻.

The velocity vectors are helpful in giving evidence of the flow pattern that the working fluid followed when the spinning disk is in motion at the bottom of the microchannel. We can qualitatively say that the counter-circulation of the fluids has a significant impact on mixing enhancement. Moreover, the spinning disk transmits momentum to the working fluid, which causes the recirculation of the fluid in the three

co-ordinates (x,y,z) along the straight microchannel. The mixing quantification of the mixture will be addressed in a later section.

6.3.1.5 Mixing at Re= 5, 10

We saw in section 6.3.1.1 of this chapter that after one second of mixing at Re=1, the liquid samples seem to be fully mixed. Therefore, in this section we will consider a mixing time of one second as the criterion to show how well the spinning disk micromixer performs at several Reynolds numbers.

First, we will see the case where the Reynolds number is equal to 5. With this study we intend to investigate how the spinning frequency of the rotating disk affects the mixing quality of the liquid samples. As seen in Figure 6.10, the concentration is not homogeneous at the channel outlet when f=3 Hz. As a consequence, the mixing degree of the mixture may not reach 90%. However, if the spinning frequency of the disk is increased to 6 Hz, the quality of the mixture is further improved. The concentration contours looked more uniform at the channel outlet than in the previous case. If the spinning frequency is increased further, for example to 9 Hz, it seems to have little effect of the concentration contours (see Figure 6.10c).

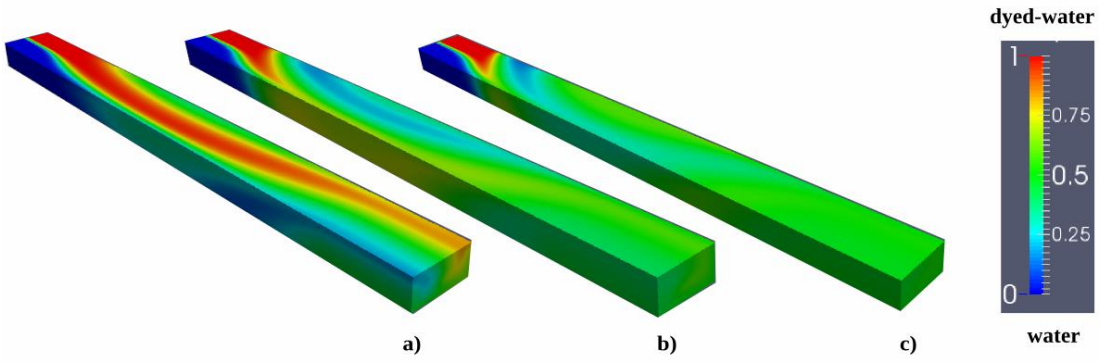

Figure 6.10 Concentration contours along the microchannel of the spinning disk mixer a) f=3 Hz, b) 6 Hz and c) 9 Hz, Re=5 and rotation of disk ↻.

Now, we will see how the spinning micromixer performs when the Reynolds number is increased to a value of 10. Three scenarios are presented in Figure 6.11, where the frequency of the spinning disk was increased in steps of 5 Hz. We see that a frequency of 5 Hz, it is not enough to reach a homogeneous mixture at the microchannel outlet. The concentration of dyed water and water are still identifiable. Nevertheless, when the actuation frequency of the rotation disk is increased to 10 Hz,

the mixing is enhanced to such a degree that the two concentrations are no longer easy to distinguish from each other (see Figure 6.11b)

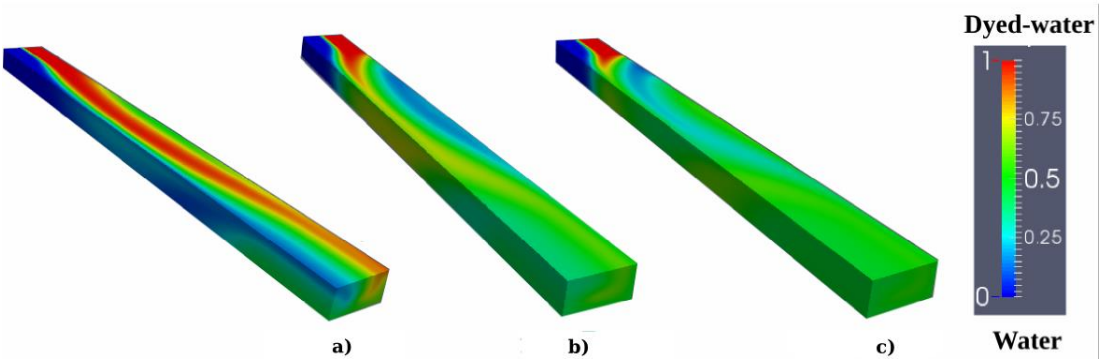

Figure 6.11 Concentration contours along the microchannel of the spinning disk mixer a) f=5 Hz, b) 10 Hz and c) 15 Hz, Re=10 and rotation of disk ↻.

As we saw in the previous case, where Re=5, increasing the frequency of the spinning disk has significant effect on enhancing mixing in the microchannel. If we visually examine the case where Re=10 and f=15 Hz, there is evidence that the concentration, along the microchannel and, more importantly at its outlet, is more homogeneous than with the other two cases. However, it seems to be a compromise between mixing quality and the energy consumption required. This point will be addressed in a later section when dealing with the quantification of the mixture.

6.3.1.6 Mixing at Re<1

So far, we have investigated, mixing at Reynolds numbers higher than 1.0 with the spinning disk micromixer. However, in numerous microfluidics applications the Reynolds number value is less than 1.0 [1], [37], [38], [39], [40]. In order to find out if the spinning disk micromixer can mix at Re<1, we performed two numerical simulations at Re=0.5 and Re=0.1. We believe that if the spinning disk micromixer can mix at such Reynolds numbers, it will be able to mix at any Re below 1. This is because the main flow velocity in the microchannel is most often the only parameter varied to reach the desired Reynolds numbers. Hence, the lower the velocity of the fluids; the more time the fluids will recirculate over the spinning disk area, leading to better mixing.

First, we consider mixing at Re=0.5. As reported above, a frequency of 2 Hz was required for mixing effectively the liquid samples at Re=1. However, if the Reynolds number is reduced to 0.5, the mean velocity of the liquids should also be reduced. We should remember that the mean flow velocity was the only variable

modified in the numerical simulations to reach the desired Reynolds number. Therefore, if the fluids flow slower at Re=0.5 than at Re=1.0, it is reasonable to reduce the frequency of the spinning disk to 1 Hz.

A time sequence of the concentration contours of the liquids to be mixed is shown in Figure 6.12 at Re=0.5. Overall, mixing seems achievable when the spinning disk frequency is just 1 Hz. The mixing quality of the mixture seems quite uniform at the microchannel outlet after just one second of mixing. The mixing of the liquid samples continued as time progressed. For example, after three seconds of mixing time, the concentration contours indicating mixing were fairly homogeneous, not only at the channel outlet, but also along the microchannel. Hence, this allowed us to conclude qualitatively that it is possible to mix two liquid samples effectively at Re=0.5 with a spinning disk frequency of just 1 Hz.

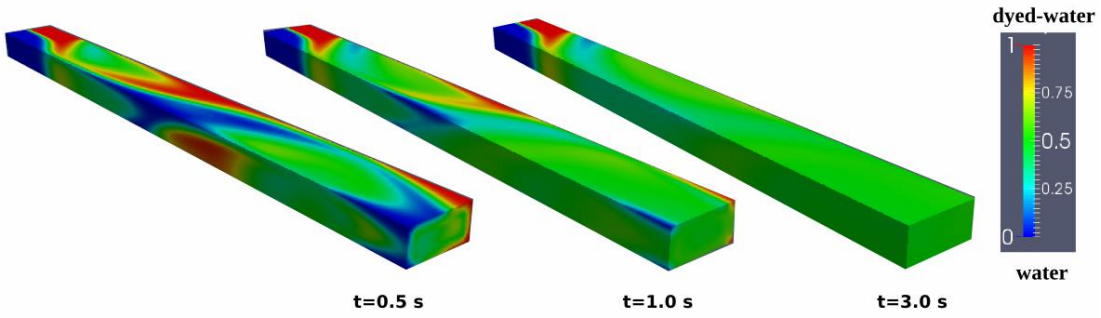

Figure 6.12 Time sequence of the concentration contours along the microchannel of the spinning disk micromixer, f=1 Hz, Re=0.5 and rotation of disk ↻.

Mixing becomes more challenging when the Reynolds number is reduced to lower values than 0.5. To investigate if the spinning disk micromixer design can mix at such low Reynolds numbers, we performed one numerical simulation considering Re=0.1 and an actuation frequency of 1 Hz. The results are shown as a time sequence of the concentration contours in Figure 6.13. Here, we can clearly see that mixing enhancement is considerably increased along the microchannel with the motion of the spinning disk.

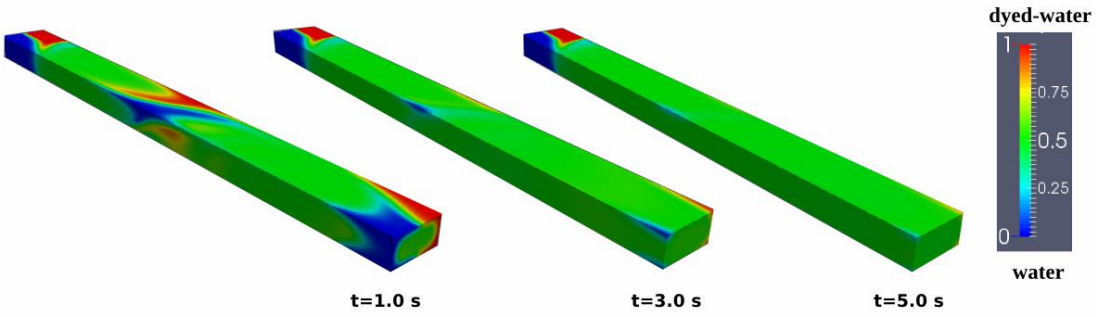

Figure 6.13 Time sequence of the concentration contours of dyed-water and water when the spinning disk is activated, f=1 Hz at Re=0.1 and rotation of disk ↻.

If we compare Re=0.5 and Re=0.1, (Figure 6.12 and Figure 6.13), we can qualitatively see that the concentration contours seem slightly more homogeneous at the channel outlet at Re=0.5 than at Re=0.1 after 1 second of mixing. This is attributed to the speed of the main flow, causing a stronger recirculation pattern which enhances mixing. However, an excellent mixing is achieved when time progresses to t=5.0 s

So far, we have investigated the mixing process when the microchannel was completely filled with two liquid samples. Although it has been very useful to visualise the flow pattern when the spinning disk was put into motion, those mixing conditions did not represent a real scenario in microfluidics. In a real scenario, mixing should take place while the liquids flow through the microchannel. We will address this issue in the next section.

6.3.2 Actuation before filling the microchannel

The way we intend to achieve mixing while the fluids flow through the channel is by putting the spinning disk into motion before the liquid samples are pumped over it. The spinning disk, we think, could force the liquid samples to mix with each other by transmitting momentum to them. This effect could promote the mixing of the liquids while they are crossing the spinning disk area. We also want to know if the actuation of the spinning disk has an effect on the fluid interface and if it is useful for enhancing the mixing quality of the final mixture.

To make a kind of comparison between the results shown above in Figure 6.6, we will keep the Reynolds number at Re=1.0 but activating the spinning disk before the fluids fill the microchannel. A time sequence of the concentration gradients of the fluids is displayed in Figure 6.14 while the liquid phase fills the microchannel. A

2D view of the microchannel is considered to make the visualisation of the fluid interface (meniscus) evident. Interestingly, the fluid interface did not significantly deform when it moved over the spinning disk area of the micromixer. The relevant findings were that mixing was considerably enhanced while the liquids flowed along each other when the spinning disk was in motion. Moreover, the fluids started to mix as soon as they were over the spinning disk, and they continued to mix while they went through it, as we observed in the case where t=0.5 s.

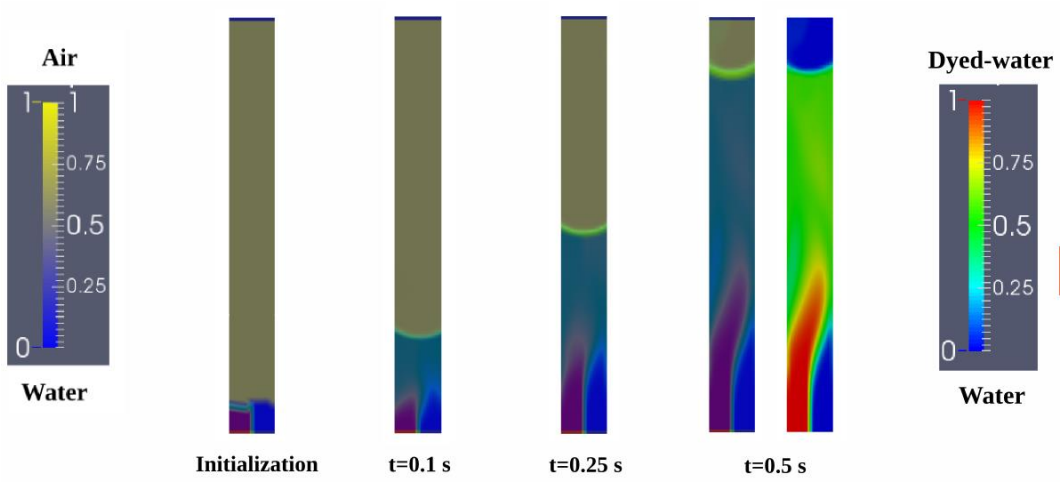

Figure 6.14 Time sequence of the concentration contours of the fluids while they flow over the spinning disk mixer, Re=1.0, f=2 Hz and rotation of disk ↻.

After looking at Re=1.0, we will now look at the rest of the Reynolds numbers considered (0.1<Re<10), which are shown in Figure 6.15. We observe that the amount of mixing along the microchannel is more uniform at Re=0.1 than any other value. In this case, the liquid samples seemed to mix just at the entrance of the spinning disk. Notice that the actuation frequency was kept constant. This condition did not seem to be fulfilled when the Reynolds number was increased to 1.0 because the concentration of dyed-water and water are still identifiable.

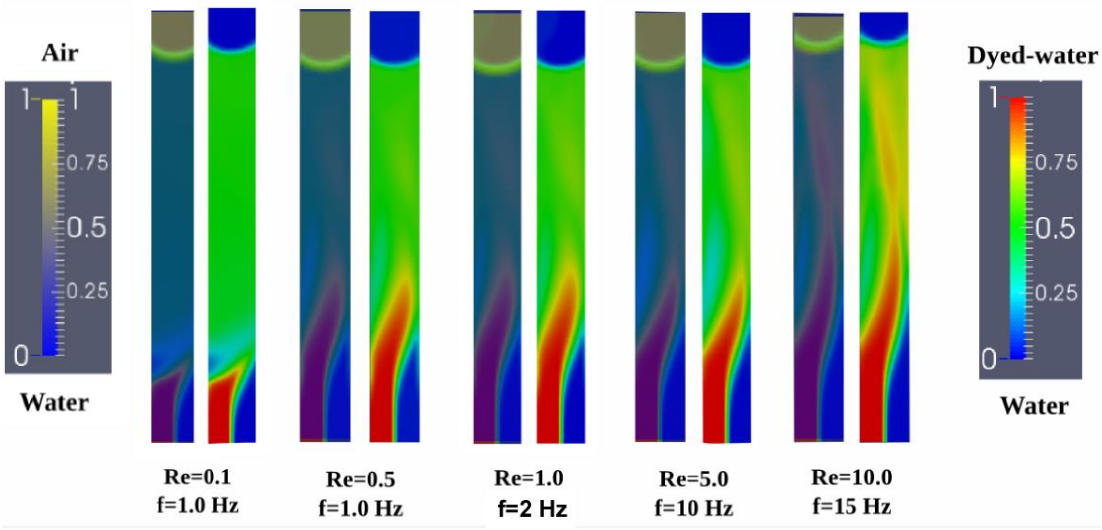

Figure 6.15 Time sequence of the concentration contours of the fluids while they flowed over the spinning disk mixer at several Reynolds numbers and rotation of disk ↻.

6.3.3 Mixing quantification

In order to quantify the mixing degree of the final mixture with the Reynolds numbers considered, the quality of the mixture was quantified as in previous chapters. Such quantification was performed at one channel width from the perimeter of the spinning disk downstream and after 3 seconds of mixing time. The results of the mixing degree are presented graphically in Figure 6.16. It can be notice that the mixing degree of the mixture is above 0.9 or 90% for Re<1 and spinning frequencies below 2 Hz. However, to reach mixing degrees of 0.9 at higher Reynolds numbers, for example at Re=5.0, the spinning frequency of the disk has to be increased to 7-8 Hz to reach a 90% mixing quality.

It is important to mention that the mixing degree for the case of Re=0.1 was relatively low, at about 77%, after 3 seconds of mixing. This poor mixing degree was because the whole mixture did not have enough time to reach the area where the mixing degree was quantified. This caused some unmixed fluid traces to remain at the channel corners, which influenced the low mixing degree. However, if the mixing degree is quantified after a longer time, for example after 5 seconds, the mixing degree target of 0.9 is also achieved.

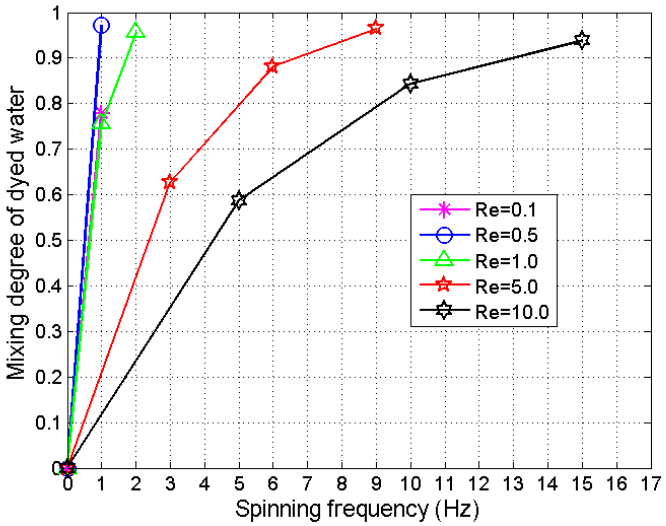

Figure 6.16 Mixing degree of dyed water at t=3 s.

6.4 Practical application of the spinning disk micromixer

The spinning disk micromixer has great possibilities to be implemented in most of the microchannel geometries frequently used in microfluidics. Although the rectangular cross-section of a microchannel is the most widely used, there are other microchannel geometries that may also be used in microfluidics. The circular, triangular, trapezoidal and semi-elliptical cross-sections shown in Figure 6.17 are some examples of potential additional micromixer designs using the spinning disk approach. The only requirement to implement the spinning disk micromixer in those cross-sections is that they should have at least one straight channel wall. From Figure 6.17, we can see that all the microchannel cross-sections fulfil that requirement except the circular one. This shows the flexibility to adapt the micromixer to most of the microchannel geometries.

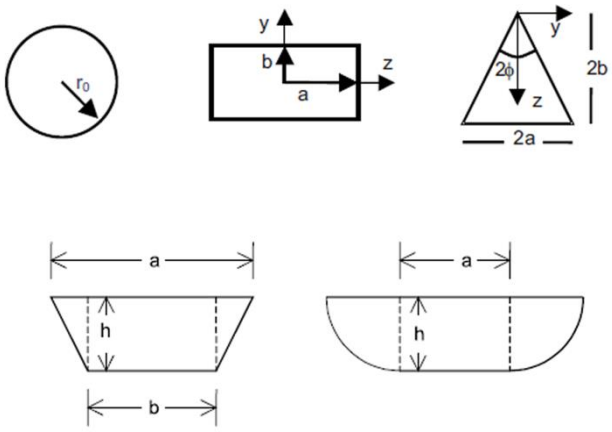

Figure 6.17 Typical microchannel cross sections in microfluidic devices [2].

We can conclude, therefore, that the spinning disk micromixer design might be implemented in many more micromixer designs with different cross-sections of microchannels. This characteristic makes the spinning disk micromixer a potential candidate for mixing enhancement in microfluidics applications for a broad range of Reynolds numbers (0.1<Re<10).

6.5 Concluding remarks

In this Chapter, an alternative micromixer design for mixing enhancement for Reynolds numbers below 10 was investigated. The micromixer consisted of a simple straight channel and a spinning disk placed at its bottom wall. The aim was to design a micromixer with the simplest possible configuration that was able to effectively mix liquid samples at low Reynolds numbers, reaching 90% mixing quality.

The filling process of the microchannel was successfully simulated including the contact angle formed by the liquid-gas-solid phases on the interior of the microchannel walls. A dynamic contact angle of 60 degrees was measured just as defined in the numerical simulations. This contact angle triggered the formation of a fluid meniscus at the liquid-gas interface where an apparent *good* mixing took place. Interestingly, the mixing area close to the meniscus did not grow while the fluids were flowing through the microchannel and mixing was attributed to the constant motion that the interface experienced to maintain its meniscus shape.

It was also demonstrated that after the filling of the microchannel with the liquid samples, poor mixing occurred between the fluids, while flowing alongside each other. The only apparent mixing took place at the fluid interface but it was not significant, which suggests that it is very complicated to mix liquid samples in straight channels at $Re<1$.

The implementation of a spinning disk at the bottom of the main microchannel generated a considerable improvement in mixing at Reynolds numbers below 10. Furthermore, the mixing time was also comparatively low to mix the sample liquids. For example, a homogenous mixture was observed after just 1 second of mixing time at $Re=1$. This remarkable mixing enhancement was due to the helical flow pattern indicated by the streamlines inside the microchannel.

Another interesting result was that mixing could be enhanced while the liquid samples flowed along the microchannel if the spinning disk was put into motion in advance.

Finally, mixing quantification suggested that it was possible to effectively mix liquid samples with the spinning disk micromixer at $Re<10$. Therefore, this micromixer

design could be utilised in electrokinetic systems [39], [178], [180] in a variety of different microchannel cross-sections.

Chapter 7

Conclusions

In this thesis we investigated two new methods to address the challenging problem of mixing in microfluidic devices. The first alternative was using the synthetic jet principle and the second was taking advantage of the multiphase flow for enhancing the mixing of two liquid samples. These two approaches were studied in some detail in order to design a micromixer able to deliver an excellent mixing quality, with consideration given to the criteria of minimum energy consumption, short mixing distance and time, a simple control system and manufacturing.

- **Mixing with synthetic jets**

Due to the difficulties encountered when fabricating and actuating a micromixer with synthetic jets, the investigation into mixing enhancement at low Reynolds numbers (Re=0.5) was approached from a macroscale viewpoint. A macromixer, in the order of a few centimetres, was designed and manufactured as the first attempt to mix two liquid samples. However, due to technical difficulties encountered in performing the mixing visualisation with this mixer design in the experiments, we proceeded to study it with the aid of 2D numerical simulations. This assumption of 2D was justified by the corresponding 3D numerical simulation, which suggested that the numerical simulations were symmetric across the mixing channel. With this strategy, the computational time to study the mixing process in the macromixer was reduced in 15%. The results of the numerical simulations showed that it is possible to mix two liquids effectively at Re=0.5 using a macromixer with four

opposite synthetic jets. The optimal operating condition to reach the mixing degree target of 90%, based on the criterion of minimum energy consumption, was at stroke length of 3.52 (Δ_{pp}=2 mm) and Strouhal number of 2.64 (f=8 Hz). Below this operating condition, the mixture quality was poor due to the lower rate of stretching and folding of the fluid interface that ultimately promotes mixing by molecular diffusion.

Since the mixing chamber volume was considerably large in the macromixer with four opposite synthetic jets as a fraction of the one all volume, an improvement was proposed which consisted of reducing the chamber volume. In terms of the mixing performance of this improved macromixer, it showed that it was possible to mix two liquid samples at Re=0.5 with just two pairs of opposite jets, which was confirmed by the 90% mixture quality achieved. Interestingly, the operating conditions to reach this mixing degree were the same as for the macromixer with four pairs of opposite jets: an actuation displacement of 2.0 mm (stroke length=1.0) and frequency of 8 Hz (Strouhal number=10.66). Although these variables coincided in both macromixers, the stroke length and Strouhal number did not due to the difference in the cavity size.

Due to the good mixing performance achieved with the macromixer with two and four synthetic jets, a further simplification of the synthetic jet macromixer was considered. The design consisted of just one pair of synthetic jets. The main improvements were made in simplifying the channel geometry, the moving frame to actuate the synthetic jets and the channel inlet configuration. With these changes, mixing was significantly enhanced when increasing the stroke length and the Strouhal number. The best operating condition to reach a mixing degree of 90% was very close to the operating conditions found in the macromixers with two and four pairs of synthetic jets. This was achieved when actuating the synthetic jets with a peak-to-peak displacement of 1.5 mm and a frequency of 6 Hz, which meant 2 Hz and 0.5 mm less than the previous macromixers. The selection of this operating condition was also based on the criterion of minimum energy consumption of the electromagnetic actuator. Once the optimal conditions were known, this macromixer was scaled down to the typical dimensions of a micromixer found in microfluidics. The results of the scaled micromixer showed that the mixing performance of the macro and micro mixers were

dramatically different. The difference was approximately 58% reduction in the mixing degree for the micromixer. Therefore, we conclude that it is not possible to study a micromixer from its macroscale counterpart.

To address the poor mixing performance of the scaled down micromixer, two modifications were made to its geometry. The synthetic jet cavities were enlarged to 7 times the channel width and the synthetic jet orifice size was reduced to a quarter of the microchannel width. The mixing performance with these geometry changes were enough to reach a mixture quality of 90% when operating the micromixer at L=10.5 (Δ_{pp}=3w/4) and Str=0.7 (f=8 Hz) at Re=0.25. The mixing performance was also qualitatively verified with Poincaré maps to visualise the distribution of small particles in the flow and show possible unmixed zones, which confirmed the mixing degree of 90%. Additionally, the Lyapunov exponent was found to be positive, indicating chaotic flow inside the micromixer which was another important factor that contributes to the good mixing performance of the mixing device.

We found that synthetic jets were very effective mechanism for mixing enhancement in a confined flow at low Reynolds numbers (Re<1) with the appropriate operating conditions. The stretching and folding of the fluid interface were the main mechanisms behind the excellent mixing, which was produced by the alternative jets injected in the mixing area (main channel). Furthermore, the distance that the liquid jets can travel when they were expelled from the synthetic jet orifice was highly dependent on the actuation frequency and the peak-to-peak displacement of the synthetic jet actuator; higher amplitudes and frequencies led to better mixing. Although a micromixer with synthetic jets could be remarkably effective for mixing enhancement in microfluidic applications, there are still some challenges that need to be addressed such as the actuator and its control system to make it a practical solution.

- **Micromixers with multiphase flow**

An alternative micromixer to the synthetic jet micromixer was proposed in order to address the technical difficulties of a synthetic jet micromixer such as suitable actuator and a complex control system. The micromixer consisted in taking advantage

of the multiphase flow for mixing enhancement at Reynolds numbers below 1.0. The geometry of this micromixer was very similar to the synthetic jet micromixer. The working principle was taking advantage of the surface tension and the fluid interface formed between the liquid-gas phases. This led to the stretching and folding of the liquid phase while it flows through the micromixer geometry. When the fluids passed through it, a remarkable mixing enhancement took place, reaching a mixing degree above 90% in just 0.17 seconds and 350 μm downstream. There are several benefits of the multiphase micromixer over synthetic jet micromixers and other micromixers, which are reported in the literature [13], [73], [86], [91], [95], [44], [101], [103], [130], [137], [140]. These are: 1) simple geometry, 2) no requirement for any control system, 3) no external energy source supply to enhance mixing, 4) no moving parts, 5) short mixing time and distance and 6) mixing degrees above 90%. All these features of the multiphase micromixer fulfil all the mini-aims stated in the introduction of this thesis, (short mixing time, simple design, minimum energy consumption, mixing degree above 90% and a simple control system), making it a very attractive option for mixing enhancement in numerous practical applications in microfluidics.

- **Spinning disk micromixer**

In microfluidics there are many applications where mixing is needed and some of them are very particular, for example, in the area of electrokinetics where the Reynolds number varies between 0.1 and 10 [178], [179]. It was proved that the effectiveness of the multiphase micromixer decreased at higher Reynolds numbers. For instance, the mixing degree was reduced by 15% when the Re=2 and 47% at Re=5.0. In an attempt to solve this poor mixing performance of the multiphase micromixer, an alternative micromixer design for mixing enhancement at Reynolds numbers up to 10 was studied. The micromixer consisted of a straight rectangular microchannel and a spinning disk placed at its bottom wall. The mixing performance of this micromixer was significant when the spinning disk was activated. The fluids experienced a helical flow pattern while flowing along the microchannel due to the spinning disk, which dramatically enhanced mixing at Re<1. An interesting feature of this micromixer is that mixing can be enhanced while the liquid samples flow along the microchannel if the spinning disk is put into motion in advance. This approach avoids wasting the precious

and expensive liquids commonly used in microfluidics. The mixing quantification suggested that it is possible to achieve mixing degrees above 90% with the spinning disk micromixer at Reynolds numbers below 10. However, the mixing performance highly depended on the angular velocity (frequency) of the spinning disk. The versatility of the spinning disk micromixer makes it a serious candidate for applications in electrokinetic systems and it can also be implemented in many microchannel cross-sections.

Recommendations for future work

Further research work is required to implement a micromixer with synthetic jets. The main limitation of this micromixer technique is a suitable actuator that fulfils the required force and displacement to promote the formation of the synthetic jets. Therefore, there is a need to design and manufacture an actuator with the following characteristics: reduced cost and size, low energy consumption and a simple control system to operate it.

Regarding the multiphase micromixer, the outstanding mixing performance and efficiency for mixing in typical Re found in microfluidic devices make it an attractive option for mixing enhancement. However, the mixing investigation was performed entirely using numerical simulations. This suggests that the manufacturing and testing of such a micromixer are the next stages to verify its mixing performance in a real scenario.

The last micromixer considered in this study was the spinning disk micromixer. The mixing performance of this device was also excellent when operating it at the adequate spinning frequency. In order to verify such a mixing performance, this micromixer should also be manufactured to perform the corresponding experiments. The advantage of this micromixer design is that the actuation of the spinning disk can be implemented using a DC motor placed at the bottom of the mixing device.

Bibliography

1. **P. Tabeling.** Introduction to Microfluidcs, Oxford University Press, 2009.

2. **N. Nguyen, S. T. Wereley.** Fundamental and applications of microfluidics, Second edition, 2006.

3. **P. S. Dittrich, A. Manz.** Lab-on-a-chip: microfluidics in drug discovery, Nature, 2006, Vol. 5, pp. 210-218.

4. **A. J. deMello.** Control and detection of chemical reactions in microfluidic systems, Review Nature, 2006, Vol. 442, pp. 394-402.

5. **H. A. Stone, S. Kim.** Microfluidics: basic issues, applications, and challenges, AIChE Journal, 2001, Vol. 47, No. 6.

6. **H. A. Stone, A. D. Stroock, A. Ajdari.** Engineering flow in small devices: microfluidics toward a lab-on-a-chip, Annual Review of Fluid Mechanics, 2004. 36, pp. 381–411.

7. **W. Tian, E. Finehout.** Microfluidics for Biological Applications, Springer Science and Business Media, 2008, p. 191.

8. **M. A. Burns, B. N. Johnson, S. N. Brahmasandra, K. Handique, J. R. Webster, M. Krishnan, T. S. Sammarco, P. M. Man, D. Jones, D. Heldsinger, C. H. Mastrangelo, D. T. Burke.** An integrated nanoliter DNA analisys device, Journal of Science, 1998, Vol. 282, pp. 484-487.

9. **J. Atencia, D. J. Beebe.** Controlled microfluidic interfaces, Journal of Nature, 2005, Vol. 437, pp. 648-655.

10. **H. Chou, C. Spence, A. Scherer, S. Quake.** A microfabricated device for sizing and sorting DNA molecules, Biophysical Journal, 1999, Vol. 96, pp. 11–13.

11. **M. W. Losey, M. A. Schmidt, K. F. Jensen.** Microfabricated multiphase packed-bed reactors: characterization of mass transfer and reactions, Journal of Industrial and Engineering Chemistry, 2001, Vol. 40, pp. 2555-2562.

12. **T. S. Sammarco, M. A. Burns.** Thermocapillary pumping of discrete drops in microfabricated analysis devices, AIChE Journal, 1999, Vol. 45, No.2, pp. 350-365.

13. **A. D. Stroock, S. K. W. Dertinger, A. Ajdari, I. Mezic, H. A. Stone, G. M. Whitesides.** Chaotic mixer for microchannels, Journal of Science, 2002, Vol. 295, pp. 647-651.

14. **J. M. Ottino, S. Wiggins.** Introduction: mixing in microfluidics, Philosophical Transactions of the Royal Society A, 2004, 362, pp. 923-935.

15. **N. T. Nguyen, Z. Wu.** Micromixers—a review, Journal of Micromechanics and Microengineering, 2005, Vol. 15, R1–R16.

16. **C. K. Harnett, J. Templeton, K. A. Dunphy-Guzman, Y. M. Senousy, M. P. Kanouff.** Model based design of a microfluidic mixer driven by induced charge electroosmosis, Journal of Lab-on-a-Chip, 2008, Vol. 8, pp. 565–572.

17. **D. J. Beebe, G. A. Mensing, G. M. Walker.** Physics and applications of microfluidics in biology, Annual Review of Biomedical Engineering, 2002, Vol. 4, pp. 261-86.

18. **I. Shestopalov, J. D. Tice, R. F. Ismagilov.** Multi-step synthesis of nanoparticles performed on millisecond time scale in a microfluidic droplet-based system, Journal of Lab-on-a-Chip, 2004, Vol. 4, pp. 316–321.

19. **B. J. Kirby.** Micro- and Nanoscale Fluid Mechanics: Transport in Microfluidics Devices, Cambridge University Press, 2010.

20. http://www.marketsandmarkets.com/Market-Reports/microfluidics-market-1305.html.

21. http://www.yole.fr/Microfluidic_Applications_Players.aspx.

22.http://www.luxresearchinc.com/news-and-events/press-releases/read/health-caremicrofluidics-marketgrow-nearly-4-billion-2020.

23.https://www.visiongain.com/Press_Release/436/Microfluidic-technologies-market-will reach 3-5bn-in2017-predicts-new-visiongain-report.

24. http://www.researchandmarkets.com/research/vgk6kv/microfluidics, (2017).

25. **W. Ehrfeld, V. Hessel, H. Löwe.** Microreactors, New technology for modern chemistry, Wiley-Vch, First Edition 2000.

26. **A. J. Tüdos, G. A. J. Besselink, R. B. M. Schasfoort.** Trends in miniaturized total analysis systems for point-of-care testing in clinical chemistry, Journal of Lab-on-a-Chip, 2001, Vol. 1, pp. 83–95.

27.http://www.lboro.ac.uk/microsites/mechman/research/ipmktn/pdf/Technology_review/an-introductionto-mems.pdf.

28.http://www.semi.org/en/mems-market-can-expect-steady-growth-structural-change-1.

29. http://www.slideshare.net/MTKDMI/mems-2013-mefyole.

30. **V. Hessel, H. Löwe, F. Schönfeld.** Micromixers—a review on passive and active mixing principles, Chemical Engineering Science, 2005, Vol. 60, Issues 8–9, pp. 2479-2501.

31. **C. Y. Lee, C. L. Chang, Y. N. Wang, L. M. Fu.** Microfluidic Mixing: A Review, International Journal of Molecular Sciences., 2011, Vol. 12, pp. 3263-3287.

32. **K. Ward, Z. H. Fan.** Mixing in microfluidic devices and enhancement methods, Journal of Micromechanics and Microengineering, 2015, Vol. 25, No. 9.

33. **G. M. Whitesides.** The origins and the future of microfluidics, Journal of Nature, 2006, Vol. 442, pp. 368-373.

34. **P. Gwynne.** Microfluidics on the move: devices offer many advantages, Biomedical Optics and Medical Imaging, 2000.

35. **A. M. Streets, Y. Huang.** Chip in a lab: Microfluidics for next generation life science research, American Institute of Physics, Journal of Biomicrofluidics, 2013, Vol. 7, pp. 011302-23.

36. **K. Jensen.** Chemical kinetics: smaller, faster chemistry, Journal of Nature, 1998, Vol. 393, pp. 735-737.

37. **S. Hardt, F. Schönfeld.** Microfluidic Technologies for Minuaturized Analysis Systems, Springer, 2007, p. 121.

38. **T. M. Squires, S. R. Quake.** Microfluidics: Fluid physics at the nanoliter scale, Journal of Review of Modern Physics, 2005, Vol. 77, pp. 977-1026.

39. **J. P. Brody, P. Yager, R. E. Goldstein, R. H. Austin.** Biotechnology at low Reynolds numbers, Journal of Biophysical, 1996, Vol. 71, pp. 3430-3441.

40. **G. S. Jeong, S. Chung, C. S. Lee.** Applications of micromixing technology, Analyst Journal, 2010, Vol. 135, pp. 460–473.

41. **A. D. Radadia.** Microfluidics for biochemical and chemical reactions, Encyclopedia of Microfluidics and Nanofluidics, Springer, 2008, p. 1195-1206.

42. **A. Soleymani, E. Kolehmainen, I. Turunen.** Numerical and experimental investigations of liquid mixing in T-type micromixers, Journal of Chemical Engineering, 2008, Vol. 135, pp. 219–228.

43. **A. Asgar, S. Bhagat, E. T. K. Peterson, I. Papautsky.** A passive planar micromixer with obstructions for mixing at low Reynolds numbers, Journal of Micromechanics and Microengineering, 2007, Vol, 17, pp. 1017–1024.

44. **A. O. E. Moctar, N. Aubry, J. Batton.** Electrohydrodynamic micro-fluidic mixer, Journal of Lab-on-a-Chip, 2003, Vol. 3, pp. 273-280.

45. **H. Berthiaux, K. Marikh, C. Gatumel.** Continuous mixing of powder mixtures with pharmaceutical process constraints, Chemical Engineering and Processing, 2008, Vol. 47, pp. 2315–2322.

46. **M. Tokeshi, T. Minagawa, K. Uchiyama, A. Hibara, K. Sato, H. Hisamoto, T. Kitamori.** Continuous flow chemical processing on a microchip by combining microunit operations and a multiphase flow network, Analytical Chemistry, 2002, Vol. 74, pp. 1565-1571.

47. **G. J. M. Bruin.** Recent developments in electrokinetically driven analysis on microfabricated devices, Journal of Electrophoresis, 2000, Vol. 21, pp. 3931-3951.

48. **E. J. Hinch.** Mixing: Turbulence and Chaos – An introduction, Kluwer Academic/ Plenum Publishers, 1999, p. 37-56.

49. **N. Nguyen.** Micromixers: Fundamentals, Design and Fabrication, Elsevier Ltd., Second edition 2012.

50. **E. Villermaux, H. Chate, J. M. Chomaz.** Why mixing? Mixing: Chaos and Turbulence, New York, 1999, p. 1.

51. **J. M. Ottino.** The Kinematics of Mixing: stretching, chaos and transport, Cambridge University Press, 1989, pp. 116.

52. **E. L. Paul, V. A. Atiemo-Obeng, S. M. Kresta.** Handbook of Industrial Mixing Science and Practice, John Wiley and Sons, Inc., 2004, p. 99.

53. **X. Niu, Y. Lee.** Efficient spatial-temporal chaotic mixing in microchannels, Journal of Micromechanics and Microengineering, 2003, Vol. 13, pp. 454–462.

54. **J. P. Gleeson.** Transient micromixing: examples of laminar and chaotic stirring, Journal of Physics of Fluids, 2005, Vol. 17, pp. 100614-8.

55. **M. A. Stremler, F. R. Haselton, H. Aref.** Designing for chaos: applications of chaotic advection at the microscale, Philosophical Transactions of the Real Society of London A, 2004, Vol. 362, pp. 1019–1036.

56. **C. Chang, R. Yang.** A particle tracking method for analyzing chaotic electroosmotic flow mixing in 3D microchannels with patterned charged surfaces, Journal of Micromechanics and Microengineering , 2006, Vol. 16, pp. 1453–1462.

57. **P. J. Cullen.** Food Mixing: Principles and Applications, A John Wiley and Sons, Ltd. Publication, 2009, p. 12.

58. **S. Kresta.** AIChE Student Conference, San Francisco, November 2, 2013.

59. **Z. Jaworskia, H. Murasiewicza.** Numerical and experimental studies of liquid-liquid mixing in a kenics static mixer, 14th European Conference on Mixing, 2012.

60. **C. Ross.** Static Mixer Designs and Applications, p. 1-10.

61. **G. Fry, P. Buck.** Static Mixers for Custody Transfer, Statiflow.

62. Verdermix static mixers, www.verdermix.com.

63. **T. J. Johnson, D. Ross, L. E. Locascio.** Rapid microfluidic mixing, Journal of Analytical Chemistry, 2002, Vol. 74, pp. 45-51.

64. **R. W. Johnson.** Handbook of fluid dynamics, Second edition 2016, Taylor and Francis Group, LLC.

65. **M. Lesieur.** Turbulence in fluid dynamics, Springer, Fourth edition 2008, p. 2.

66. **J. M. Ottino.** Mixing chaotic advection and turbulence, Annual Review of Fluid Mechanics, 1990, Vol. 22, pp. 207-53.

67. **P. Graveson, J. Branjeberg, O. S. Jensen.** Microfluidics—a review. Journal of Micromechanics and Microengineering, 1993, Vol. 3, Issue 4, pp. 168–182.

68. **H. Aref.** The development of chaotic advection, Journal of the American Institute of Physics, Physics of Fluids, 2002, Vol. 14, pp. 1315–1325.

69. **A. E. Fick.** Poggendorffs Annalen der Physik, (1855a). pp. 94, 59.

70. **J. B. Fourier.** Theorie analitique de la chaleur, 1822, Paris.

71. **H. Bruus.** Theorical microfluidics, Oxford University Press, 2008, p. 95.

72. **A. Einstein.** Investigations on the theory of the Brownian movement, Dover Publications, Inc., 1956.

73. **P. Hinsmann, J. Frank, P. Svasek, M. Harasek, Bernhard Lendl.** Design, simulation and application of a new micromixing device for time resolved infrared

spectroscopy of chemical reactions in solution, Journal of Lab-on-a-Chip, 2001, Vol. 1, pp. 16–21.

74. **H. Mobius, W. Ehrfeld, V. Hessel, T. Richter.** Sensor controlled processes in chemical microreactors, The 8th International Conference on Solid-State Sensors and Actuators, Stockholm, Sweden, 1995, pp. 775-778.

75. **M. Koch, H. Witt, A. G. R. Evans, A. Brunnschweiler.** Improved characterization technique for micromixers, Journal of Micromechanics and. Microengineering, 1999, pp. 156–158.

76. **F. G. Bessoth, A. J. deMello, A. Manz.** Microstructure for efficient continuous flow mixing, Journal of Analytical Communications, 1999, Vol. 36, pp. 213–215.

77. **J. B. Knight, A. Vishwanath, J. P. Brody, R. H. Austin.** Hydrodynamic focusing on a silicon chip: mixing nanoliters in microseconds, The American Physical Society, Physical Review Letters, 1998, Vol. 80, No 17, pp. 3863-3866.

78. **G. M. Walker, M. S. Ozers, D. J. Beebe.** Cell infection within a microfluidic device using virus gradients, Journal of Sensors and Actuators B: Chemical, 2004, pp. 347–355.

79. **T. M. Floyd, M. A. Schmidt, K. F. Jensen.** Silicon micromixers with infrared detection for studies of liquid-phase reactions, Journal of Industrial and Engineering Chemistry Research, 2005, Vol. 44, No 8, pp. 2351-2358.

80. **H. Aref.** Stirring by chaotic advection, Journal of Fluid Mechanics, 1984, Vol. 143, pp. 1–21.

81. **H. Aref, B. Balachandar.** Chaotic advection in stoke flows, Journal of Physics of Fluids, 1986, Vol. 29, Issue 11, pp. 3515-3521.

82. **J. Chaiken, R. Chevray, M. Tabor, Q. M. Tan.** Experimental study of lagrangian turbulence in a Stokes flow, Proceedings of the Royal Society of London A, 1986, Vol. 408, pp. 164-174.

83. **H. Aref.** Chaotic advection of fluid particles, Journal of the Philosophical Transactions of the Royal Society A, 1990, Vol. 333, pp. 273–288.

84. **R. H. Liu, M. A. Stremler, K. V. Sharp, M. G. Olsen, J. G. Santiago, R. J. Adrian, H. Aref, D. J. Beebe.** Passive mixing in a three-dimensional serpentine

microchannel, Journal of Microelectromechanical Systems, 2000, Vol. 9, No. 2, pp. 190-197.

85. **H. Song, M. R. Bringer, J. D. Tice, C. J. Gerdts, R. F. Ismagilov.** Experimental test of scaling of mixing by chaotic advection in droplets moving through microfluidic channels, Journal of Applied Physics Letters, 2003, Vol. 83, No 22, pp. 4664-4666.

86. **D. S. Kim, S. H. Lee, T. H. Kwon, C. H. Ahn.** A serpentine laminating micromixer combining splitting recombination and advection, Journal of Lab-on-a-Chip, 2005, Vol. 5, pp. 739–747.

87. **C. Y. Lee, C. F. Lin, M. F. Hung, R. H. Ma, C. H. Tsai, C. H. Lin, L. M. Fu.** Experimental and numerical investigation into mixing efficiency of micromixers with different geometric barriers, Materials Science Forum, 2006, Vol. 505-507, pp. 391-396.

88. **Z. Chen, M. R. Bown, B. Osullivan, J. M. MacInnes, R. W. K. Allen, M. Mulder, M. Blom, R. van't Oever.** Performance analysis of a folding flow micromixer, Journal of Microfluidics and Nanofluidics, 2009, Vol. 6, pp. 763–774.

89. **S. Hardt, H. Pennemann, F. Schonfeld.** Theoretical and experimental characterization of a low Reynolds number split-and-recombine mixer, Journal of Microfluidics and Nanofluidics, 2006, Vol. 2, pp. 237–248.

90. **R. Tsai, C. Wu.** An efficient micromixer based on multidirectional vortices due to baffles and channel curvature, Journal of Biomicrofluidics, 2011, Vol. 5, pp. 014103-13.

91. **A. A. Deshmukh, D. Liepmann, A. P. Pisano.** Continuous micromixer with pulsatile micropumps, 2000, Berkeley Sensor and Actuator Center, pp. 73-76.

92. **I. Glasgow, N. Aubry.** Enhancement of microfluidic mixing using time pulsing, Journal of Lab-on-a-Chip, 2003, Vol. 3, pp. 114–120.

93. **Y. B. Ma, M. Fields, C. P. Sun, F. Y. Zhang, J. C. Liao, Y. Li, B. M. Churchill, C. M. Ho.** Microfluidic T-form mixer utilizing pressure disturbances, Nano Science and Technology Institute, 2006, Vol. 2, pp. 651-654.

94. **L. H. Lu, K. S. Ryu, C. Liu.** A magnetic microstirrer and array for microfluidic mixing, Journal of Microelectromechanical Systems, 2002, Vol. 11, No. 5, pp. 462-469.

95. **K. S. Ryu, K. Shaikh, E. Goluch, Z. Fan, C. Liu.** Micro magnetic stir-bar mixer integrated with parylene microfluidic channels, Journal of Lab-on-a-Chip, 2004, Vol. 4, pp. 608-613.

96. **H. H. Bau, J. Zhong, M. Yi.** A minute magnetohydrodynamic (MHD) mixer, Journal of Sensors and Actuators B, 2001, Vol. 79, pp. 207-215.

97. **D. Oh, J. S. Jin, J. H. Choi, H. Kim, J. S. Lee.** A microfluidic chaotic mixer using ferrofluid, Journal of Micromechanics and Microengineering, 2007, Vol. 17, pp. 2077-2083.

98. **G. G. Yaralioglu, I. O. Wygant, T. C. Marentis, B. T. Khuri-Yakub.** Ultrasonic mixing in microfluidic channels using integrated transducers, Journal of Analytical Chemistry, 2004, Vol. 76, pp. 3694-3698.

99. **K. Yasuda.** Non Destructive, non contact handlig method for biomaterials in microchamber by ultrasound, Sensors and Actuators B, 2000, Vol. 64, pp. 128-135.

100. **Z. Yang, S. Matsumoto, H. Goto, M. Matsumoto, R. Maeda.** Ultrasonic micromixer for microfluidic systems, Journal of Sensors and Actuators B, 2001, Vol. 93, Issue 3, pp. 266-272.

101. **L. Jang, S. Chao, M. R. Holl, D. R. Meldrum.** Resonant mode-hopping micromixing, Sensors and Actuators A 138, 2007, Vol. 138(1), pp. 179–186.

102. **T. Luong, V. Phan, N. Nguyen.** High-throughput micromixers based on acoustic streaming induced by surface acoustic wave, Journal of Microfluidics and Nanofluidics, 2011, Vol. 10, pp. 619-625.

103. **A. A. Darhuber, J. P. Valentino, J. M. Davis, S. M. T. S. Wagner.** Microfluidic actuation by modulation of surface stresses, Jounal of Applied Physics Letters, 2003, Vol. 82, No 4, pp. 657-659.

104. **B. Xu, T. N. Wong, N. Nguyen, Z. Che, J. C. K. Chai.** Thermal mixing of two miscible fluids in a T-shaped microchannel, Journal of Biomicrofluidics, 2002, Vol. 4, pp. 044102-12.

105. **H. Mao, T. Yang, P. S. Cremer.** A microfluidic device with a linear temperature gradient for parallel and combinatorial measurements, Journal of the American Chemical Society, 2002, Vol. 124, pp. 4432-4435.

106. **J. Tsai, L. Lin.** Active microfluidics mixer and gas bubble filter driven by thermal bubble micropump, Journal of Sensors and Actuators A, 2002, Vol. 97-98, pp. 665-671.

107. **L. Chen, X. Zhang, J. Okajima, S. Maruyama.** Numerical investigation of near-critical fluid convective flow mixing in microchannels, Journal of Chemical Engineering, 2013, Vol. 97, pp. 67-80.

108. **J. T. Edward.** Molecular volumes and the Stokes-Einstein equation, 1970, Vol. 47, Issue 4, pp. 261-270.

109. **G. Jenkins, C. D. Mansfield.** Microfluidic Diagnostics Methods and Protocols, Springer Science and Business Media, LLC., 2013.

110. **J. Berthier, P. Silberzan.** Microfluidics for Biotechnology, Artech House, 2010, Second edition, p. 1.

111. **H. A. Stone.** Dynamics of drop deformation and breakup in viscous fluids, Annual Review of Fluid Mechanics, 1994, Vol. 26, pp. 65-102.

112. **S. G. Kandlikar.** Heat Transfer and Fluid Flow in Minichannels and Microchannels, Elsevier Ltd., First edition 2006.

113. **L Capreto, W. Cheng, M. Hill, X. Zhang.** Mixing within microfluidics devices, Topics of Current Chemistry Journal, 2011, 304, pp. 27–68.

114. **S. Shoji, M. Esashi.** Microflow devices and systems, Journal of Micromechanics and Microengineering, 1994, Vol. 4, pp. 157-171.

115. **I. Glasgow, S. Lieber, N. Aubry.** Parameters influencing pulsed flow mixing in microchannels, Journal of Analytical Chemistry, 2004, Vol. 76, No 16, pp. 4825-4832.

116. **M. Jain, B. Puranik, A. Agrawal.** A numerical investigation of effects of cavity and orifice parameters on the characteristics of a synthetic jet flow, Journal of Sensors and Actuators A, 2011, Vol. 165, pp. 351-366.

117. **M. Jabbal, J. Wu, S. Zhong.** The performance of round synthetic jets in quiescent flow, The Aeronautical Journal, 2006, pp. 385-392.

118. **M. B. Gillespie, W. Z. Black, C. Rinehart, A. Glezer.** Local convective heat transfer from a constant heat flux flat plate cooled by synthetic air jets, Journal of Heat Transfer, 2006, Vol. 128, pp. 990-1000.

119. **M. Jain, B. Puranik, A. Agrawal.** A numerical investigation of effects of cavity and orifice parameters on the characteristics of a synthetic jet flow, Journal of Sensors and Actuators, 2011, A 165, pp. 351–366.

120. **S. Davis, A. Glezer.** Mixing control of fuel jets using synthetic jet technology, Velocity field measurements, 37th Aerospace Sciences Meeting and Exhibit, Aerospace Sciences Meetings, American Institute of Aeronautics and Astronautics, 1999.

121. **R. Mittal, P. Rampunggoon.** On the virtual aeroshaping effect of synthetic jets, Journal of Physics of Fluids, 2002, Vol. 14, No. 4, pp. 1533-1536.

122. **V. Timchenko, J. Reizes, E. Leonardi.** A numerical study of enhanced microchannel cooling using a synthetic jet actuator, 15th Australian Fluid Mechanics Conference, 2004.

123. **A. Glezer, M. Amitay.** Synthetic jets, Annual Review of Fluid Mechanics Journal, 2002, Vol, 34, pp. 503–29.

124. **D. McCormick.** Boundary layer separation control with directed synthetic jets, 38th Aerospace Sciences Meeting and Exhibit, 2000, American Institute of Aeronautics and Astronautics.

125. **R. Holman, Y. Utturka, R. Mittal, B. L. Smith, L. Cattafesta.** Formation criterion for synthetic jets, AIAA Journal, 2005, Vol. 43, No. 10, pp. 2110-2116.

126. **Y. Chen, S. Liang, K. Aung, A. Glezer, J. Jagoda.** Enhanced mixing in a simulated combustor using synthetic jet actuators, 37th Aerospace Sciences Meeting and Exhibit, Aerospace Sciences Meetings, American Institute of Aeronautics and Astronautics, 1999.

127. **I. M. Milanovic, K. B. M. Q. Zaman.** Synthetic jets in crossflow, AIAA Journal, 2005, Vol. 43, No. 5, pp. 929-940.

128. **M. Jabbal, S. Zhong.** The near wall effect of synthetic jets in a boundary layer, International Journal of Heat and Fluid Flow, 2008, Vol. 29, pp. 119–130.

129. **Y. Kamotani, I. Greber.** Experiments on a turbulent jet in a crossflow, AIAA Journal, 1972, Vol.. 10, No. 11, pp. 1425-1429.

130. **T. Mautner.** Application of the synthetic jet concept to low Reynolds number biosensor microfluidic flows for enhance mixing: a numerical study using the

lattice Boltzmann method, Journal of Biosensors and Bioelectronics, 2004, Vol. 19, pp. 1409-1419.

131. **R. Duvigneau.** http://num3sis.inria.fr/blog/synthetic-jet-simulations, 2014.

132. **Q. Xia, S. Zhong.** Liquids mixing enhanced by multiple synthetic jet pairs at low Reynolds numbers, Journal of Chemical Engineering Science, 2013, Vol. 102, pp. 10-23.

133. **Q. Xia.** Enhancement of liquids mixing using active pulsation in the laminar flow regime, PhD thesis, 2012, pp. 181-197.

134. **D. S. Kercher, J. Lee, O. Brand, M. G. Allen, A. Glezer.** Microjet cooling devices for thermal management of electronics, IEEE Transactions on Components and Packing Technologies, 2003, Vol. 26, No 2, pp. 359-366.

135. **C. Lee, G. Hong, Q. P. Ha, S. G. Mallinson.** A piezoelectrically actuated micro-synthetic jet for active flow control, Journal of Sensors and Actuators A, 2003, Vol. 108, pp. 168-174.

136. **N. Nguyen, X. Huang, T. K. Chuan.** MEMS-Micropumps: A Review, Journal of Fluids Engineering, 2002, Vol. 124, pp. 384-392.

137. **A. Günther, S. A. Khan, M. Thalmann, F. Trachsel, K. F. Jensen.** Multiphase microfluidics: from flow characteristics to chemical and materials synthesis, Journal of Lab-on-a-Chip, 2006, Vol. 6, pp. 1487-1503.

138. **S. Okushima, T. Nisisako, T. Tori, T. Higuchi.** Controlled production of monodisperse double emulsions by two-step droplet breakup in microfluidic devices, Langmuir Journal, 2004, Vol. 20, Issue 23, pp. 9905-9908.

139. **Y. K. Suh, S. Kang.** A review on mixing in microfluidics, Journal of Micromachines, 2010, Vol. 1, No 3, pp. 82-111.

140. **M. R. Bringer, C. J. Gerdts, H. Song, J. D. Tice, R. F. Ismagilov.** Microfluidic systems for chemical kinetics that rely on chaotic mixing in droplets, Philosophical Transactions of the Royal Society of London A, 2004, Vol. 362, pp. 1087-1104.

141. **A. Liau, R. Karnik, A. Majumdar, J. H. D. Cate.** Mixing crowded biological solutions in milliseconds, Journal of Analytical Chemistry, 2005, Vol. 77, pp. 7618-7625.

142. **P. Paik, V. K. Pamula, R. B. Fair.** Rapid droplet mixers for digital microfluidic systems, Journal of Lab-on-a-Chip, 2003, Vol. 3, pp. 253-259.

143. **P. Garstecki, M. J. Fuerstman, M. A. Fischbach, S. K. Sia, G. M. Whitesides.** Mixing with bubbles: a practical technology for use with portable microfluidic devices, Journal of Lab-on-a-Chip, 2006, Vol. 6, pp. 207-212.

144. **K. Tung, C. Li, J. Yang.** Mixing and hydrodynamic analysis of a droplet in a planar serpentine micromixer, Journal of Microfluidics and Nanofluidics, 2009, Vol. 7, pp. 545-557.

145. **M. Rhee, M. A. Burns.** Drop mixing in a microchannel for lab-on-a-chip platforms, Langmuir Journal, 2008, Vol. 24, pp. 590-601.

146.https://www.piceramic.com/en/products/piezoceramic-actuators/linear-actuators/.

147. http://www.solidworks.co.uk/ (2014).

148. **B. J. Tensi, F. Paille, G. Dury.** Modification of the wake behind a circular cylinder by using synthetic jets, Journal of Visualization, 2002, Vol. 5, No.1, pp. 37-44.

149. **J. F. Swindells, C. F. Snyder, R. C. Hardy, P. E. Golden.** Viscosities of sucrose solutions at various temperatures: Tables of recalculated values, Supplement of National Bureau of Standards Circular 440, Issued July 31, 1958.

150.http://www.reevesart.com/products/acrylic_colour/fine_artist_quality_acrylic_colour/.

151. **J. Voldman, M. L. Gray, M. A. Schmidt.** An integrated liquid mixer/valve, Journal of Microelectromechanical Systems, 2000, Vol. 9, No. 3, pp. 295-302.

152. **V. Haverkamp, W. Ehrfeld, K. Gebauer, V. Hessel, H. Löwe, T. Richter, C. Wille.** The potential of micromixers for contacting of disperse liquid phases, Journal of Analytical Chemistry, 1999, Vol. 364, pp. 617-624.

153. **A. E. Kamholz, B. H. Weigl, B. A. Finlayson, P. Yager.** Quantitative analysis of molecular interaction in a microfluidic channel: the T-sensor, Journal of Analytical Chemistry, 1999, Vol, 71, pp. 5340-5347.

154. **D. B. Kenkamp, A. Desai, X. Yang, Y. Tai, E. M. Marzluff, S. L. Mayo.** Microfabricated silicon mixers for submillisecond quench-flow analysis, Journal of Analytical Chemistry, 1998, Vol. 70, pp. 232-236.

155. **M. Zlokarnik.** Stirring: Theory and Practice, Wiley-Vch, 2001, p.101.

156. **F. Alberini, M. J. H. Simmons, A. Ingrama, E. H. Stitt.** Assessment of different methods of analysis to characterise the mixing of shear-thinning fluids in a Kenics KM static mixer using PLIF, Journal of Chemical EngineeringScience, 2014, Vol. 112, pp. 152.

157. **J. D. Zhan.** Methods of Bioengineeing: Biomicrofabrication and biomicrofluidics, Artech House, 2010.

158. https://uk.mathworks.com/products/matlab.html.

159. https://www.dantecdynamics.com/particle-image-velocimetry.

160. **G. W. Hart.** Multidimensional Analysis: Algebras and Systems for Science and Engineering, Springer Science and Business Media, 1995.

161. **D. C. Montgomery.** Design and Analysis of Experiments, Fifth edition, 2001, John Wiley and Sons, Inc.

162. SAS Institute Inc. 2012. JMP 10 Design of Experiments Guide. Cary, NC: SAS Institute Inc.

163. **R. H. Myers, D. C. Montgomery, C. M. Anderson-Cook.** Response Surface Methodology, Third edition, 2009, John Wiley and Sons, Inc.

164. **C. Kleinstreuer.** Microfluidics and Nanofluidics: Theory and Selected Applications, 2014, John Wiley and Sons, Inc., p. 61.

165. **J. F. Wendt.** Computational fluid dynamics, An introduction, A von Karman Institure book, Springer-Verlag, 1992.

166. http://www.ansys.com/Products/Fluids/ANSYS-Fluent.

167. ANSYS Fluent 12.0 User's Guide, ANSYS, Inc., 2009.

168. **O. Zikanow.** Essential Computational Fluid Dynamics, John Wiley and Sons, Inc., 2010, p. 26.

169. http://www.dolomite-microfluidics.co.uk/ (consulted 2014).

170. **Y. A. Cengel, M. A. Boles.** Thermodynamics, An Engineering Approach, Fifth edition, 2006.

171. Fluent 14.0 User's Guide, Modelling Discrete Phase.

172. **M. Heule, A. Manz.** Sequential DNA hybridisation assays by fast micromixing, Journal of Lab-on-a-Chip, 2004, Vol. 4, pp. 506-511.

173. **N. B. Vargaftik, B. N. Volkov, L. D. Voljak.** International tables of the surface tension of water, Journal of Physical Chemistry, 1983, Vol. 12, No 3.

174. **J. Berthier.** Microdrops and digital microfluidics, William Andrew Inc., 2008, p. 12.

175. http://www.openfoam.org/features/standard-solvers.php.

176. **D. Li.** Encyclopedia of Microfluidics and Nanofluidics, Springer Science and Business Media, 2008, p. 70.

177. **C. Ho.** Microflows and nanoflows, Fundamentals and simulation, 2005, Springer Inc., p. 315.

178. **D. Li.** Electrokinetics in Microfluidics, Vol. 2, Elseiver Ltd., 2004, p. 232.

179. **D. Erickson, D. Li.** Influence of surface heterogeneity on electrokinetically driven microfluidic mixing, Langmuir Journal, 2002, Vol. 18, pp. 1883-1892.

180. **M. Z. Bazant, T. M. Squires.** Induced-charge electrokinetic phenomena: theory and microfluidic applications, Journal of Physical Review Letters, Vol. 92, No 6, pp. 066101-066104.

181. http://www.openfoam.com.

182. http://www.ni.com/labview/ (National Instruments).

183. **H. Kinoshita, S. Kaneda, T. Fujii, M. Oshima.** Three-dimensional measurement and visualization of internal flow of a moving droplet using confocal micro-PIV, Journal of Lab-on-a-Chip, 2007, Vol. 7, pp. 338-346.

184. **J. G. Santiago, S. T. Wereley, C. D. Meinhart, D. J. Beebe, R. J. Adrian.** A particle image velocimetry system for microfluidics, Journal of Experiments in Fluids, 1998, Vol. 25, pp. 316-319.

Appendix A

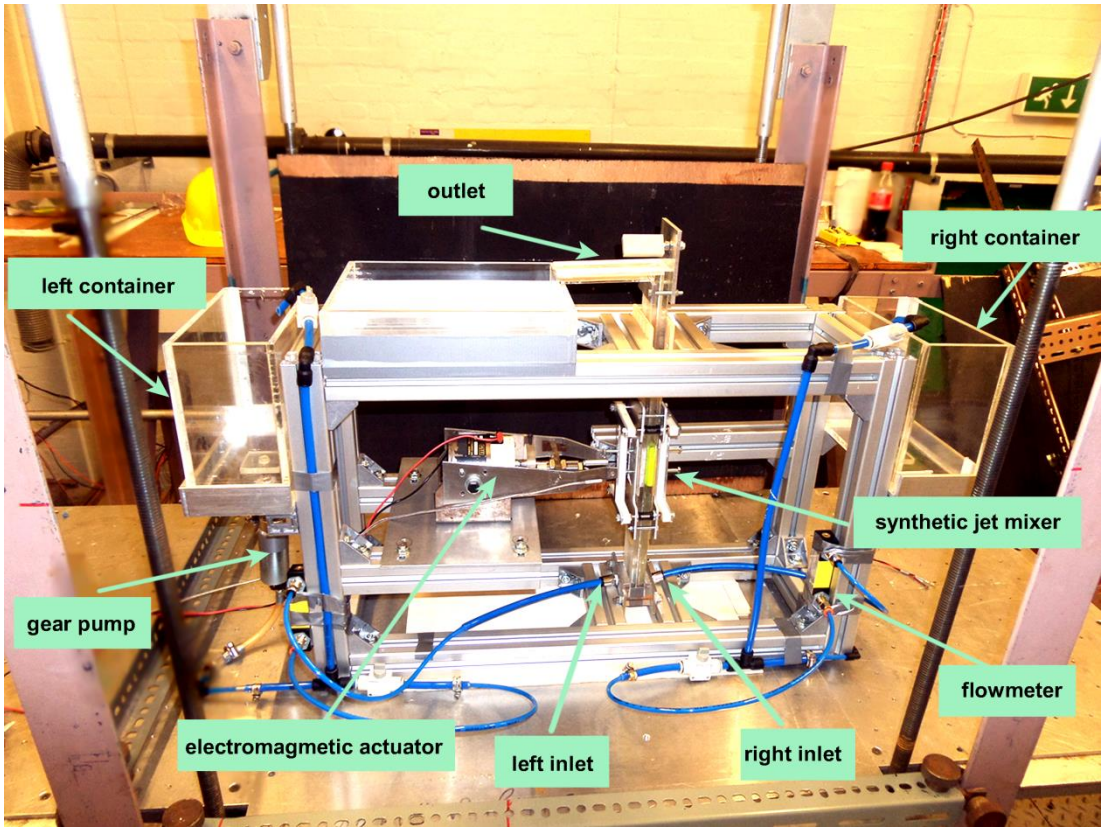

Test rig of the macromixer with four pairs of opposite synthetic jets

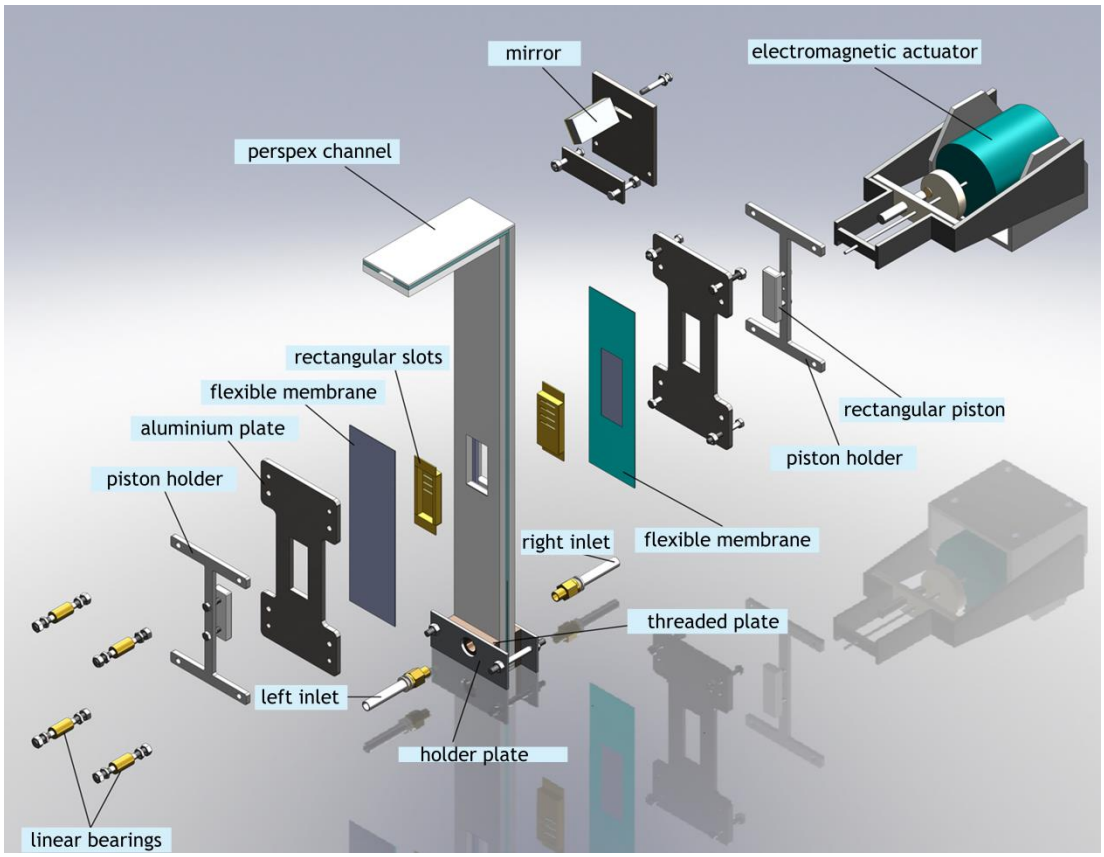

Exploded view of the macromixer with four pairs of opposite synthetic jets

Appendix B

User-defined Functions (UDFs) coded in C language

```
#include "udf.h"                                    /*Library to load the udf features */

                    /*Velocity profile for one half of the channel */
DEFINE_PROFILE(velocity_profile_left, thread, position)
{
real x[ND_ND];
real r;                                             /*Variable to define the channel radius */
face_t f;
real mean_vel = 0.000125;                           /*Mean velocity in the rectangular channel */
real vel_max = mean_vel*1.5;   /*Maximum flow velocity in the rectangular channel */
real radius_channel = 0.004/2.0;                            /*Channel height over two*/
        begin_f_loop(f,thread)
        {
        F_CENTROID(x, f, thread);
         r = x[0];                                  /*Velocity profile along the x-coordinate */
        F_PROFILE(f,thread,position)=vel_max*(1.0(r*r)/(radius_channel*radius_cha
         nnel));
        }
        end_f_loop(f, thread)
}

                    /*Velocity profile for the other half of the channel */
DEFINE_PROFILE(velocity_profile_right, thread, position)
{
real x[ND_ND];
real r;                                             /*Variable to define the channel radius */
face_t f;
real mean_vel = 0.000125;                           /*Mean velocity in the rectangular channel */
real vel_max = mean_vel*1.5;          /*Max. flow velocity in the rectangular channel */
```

```
real radius_channel = 0.004/2.0;                    /*Channel height over two*/
        begin_f_loop(f,thread)
        {
         F_CENTROID(x, f, thread);
         r = x[0];                          /*Velocity profile along the x coordinate */
        F_PROFILE(f,thread,position)=vel_max*(1.0(r*r)/(radius_channel*radius_ch
        annel));
        }
         end_f_loop(f, thread)
}
```

/* User-defined Function (UDF) for dynamic mesh simulation */

```
DEFINE_CG_MOTION(velocity_mesh_motion, dt, cg_vel, cg_omega, time, dtime)
{
real t;                    /* Variable to determine the current time of the simulation */
real vp;                                        /* Variable of the oscillating motion */
real pi=3.1416;                                          /* Constant value of pi */
real delta = 0.0035;                          /* Diaphragm displacement in metres */
real frequency = 2.0;                                  /* Oscillating frequency in Hz */
real fluent_time=0.0;                    /* Time at which this udf is called by Fluent*/
t=time-fluent_time;    /* Current time calculated by Fluent minus the time at which the
mesh motion is called */
        vp = pi*delta*frequency*cos(2.0*pi*frequency*t);        /* Motion equation */
cg_vel[0] = vp;              /* Oscillating motion values applied to the x-coordinate*/
cg_vel[1] = 0.0;
cg_vel[2] = 0.0;
                    /*No angular velocity in any of the x,y,z co-ordinates*/
cg_omega[0] = 0.0;
cg_omega[1] = 0.0;
cg_omega[2] = 0.0;
}
```

/* User-defined Function (UDF) for defining the fluid zones (water and dyed water */

```
DEFINE_INIT(my_init_func,d)
{
cell_t c;
Thread *t;
real xc[ND_ND];
                                        /* loop over all the cell threads in the domain */
        thread_loop_c(t,d)
        {
        begin_c_loop_all(c,t)                                   /* loop over all cells */
        {
        C_CENTROID(xc,c,t);
        if (  xc[0] > 0.0   )              /* if the co-ordinate x is greater than zero */
        C_YI(c,t,0)=1.0;                 /* the fluid domain is defined as 100% dyed */
        }
        end_c_loop_all(c,t)
        }
}

DEFINE_ON_DEMAND(Set_dye_on_demand)
{
Domain*d;
cell_t c;
Thread*t;
 real xc[ND_ND];
                                        /* loop over all cell threads in the domain */
        d = Get_Domain (1);
        thread_loop_c(t,d)
        {
            begin_c_loop_all(c,t)                               /* loop over all cells */
        {
```

```
        C_CENTROID(xc,c,t);
        if( (xc[0] >0.0 ) )                 /* if the co-ordinate x is greater than zero */
        C_YI(c,t,0)=1.0;                    /* the fluid domain is defined as 100% dyed */
        }
        end_c_loop_all(c,t)
        }
}
```

Appendix C

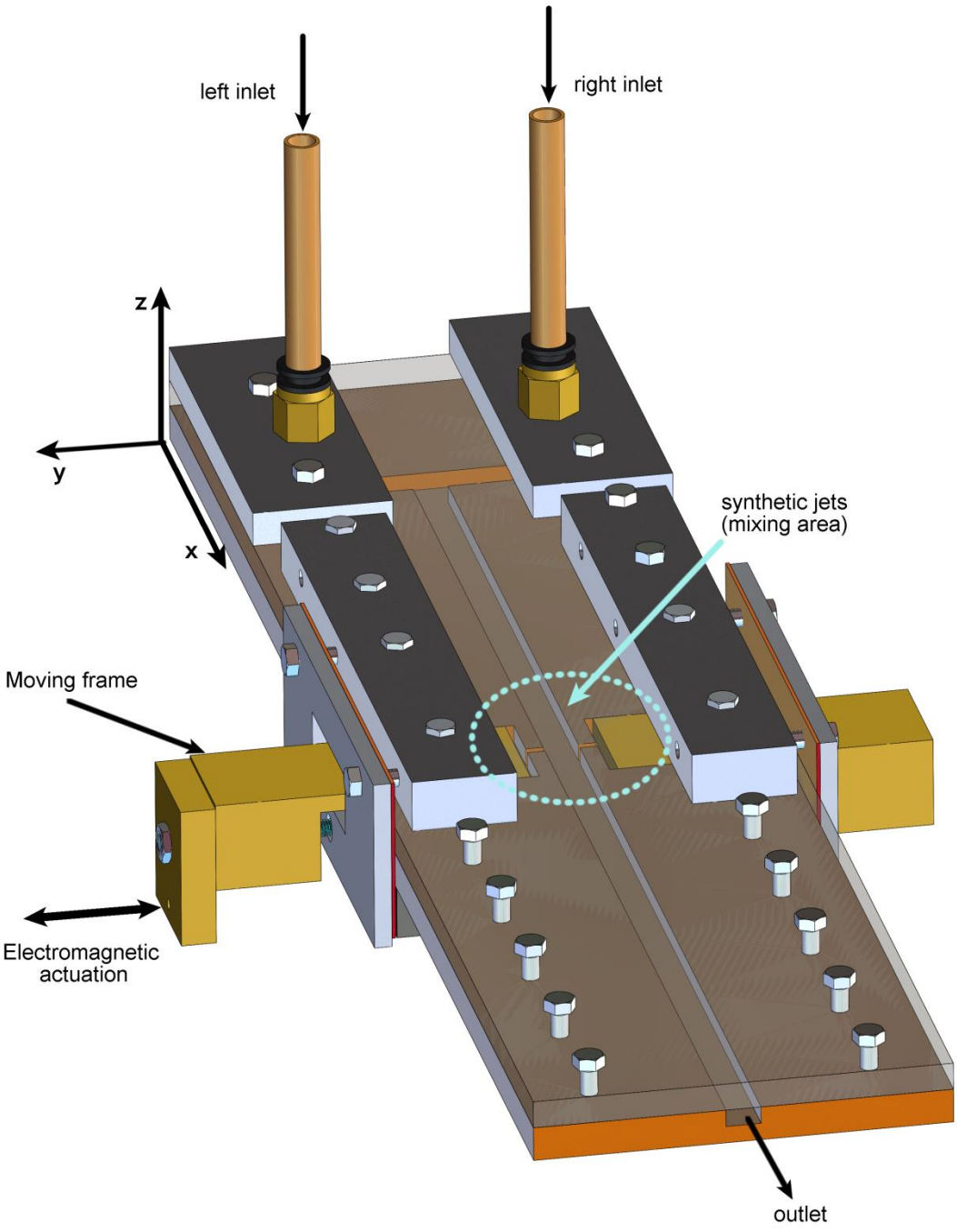

Macromixer with one pair of opposite synthetic jets

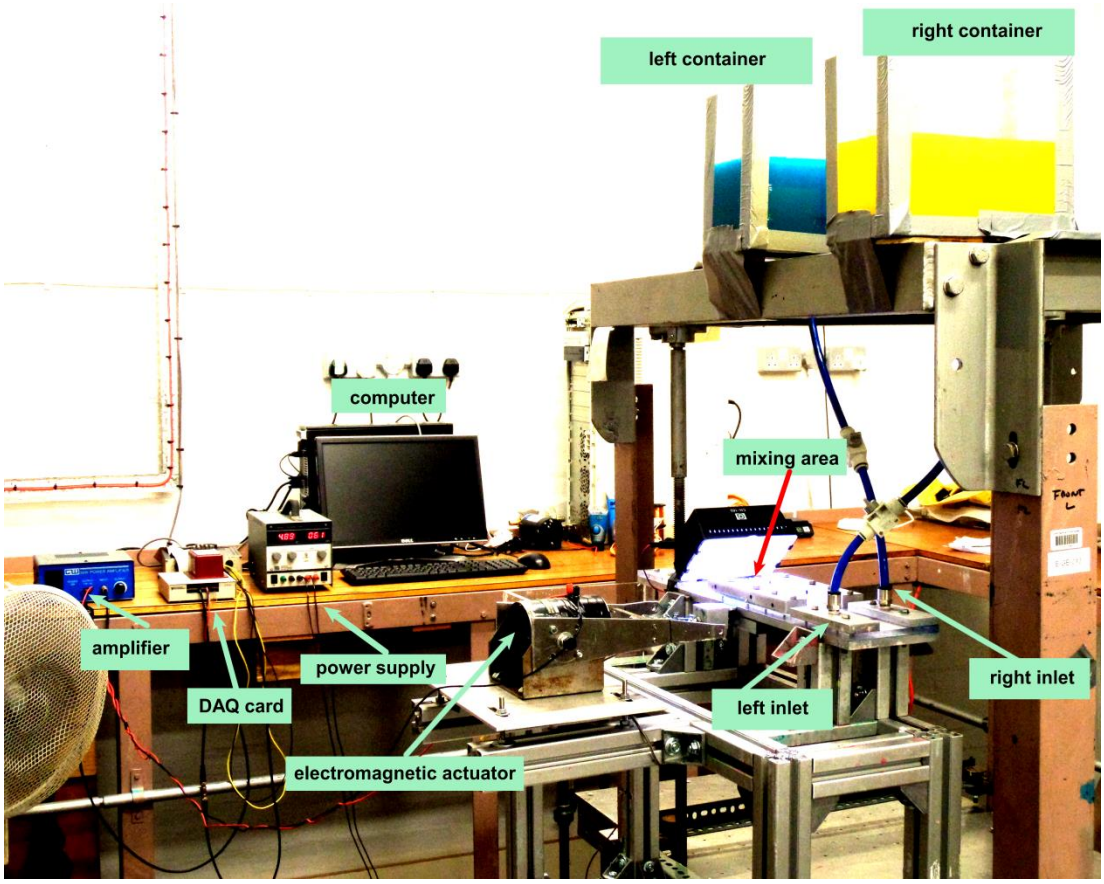

Test rig of the macromixer with one pair of opposite synthetic jets